Advective interfacial exchange in permeable sediments driven by surface gravity waves and its ecological consequences

Dissertation
zur Erlangung des
Doktorgrades der Naturwissenschaften
im Fachbereich 5
der Universität Bremen

vorgelegt von

Elimar Precht
Bremen
2003

Tag des Kolloquiums:

24. April 2003

Gutachter:

Herr Prof. Dr. Bo Barker Jørgensen

Herr PD Dr. Matthias Zabel

Prüfer:

Herr Prof. Dr. Gerhard Bohrmann

Herr Prof. Dr. Michael Schlüter

Table of Contents

Abstract

Sandy sediments, as they are common in coastal and shelf environments, are highly permeable and allow advective pore water exchange across the sediment-water interface driven by pressure differences at the sediment surface (Huettel and Webster 2001). This process has been addressed and quantified for unidirectional flow in a number of studies, and it has been suggested that advective exchange may play a significant role in global biogeochemical cycling of matter (Huettel et al. 1998), as permeable sediments are abundant on the continental shelves (de Haas et al. 2002). Advective exchange driven by oscillating flows, as induced by surface gravity waves in shallow water, has received less attention in previous works although waves affect large areas of the global shelves.

The aim of this thesis was to investigate and quantify advective exchange between permeable sediments and overlying water driven by surface gravity waves and to demonstrate the influence of this exchange on the sedimentary oxygen dynamics. For this purpose and to assess the effects of the waves on transport and reaction in permeable sands, laboratory wave tank experiments and in-situ studies were conducted using inert tracers and planar oxygen optode measurements.

The wave tank experiments demonstrated that shallow water waves can increase solute exchange between sandy sediment and overlying water up to 50-fold relative to diffusive exchange. This wave-generated interfacial exchange was mainly driven by the pressure gradients generated by the interaction of oscillating boundary flows and sediment wave ripples that formed on the initially level sediment surface. Below ripple topography, a pore water flow field with a regular pattern of intrusion and release zones developed that migrated with ripple propagation. The ensuing filtering rates in the wave tank ranged from 60 L m^{-2} d^{-1} to 590 L m^{-2} d^{-1} and exceeded the solute exchange rates caused by hydrostatic wave pumping (38 L m^{-2} d^{-1}) and molecular diffusion (corresponding to 10 to 12 L m^{-2} d^{-1}). The results revealed that oscillating flows drive advective exchange in similar manner and magnitude as unidirectional flows.

To verify that the processes observed in the wave tank also occur in natural environments, the wave tank experiments were succeeded by observations of pore water flow fields in a rippled coastal sand bed exposed to oscillating boundary flows, and in-situ measurements of pore water flow velocities. The measurements were carried out on Giglio Island (Italy) at

50 to 70 cm water depth during a phase of very low wave energy. Pore water visualisation experiments revealed flow fields with intrusion of water in the ripple troughs and pore water release at the ripple crests very similar to the flow fields we observed in the wave tank experiments with the difference that the natural wave ripples and the pore water flow fields were about 10 times larger than those recorded in the laboratory. Additionally, a novel optode technique was introduced that permitted direct pore water flow velocity measurements using a fluorescent tracer. Averaged pore water velocity in the upper 6 cm of sediment underneath the ripple crest was 26 cm h^{-1} and reached up to 40 cm h^{-1} 0.5 cm below the sediment surface. Thus, advective transport exceeded transport by molecular diffusion by at least 3 orders of magnitude. From the pore water velocities and ripple spacing, it could be inferred that approx. 140 L m^{-2} d^{-1} of water were filtered through the sediment by the waves, which correlated well with the findings of the previous wave tank experiments.

In order to assess the effect of wave-induced pore water exchange on the oxygen dynamics in the sediment and its biogeochemical implications, wave tank experiments with natural sandy sediment and a planar oxygen optode were carried out.

The planar optode technique allowed direct 2-dimensional surveillance of the oxygen distribution in the sediment and overlying water and the experiments demonstrated that wave-driven advective pore water flow changed the spatial and temporal oxygen distribution in the upper sediment layer. Oxygenated water intruding in the ripple troughs and deep anoxic pore water drawn to the surface under the ripple crests created an undulating oxic-anoxic boundary within the upper sediment layer mirroring the topographical features of the sediment bed. Magnitudes of pore water flow and sedimentary oxygen consumption determined the spatial dimensions of the oxic zones. Horizontal oxygen concentration gradients developed that were in the same order of magnitude as those in the vertical. The oxygen optode showed that migrating wave ripples were trailed by their pore flow field alternately exposing sediment volumes to oxic and anoxic pore water until the ripple movement became too rapid (experimental threshold $\approx$ 20 cm h^{-1}) for the pore water to follow. Rapid ripple migration, thus, produced a continuous oxic surface layer that inhibited the release of reduced substances from the bed, which under slowly migrating ripples was possible through the anoxic vertical upwelling zones. Swift, dramatic

changes in oxygen concentration in the upper layers of permeable sea beds due to surface gravity waves challenge sedimentary organisms and affect organic matter mineralisation in the bed.

The wave-induced advective pore water exchange processes and filtration investigated here are ecologically and biogeochemically relevant as permeable sandy sediments are very abundant on the continental shelf and large areas (water depth < 100 m) of the shelf are permanently or episodically affected by hydrodynamic forcing through waves. More specifically, the wave-influenced continental shelf may be subdivided into two zones: a shallow zone (water depth < wavelength/2), where wave orbital motion at the sea floor creates ripples and causes topography-related permanent or episodic advective filtering and a deeper zone (wavelength/2 < water depth < wavelength), where wave pumping enhances interfacial exchange by hydrostatic pressure oscillations.

Thus, large shelf areas may be effective filter systems for particulate matter. The highly dynamic oxygen concentrations of the sediments, with mobile horizontal oxygen concentrations gradients in the same order of magnitude as in those in the vertical, reveal that advective transport cannot only filter particulate matter but could also enhance mineralisation in these sandy beds by constantly transporting oxygen-rich water into the particle-rich surface layers of these sediments. Surface gravity waves thereby could largely affect suspended particle concentration and cycling of matter in the coastal and continental shelf environment.

Zusammenfassung

In permeablen Sedimenten wie Schelfsanden, führen Druckgradienten an der Sedimentoberfläche zu advektivem Porenwasseraustausch zwischen Sediment und Wasser (Huettel und Webster 2001). Dieser Prozess wurde für gerichtete Strömungen in einer Anzahl von Arbeiten untersucht und quantifiziert. Daraus folgte die Vermutung, dass advektiver Austausch aufgrund der Häufigkeit permeabler Sedimente auf dem kontinentalen Schelf (de Haas et al. 2002) eine bedeutende Rolle im globalen biogeochemischen Stoffkreislauf spielen könnte (Huettel et al. 1998). Im Gegensatz zu advektivem Austausch verursacht durch gerichtete Strömungen hat advektiver Austausch durch oszillierende Strömungen, wie sie Oberflächenwellen in flachem Wasser hervorrufen, in bisherigen Arbeiten weniger Beachtung gefunden, obwohl große Schelfgebiete von Wellen beeinflusst sind.

Ziel der vorliegenden Arbeit war, den wellengetriebenen advektiven Austausch zwischen permeablen Sedimenten und der Wassersäule zu untersuchen und zu quantifizieren. Desweiteren sollte der Einfluss dieses Austausches auf die Sauerstoffdynamik im Sediment nachgewiesen werden. Dazu und um den Einfluss von Wellen auf Transport und Reaktionen im Sediment abzuschätzen, wurden Wellenkanalversuche sowie in situ Experimente mit inertem Tracer und planaren Sauerstoffoptoden durchgeführt.

Die Wellenkanalversuche zeigten, dass Flachwasserwellen den Austausch gelöster Substanzen zwischen sandigem Sediment und Wasser im Vergleich zu diffusivem Austausch um bis zu 50-fach erhöhen können. Der welleninduzierte Austausch zwischen Sediment und Wasser wurde vor allem hervorgerufen durch Druckgradienten, entstanden durch die Wechselwirkung zwischen oszillierender Strömung und auf der anfänglich glatten Sedimentoberfläche gebildeten Wellenrippeln. Unterhalb der Rippeltopographie bildete sich ein regelmäßiges Porenwasserströmungsmuster mit Zonen, in denen Wasser in das Sediment eindrang und Zonen, aus denen Porenwasser austrat. Dieses Strömungsmuster war an die Rippeltopograhie gebunden und migrierte mit ihr. Die aus dem Porenwasseraustausch resultierenden Filterungsraten lagen zwischen 60 L m^{-2} d^{-1} und 590 L m^{-2} d^{-1} und übertrafen damit deutlich den Austausch durch "Wellenpumpen" (angetrieben durch hydrostatische Druckunterschiede, 38 L m^{-2} d^{-1}) und molekulare

Diffusion (entsprechend 10 bis 12 L m^{-2} d^{-1}). Oszillierende Strömungen verursachten damit advektiven Austausch in ähnlicher Weise und Größenordnung wie gerichtete Strömung.

Um zu überprüfen, ob die im Wellenkanal beobachteten Prozesse auch in der Natur vorkommen, wurden anschließend in Feldmessungen in einem küstennahen Sand Porenwasserströmungsmuster visualisiert und Porenwassergeschwindigkeiten gemessen. Die Messungen wurden auf der Isola del Giglio (Italien) in 50 bis 70 cm Wassertiefe in einer Phase mit sehr niedriger Wellenenergie durchgeführt. Die Porenwasser-Visualisierungs-Experimente zeigten Eindringen von Wasser in den Rippeltrögen und Porenwasseraustritt an den Rippelkämmen. Dieses Muster entsprach dem im Labor beobachteten, obwohl die räumlichen Ausmaße der Rippeln und des sich bildenden Strömungsmusters etwa 10 mal größer waren als im Labor. Desweiteren wurde eine neuartige Optoden-Technik angewandt, die direkte Messungen der Strömungsgeschwindigkeit des Porenwassers im Sediment mit Hilfe fluoreszierenden Tracers erlaubte. In den Messungen lag die durchschnittliche Porenwassergeschwindigkeit unterhalb der Rippelkämme in den oberen 6 cm des Sediments bei 26 cm h^{-1} und erreichte 40 cm h^{-1} 0.5 cm unterhalb der Sedimentoberfläche. Auf diese Weise war der advektive Transport um mehr als drei Größenordnungen schneller als der Transport durch molekulare Diffusion. Aus den gemessenen Porenwassergeschwindigkeiten und den Rippelkammabständen wurde errechnet, dass ca. 140 L m^{-2} d^{-1} Wasser von den Wellen durch das Sediment gefiltert wurden, was in sehr guter Übereinstimmung mit den Laborergebnissen steht.

Um den Einfluss des welleninduzierten Porenwasseraustausches auf die Sauerstoffdynamik im Sediment und die damit verbundenen biogeochemischen Auswirkungen zu untersuchen, wurden Versuche im Wellenkanal mit natürlichem sandigen Sediment und einer planaren Sauerstoffoptode durchgeführt.

Die planare Optode erlaubte direkte 2-dimensionale Messungen der Sauerstoffverteilung in Sediment und darüberliegendem Wasser. Welleninduzierte advektive Porenwasserströme beeinflussten die zeitliche und räumliche Verteilung des Sauerstoffs in den oberen Sedimentschichten. In den Rippeltrögen in das Sediment eindringendes sauerstoffreiches Wasser und an den Rippelkämmen austretendes sauerstoffarmes Porenwasser aus tieferen Sedimentschichten schufen eine undulierende, oxisch-anoxische Grenzschicht in den

oberen Sedimentlagen, die die Sedimenttopographie widerspiegelte. Das Ausmaß der Porenwasserströmung und die Sauerstoffzehrung des Sediments bestimmten die räumliche Ausdehnung der oxischen Zonen im Sediment. Horizontale und vertikale Sauerstoffgradienten im Sediment lagen in der selben Größenordnung. Die Optodenmessungen zeigten außerdem, dass die Porenwasserströmung migrierenden Wellenrippeln folgte, wodurch Sediment alternierend oxischem und anoxischem Porenwasser ausgesetzt sein konnte, bis die Rippelgeschwindigkeit so hoch wurde (experimenteller Schwellenwert $\approx$ 20 cm h^{-1}), dass das Porenwasser nicht mehr folgen konnte. Somit erzeugten schnelle Rippeln eine durchgängige, sauerstoffreiche Oberflächenschicht im Sediment, die die Freisetzung reduzierter Substanzen aus dem Sediment verhinderte. Unter sich langsam bewegenden Rippeln war eine solche Freisetzung durch die vertikalen Zonen, in denen anoxisches Porenwasser an die Sedimentoberfläche drang, möglich. Rasche, welleninduzierte, dramatische Veränderungen der Sauerstoffkonzentration in den Oberflächenhorizonten permeabler Sedimente stellen eine Herausforderung für die im Sediment lebenden Organismen dar und haben Einfluss auf die Mineralisation organischen Materials.

Die in dieser Arbeit untersuchte welleninduzierte Filtration und der advektive Porenwasseraustausch sind ökologisch und biogeochemisch relevant, da sandige permeable Sedimente auf dem kontinentalen Schelf sehr häufig sind und große Gebiete des Schelfs (Wassertiefe < 100 m) permanent oder episodisch von Wellen beeinflusst sind. Der von Wellen beeinflusste kontinentale Schelf kann somit in zwei Zonen unterteilt werden: eine flache Zone (Wassertiefe < Wellenlänge/2), in der Orbitalbewegungen durch Wellen Rippeln am Seegrund entstehen lassen und an die Sedimenttopographie gebundene, permanente oder episodische advektive Filtration stattfindet, und eine tiefere Zone (Wellenlänge/2 < Wassertiefe < Wellenlänge), in der hydrostatisches Wellenpumpen den Austausch zwischen Sediment und Wasser verstärkt.

Große Gebiete des Schelfs können daher effektive Filterungssysteme für partikläres Material darstellen. Die hochdynamischen Sauerstoffkonzentrationen in den Sedimenten, mit mobilen horizontalen Sauerstoffkonzentrationsgradienten vergleichbar den vertikalen, machen deutlich, dass advektiver Transport nicht nur partikuäres Material durch das Sediment filtern kann, sondern möglicherweise die Mineralisation in sandigem

Meeresgrund durch ständigen Transport sauerstoffreichen Wassers in die partikelreichen Oberflächenhorizonte solcher Sedimente erhöhen kann. Demnach könnten Oberflächenwellen einen großen Einfluss auf die Konzentration suspendierter Partikel und die Stoffkreisläufe in Küsten- und Schelfgewässern haben.

1. Introduction

The focus of this study lies on interfacial exchange between permeable, sandy sediments and overlying water that is driven by shallow water waves. It will be shown that pore water flows in sandy sediments can be driven by wave-induced oscillating boundary flows interacting with sediment topography. The studied processes require shallow water depths, sandy sediments and hydrodynamic forcing by waves to occur. All those can be found in the continental shelf environment.

1.1. The Continental Shelf

The continental shelf is part of the ocean margins that, in the broad sense, comprise the area of the world oceans situated between the shoreline and the deep ocean. The ocean margins consist, in seaward direction, of the continental shelf, the shelf break and the continental slope and rise. The continental shelf with its characteristic gentle slope of typically 0.1° or less extends from the coast to its seaward limit, the shelf break, which separates it from the continental slope with an average slope of about 4°(Wollast 2002). The water depth of the shelf break is variable and depends on the characteristics of the respective shelf but it is typically situated at a water depth of approx. 130 m although it may also lie considerably deeper (200 m, in exceptional cases up to 350 m). The overall global length of the shelf break is about 320 000 km and with an average width of 85 km, the continental shelf comprises approximately 7.5 % of the world ocean surface (Wollast 2002). In spite of this small percentage, the shelf areas are very important for the global biogeochemical cycling of matter, as the continental shelves, together with the continental slope, represent the link between the terrestrial environment and the open ocean. Compared to average oceanic surface waters, the continental shelf seas commonly show an elevated primary productivity and contribute 18 to 33 % (lowest and highest estimates, respectively) to the global ocean primary production (Wollast 1991). Only a small fraction of the primarily produced organic carbon on the shelf is utilised by zooplankton, and most of it ends up as detrital organic carbon (Wollast 1991). Additionally, the continental shelf receives large inputs of terrestrial material through rivers. Most of the riverine sediment transported into the ocean is deposited on the shelf, the bulk of it being deposited on the fans and cones off large rivers. For example, of the fluvial load of the ten largest rivers, that contribute approximately one

third to the global riverine input into the ocean, only 25 to 30 % escape the shelf break and reach the ocean basins (Milliman 1991). Most (>95 %) of the organic carbon introduced onto the continental shelf by primary production and imported from the continents and oceans is mineralised in the water column and the sediments. Considerable amounts of organic carbon are buried only locally, where hydrological and sedimentological settings are favourable, like on the continental slopes, in canyons and deep-sea fans (de Haas et al. 2002) or deltaic systems. Still, the ocean margin areas are the most important areas of calcium carbonate and organic carbon accumulation and burial (Ver et al. 1999; Zabel and Hensen 2002).

Today, the coastal continental shelf seas receive increased attention to evaluate the effects of anthropogenic eutrophication through agriculture, river manipulation (leading e.g. to increased soil erosion and nutrient leaching), tourism and marine aquaculture. The response of the natural system to eutrophication may show in gradual trends, but may also lead to seemingly unpredictable oscillations. Presently, it seems hard to diagnose if the changes recorded in continental shelf systems are the result of excessive nutrient release, changing climatic cycles or an effect of a higher data density and quality (Smetacek et al. 1991).

1.1.1. Geological settings

The Quaternary (the last 1.8 Ma) is characterised by a number of continental glaciations and deglaciations that caused frequent dramatic eustatic fluctuations of the sea level. Compared to the average conditions in the Quaternary, the present sea level is at an exceptional high-stand. As the glacial periods lasted for much longer than the interglacials, the sea level has been lower than it is today for at least 90 % of the last million years. The last sea level high-stand comparable to the present conditions was reached during the last interglacial 120 – 130 ka bp (before present). During the last glaciation, the global sea level development was governed by a gradually undulating regression reaching a low stand of up to 125 ± 5 m below the present sea level (Fleming et al. 1998) during the last glacial maximum centered at 21 ka bp (Mix et al. 2001). The post-glacial sea level rise was characterised by an initial moderate transgression of approx. 6 m ka^{-1} from 21 to 17 ka bp, followed by a sea level rise of approx. 10 m ka^{-1} in the next 10 ka (Fleming et al. 1998). Thus the present sea level was nearly reached about 7 ka bp (Lambeck and Chappell 2001).

For the continental shelf areas, the present exceptional sea level high stand means that large areas of the shelf have been exposed to terrestrial conditions during most of the later Quaternary with terrestrial sediments being deposited. The terrestrial input of sediments to the ocean at low sea level bypassed the then exposed shelf and sediments were directly discharged into the ocean basins (McCave 2002). As the lengths of interglacial periods with sea level high-stands and marine conditions on the continental shelves were much shorter than the glacial periods with terrestrial conditions on the shelves, the sediments of the shelf were in disquilibrium with the hydrodynamic conditions. This is also the present situation; the few thousand years that the shelf has been a fully marine environment during the Holocene were not sufficient to reach a sedimentary equilibrium.

1.1.2. Sediments

Most of today's global sedimentation takes place on the continental margins. As much as 90 % of the sediment that is generated by erosion on land is deposited on the continental margins, mainly in the deltaic cones. Among the factors controlling the deposition on the continental shelf are climate and tectonics of the landmasses neighbouring the shelf sea, the type of the continental margin (convergent or passive), sea level fluctuations, and the hydrodynamics of the shelf sea itself (McCave 2002). The sediments of the continental shelves were classified into six main classes by Emery (1968): detrital (sediment presently supplied to the shelf), biogenic (e.g. shell debris, faecal pellets), residual (in-situ weathering of rock outcrops), authigenic (e.g. glauconite, phosphorite, etc.), volcanic and relict. The bulk of the sediments deposited on the continental shelf today are of detrital, i.e. terrestrial, origin, transported into the oceans by streams from the continents.

Relict sediments are sediments that were deposited in equilibrium with their environment in the geological past but the depositional environment changed and the time that elapsed was not ample to regain a new equilibrium by burial or erosion. Because of the aforementioned short time that has elapsed since the sea level reached its present stand, the sediment load transported onto the shelf so far was neither sufficient to bury these relict sediments completely nor was the hydrodynamic forcing large enough to fully rework these sediments. Therefore large areas of today's shelf areas are covered by coarse relict

sediments (Emery 1968). The percentage was estimated to be 68 % (Emery 1968), however, more recent studies have shown that the proportion of relict sediment is considerably smaller (<50 %) because large areas of the Arctic shelves are covered by recent sediments (Johnson and Baldwin 1986). Due to the decreased hydrodynamic forcing with increasing water depth, grain size of recent sediments decreases with increasing water depth across the shelf so that the presence of relict sediments is shown, e.g., by coarse sands with a narrow grain size spectrum lying seaward of finer, less sorted sands. The deposition of sandy sediments on the inner shelf and the presence of large relict sediment areas further offshore mean that large areas of the shelf are sandy.

Sandy sediments are permeable, which means that they allow pore water movement through their interstices. A wealth of studies has been conducted on the sediment properties of the continental shelves showing the occurrence of sands in the continental shelf environment in a large variety of sedimentological settings and water depths. Sands have been reported e.g. at water depths of 2.5 m (Agrawal and Aubrey 1992), 15 m (Traykovski et al. 1999), 20 – 45 m (Black and Oldman 1999), 39 m (Li and Amos 1998) and 56 m (Li and Amos 1999). A comprehensive overview of the sedimentological settings of different shelf seas is given by de Haas et al. (2002).

1.1.3. Sediment topography

Ripple marks are present as undulations on a non-cohesive surface, although they may also be found infrequently in muddy sediments as well. They are produced as a result of the interaction of oscillating or unidirectional currents and a sediment surface. Oscillating currents as induced by surface gravity waves form wave ripples, which are periodic undulations of the seabed with the crests sharper than the troughs and symmetry with respect to their crests and troughs (Blondeaux et al. 2000). Ayrton (1910) made general observations on the development and behaviour of ripples and the water motion above them. She showed that ripple formation in general is strongly related to the appearance of vortices in the flow. Bagnold (1946) studied the behaviour of wave ripples quantitatively and distinguished rolling-grain ripples from vortex ripples. Rolling grain ripples are initially formed on a smooth sandy sediment surface subjected to wave action when grains are moved as bedload. Vortex ripples form after rolling-grain ripples exceed a critical

height and a vortex forms in the lee of the crests, which is the typical case in nature. Wave ripple formation is qualitatively understood today and it is known that any perturbation of a flat bed under wave action tends to grow so steep that the flow separates behind it forming a strong vortex. This vortex can sweep sand from the lee-side trough to the crest and increase its steepness (Nielsen 1981). Depending on the characteristics of the free flow, the sediment and the perturbation, length and height of ripples grow until a certain stable geometry is reached. A number of models for the evolution, dynamics and geometry of wave-generated ripples were developed and are compiled in Sleath (1984). Four more recent models were compared by O'Donoghue and Clubb (2001). Wiberg and Harris (1994) distinguished orbital, anorbital and suborbital wave ripples. Most wave ripples on highly energetic shelves with long period-waves (T = 8 s and T = 12 s) are anorbital ripples with a ripple spacing that is dependent on the sediment grain size. Wiberg and Harris (1994) also predicted the effects of water depth, wave height, wave period and sediment grain size on ripple formation. They calculated that orbital ripples could form at a water depth of 100 m with a wave period of 12 s, 4 m wave height and a sediment grain size of 250 μm, conditions found on the continental shelf during storm events creating large surface waves. This was confirmed by a large number of field observations, e.g. in side-scan sonar surveys. In more detail, ripples of wavelengths ranging from 9 to >100 cm have been reported from different water depths from the continental shelf by e.g. Agrawal and Aubrey (1992); Black and Oldman (1999) or Cacchione et al. (1999). Therefore, sand ripples can be expected to be very abundant features of the sea floor on the continental shelf consisting of sandy sediments. They will be most abundant and best developed in those areas of the shelf where waves constantly (or frequently) agitate the bed. This area, defined as "inner shelf" by Wright (1995), typically extends to water depths of 30 m, although its limit may be deeper on very energetic shelves and lower on sheltered epicontinental shelves. The frequency of bed agitation through waves during storm events decreases with increasing water depth, therefore in deeper areas of the shelves, processes eradicating ripple topography like bioturbation will be more effective. Fig. 1 shows a side-scan sonar image of rippled sandy sediments from the Baltic Sea.

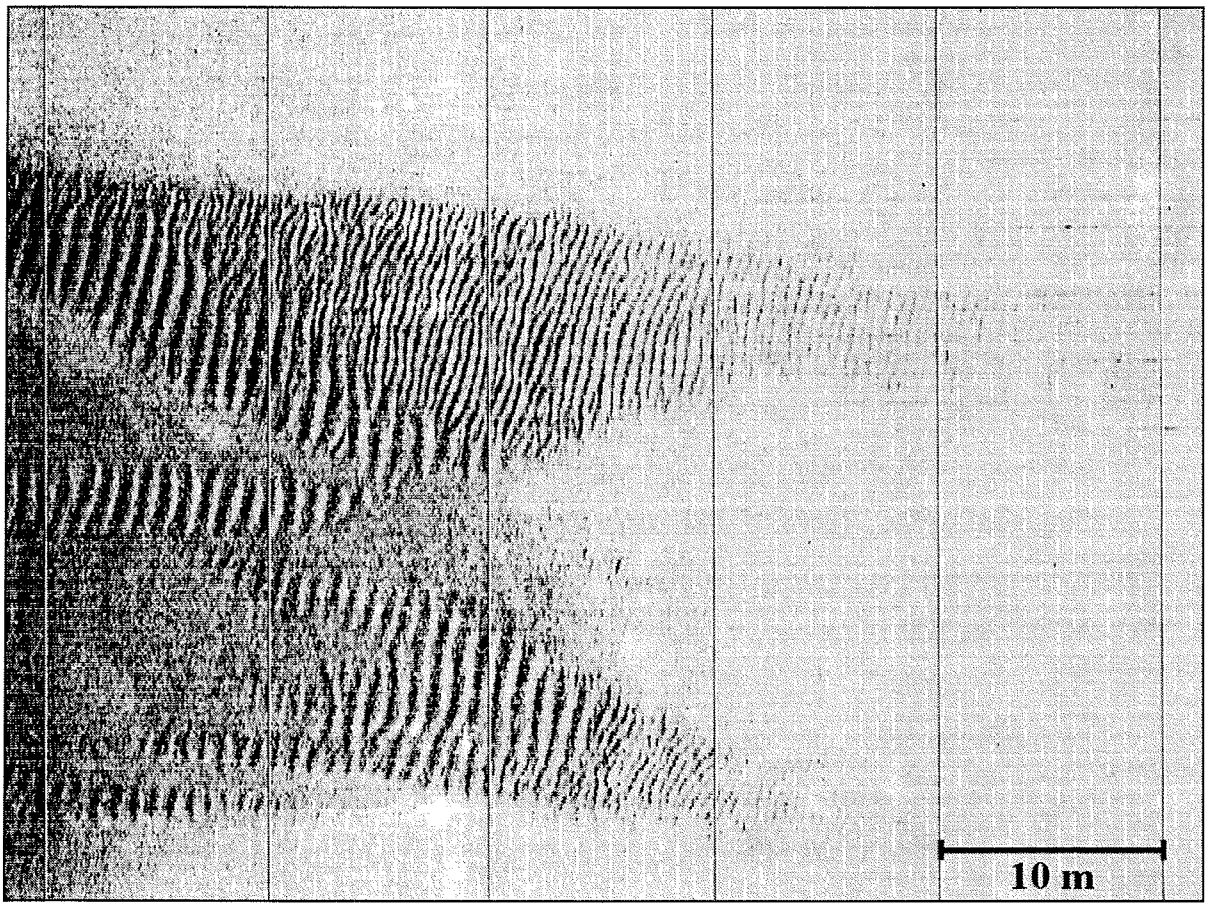

Fig. 1: Side-scan sonar image from the Baltic Sea (Tromper Wiek) at 10 m water depth. On the left, there is coarse sand showing large wave ripples of two different wavelengths (approx. 1 and 0.5 m). The bright grey areas on the right are fine sands partly covering the coarse sand. Here, smaller ripples can be expected, but their size is below the resolution of the sonar system. Image courtesy of Arbeitsgruppe Hydroakustik, Institut für Geowissenschaften der Univ. Kiel.

1.1.4. Hydrodynamics

The previously described sedimentary settings and sediment topography features of the continental shelf are results of hydrodynamic forcing. Wind stress at the air-sea interface imparts kinetic energy to the water in form of ocean currents and surface gravity waves. Both unidirectional and wave-induced currents control sediment transport and composition and seabed topography.

Surface gravity waves generated by wind on the surface of the ocean have periods of 3 to 25 s and it can be approximated that they induce oscillating currents at a solid boundary, i.e. the sea floor, when the water depth is smaller than half the wavelength (Fig. 2) (Denny

1988). Wave-induced peak bottom velocities at the sediment surface increase when the waves move into shallower water (Kawamata 1998).

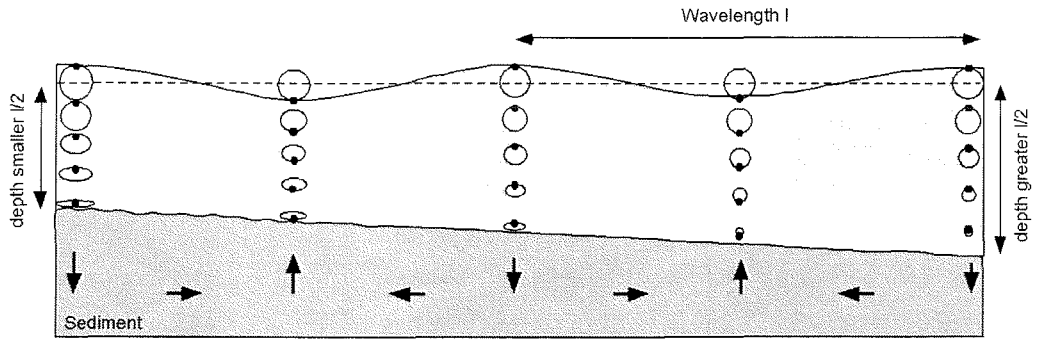

Fig. 2: Schematic drawing of shallow water waves inducing oscillating flow at the sea floor when the water depth is smaller than wavelength/2. The arrows in the sediment indicate the directions of pore water flow induced by hydrostatic pressure oscillations ("wave pumping", not to scale).

The extent of the shelf areas affected by waves was numerically assessed by Harris and Coleman (1998) with the result that wave climate in the North Atlantic was such that quartz sands of 100 μm diameter would be mobilised down to a depth of 234 m at least once over a 3-year period. These authors also stated that wave-induced flow exceeds the mobilisation threshold for such a sediment 10 to 50 % of the time in large areas of the Southern North Sea.

Apart from the ubiquitous surface gravity waves, wind forcing may also drive along-shelf and across-shelf (upwelling and downwelling) flows. Additionally, directed flows are caused by tidal currents or buoyancy effects (positive and negative). Some of the important transport phenomena on the inner continental shelf are summarised in Fig. 3 that also includes internal waves, infragravity oscillations and surf-zone processes.

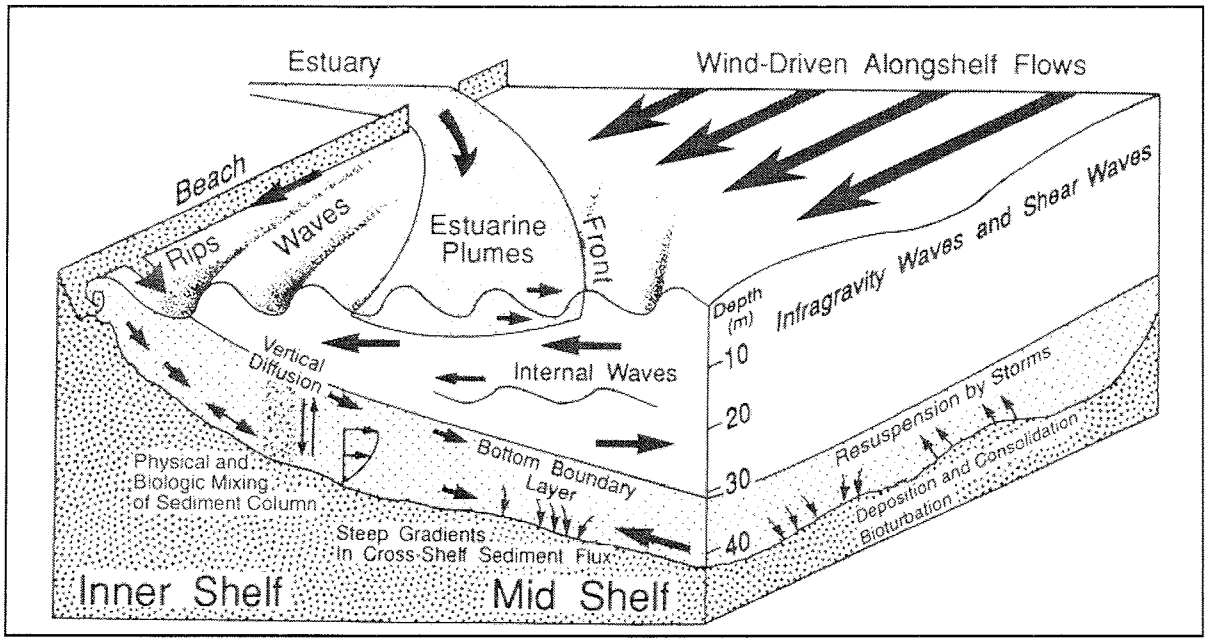

Fig. 3: Conceptual diagram illustrating physical transport processes on the inner shelf. (from Nittrouer and Wright, Reviews of Geophysics, Vol. 32, pp 90, 1994 © 1994 by the American Geophysical Union).

Most particulate transport occurs in the water column close to the sea bed, therefore the physical processes are effective where and when they influence the bottom boundary layer causing shear stresses sufficient to erode and transport particulate material. The bottom boundary layer in the continental shelf environment affected by waves is characterised by a thin (1 – 10 cm thick) oscillatory boundary layer nested within a much thicker boundary layer of tidal or wind-driven currents. The coupling of hydrodynamic forcing by currents and surface gravity waves strongly influences across-shelf transport, and during storms, their combined effects can transport suspended material tens of kilometres seaward (Nittrouer and Wright 1994).

Wind stress, bottom friction and buoyancy forces exert considerable influence on advection and mixing processes of the water masses along coastal margins that affect the flux of material. Their interplay results in the considerable complexities in circulation encountered along continental margins: e.g., a wind of 20 m s^{-1} can vertically homogenise a water column 100 m thick if there is no input of buoyancy (Blanton 1991).

1.2. Sediment – water exchange processes

In cohesive, fine-grained sediments, the major driving forces for solute transport are molecular diffusion, bioturbation, and bioirrigation (Berner 1980; Aller 1982). Molecular diffusion prevails in muddy sediments in which benthic macroorganisms are absent, such as anoxic basins and also is the main process that drives interfacial exchange in most deep see locations. The magnitude of biological transport relative to other transport mechanisms is primarily controlled by the abundance and activity of macrobenthic organisms.

Biogenic transport activity is usually most intense near the sediment-water interface where benthos are numerous. The search for food and the construction of burrows may efficiently mix the upper sediment layers and disrupt the original sedimentary fabric. This is particularly relevant for solid phase fluxes.

Filter-feeding benthic organisms may transport substantial amounts of water for nourishment and respiration through their bodies and burrows, thereby pumping bottom water to deeper sediment layers and vice versa. Filter-feeding thus may provide a rapid and efficient pathway for solutes and particulate matter into and out of the sediment and locally increases oxygen penetration depth (Riisgard and Larsen 2000; Aller 2001; Haese 2002).

Interfacial exchange both in cohesive and sandy sediments may also be driven by other processes like submarine groundwater discharge (e.g. Moore 1996; Corbett et al. 1999) or through gas seeps (O'Hara et al. 1995). Additionally, lateral compression, sediment compaction and dehydration of clay minerals at convergent continental margins may cause an upward pore water flow and discharge of fluids from the seafloor at vent and seep sites. A common feature of these transport processes related to different geological settings and driving forces is the fast transfer of dissolved gaseous constituents from the sediment into the bottom water (Schlüter 2002).

1.3. Pore water exchange in permeable sediments

In sandy sediments, permeability allows the flow of pore water through the interstices, with the flow rate being proportional to permeability and pressure gradient (Darcy 1856). A sediment permeability larger than 10^{-12} m^2 allows advective pore water flow driven by pressure gradients that is faster than diffusive transport (Huettel and Gust 1992), which may

lead to rapid sediment-water exchange of solutes and particulate matter. According to Bernoulli's law, total pressure remains constant along any streamline. Locally decelerated flow brings about an increase of hydrostatic pressure and flow acceleration induces a decrease of hydrostatic pressure. Thus, a boundary current flowing over a topographic feature of the seafloor generates a zone of increased pressure at the front slope and to a lesser extent behind the structure and a zone of reduced pressure leewards near the top of the obstruction (Fig. 4). Pressure gradients of less than 1 Pa cm^{-1} can cause significant pore water flow through the upper layers of sandy sediments (Huettel and Gust 1992). This advective transport can exceed the transport by molecular diffusion by several orders of magnitude (Huettel and Webster 2001).

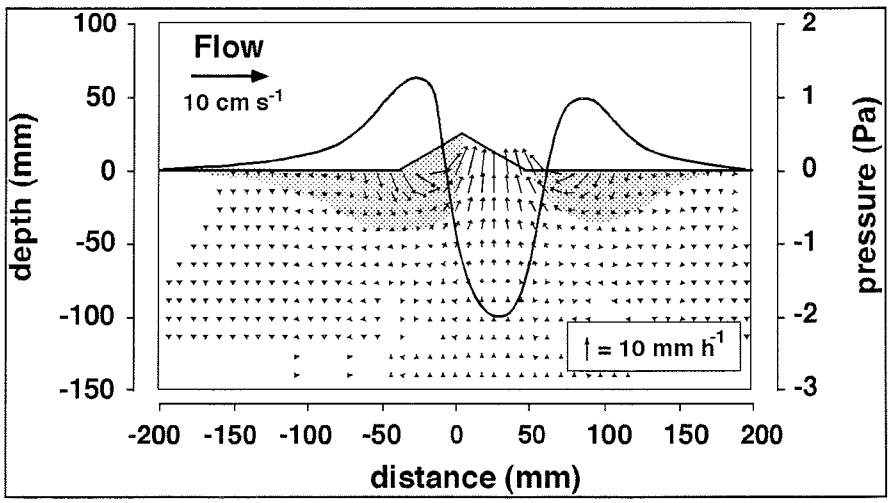

Fig. 4: Schematic drawing of the advective pore water flow field under sediment topography exposed to unidirectional flow in a straight open channel. The solid curved line depicts the pressure distribution at the sediment-water interface. Shaded areas mark the intrusion zones of water, and the arrows in the sediment show direction and magnitude of advective pore water flow (from Huettel and Rusch, Limnology and Oceanography, Vol. 45(3), pp 534, 2000, © 2000 by the American Society of Limnology and Oceanography, with permission.)

1.3.1. Exchange driven by density differences

Unstable density gradients in interstitial waters may lead to pore water motion and thus solute exchange (convection). Musgrave and Reeburgh (1982) presented in-situ observations for this phenomenon from a freshwater lake. During autumn cooling, a destabilising temperature gradient developed between cooled bottom water and warmer pore water, leading to convective pore water flow and thus heat flux across the sediment

water interface. The authors did not measure solute transport but concluded that, as solute diffusivities are typically up to 3 orders of magnitude lower than the thermal diffusivity, solutes are more susceptible to increased transport by convection than heat. This convective transport by temperature differences was also described by Rocha (1998) from intertidal sediments in an estuary. During lowtide, the exposed sediments experience warming, which leads to an inverse density gradient between pore and bottom water when the tidal flats are flooded. These authors found that up to 75 % of NH_4^+ that had accumulated in the sediment could convectively be flushed from the sediment during flooding. This work was extended by Rocha (2000) who found that this mechanism may affect sediment depths of at least 10 cm. When the right pre-conditions are met, this mechanism may transport oxygen and fresh metabolites into the sediment and release solutes from the sediment. The importance of this convective solute transport stems from the fact that it may occur on a daily basis and is three orders of magnitude faster than transport by molecular diffusion alone.

Convective transport may also occur through density differences due to salinity, which might be important in regions subject to significant temporal variations in salinity such as estuaries. Interfacial exchange by this effect will occur when dense bottom waters with a high salinity overlie sediment with pore water with lower salt content and therefore lower density, which leads to gravitational instability. This was studied by Webster et al. (1996) in a flume study, who found that convective transport can be much more important for solute transport than molecular diffusion. Additionally, these authors discussed that convective transport may open pathways across the sediment-water interface for substances only soluble under anoxic conditions such as iron, manganese or phosphate.

1.3.2. Beach percolation

Riedl and Machan (1972) conducted measurements of flow speed in the interstitial of the surf zone of sandy beaches, and distinguished three effects that could drive pore water flow through the beach face. Firstly, the tide may create changing ground water levels within the beach. The other two processes Riedl and Machan (1972) pointed out to be effective on the beach were the swash run-up of the waves ahead of the tide partly percolating the beach and so-called wave pumping due to hydrostatic pressure differences between wave crests and troughs.

The tidal effects on beach ground water flow were studied in detail by Nielsen (1990). During high tide, water percolates the beach leading to a time-averaged water table in the beach standing considerably above the mean sea level even though during low tide, the beach is drained. This process leads to substantial exchange between beach ground water and seawater. This could be verified and quantified by Webster et al. (1994) who measured pore water exchange through tidal filling and draining of intertidal sediments in an estuary by measuring radium isotopes.

The effects of waves running up the beach and partly percolating it received further attention by Longuet-Higgins (1983) in a wave tank study. It could be shown that water percolates the beach down to depths that are comparable to the distance covered by the wave set-up. This beach groundwater ideally flows on circular pathways through the beach back into the sea. Swash infiltration-exfiltration was quantified by Turner and Masselink (1998) by measuring vertical pore pressure gradients, showing that time-averaged flow velocity through the sediment was in the range of 360 cm h^{-1}. Li and Barry (2000) confirmed these results and found that while the averaged flow behaviour is characterised by continuous circulation due to wave set-up, there is also a periodic local ground water circulation due to progressive bores. Bores may be formed when waves propagate into shallower water and in lower parts of the beach, the run-up of bores may cause pore water pressure differences in the beach and therefore induce in- and exfiltration of pore water.

The results on overall water filtration through beaches through tidal and wave effects were quantified and compiled by McLachlan (1989) who found filtration rates of water in the range of tens of m^3 m^{-1} d^{-1} through beach faces, which agrees well with the findings of Riedl and Machan (1972). Other factors driving ground water flow through beaches are precipitation, ground water discharge and bioturbation. A comprehensive review of the physical processes driving interstitial flow in beaches and its effects on pore water chemistry and the interstitial ecology is given by McLachlan and Turner (1994).

In the lower parts of the beach and the near-shore zone, exchange between sediment and water may also be driven by release of pore water by resuspension and subsequent sedimentation and trapping of "fresh" pore water. Sediment resuspension in the surf zone is mainly driven by vortices induced by bores and breaking waves (Voulgaris and Collins 2000). The average sand mixing depth due to resuspension can be correlated with the

significant wave height at breaking (Ciavola et al. 1997) and is also the horizon from which pore water is regularly released by reworking.

1.3.3. Effects of unidirectional boundary flow

Unidirectional near-bottom current flowing over morphological features of biogenic or physical origin of permeable sediment leads to advective porewater flows and thus sediment-water-interfacial fluxes.

Thibodeaux and Boyle (1987) conducted a flume study and found that unidirectional currents flowing over sediment ripples induced significant interstitial flows that could enhance the mobility of chemicals and thermal energy in porous sediment beds down to depths 5 times the ripple height. This work was extended by Savant et al. (1987) who employed sandy (mean diameter = 0.37 mm) instead of pebbly (mean diameter = 8 mm) sediment and found pore water velocities of up to 26 cm h^{-1}.

Numerical models to quantify the pressure perturbation developing around a stationary bedform and the resulting flux of solutes into and out of the sediment bed under unidirectional flow were developed by Elliott (1990). The trapping and release of pore water by and from the sediment gains in importance compared to advective interfacial solute exchange if the bedforms are non-stationary and migrate faster than the pore water velocity. Elliott's (1990) work on advective solute exchange for a streambed with stationary and non-stationary bedforms and nonsorbing solutes was extended by Elliott and Brooks (1997a; 1997b). The impact of these exchange processes on the transport of oxygen into and out of stream beds was addressed by Rutherford et al. (1993; 1995), who inferred that up to 60 % of the deoxygenation rate of the river studied could be explained by oxygen uptake in the upper sediment layers. In natural streams, not only non-sorbing solutes may be transferred across the sediment-water interface. Therefore, Eylers et al. (1995) studied the transport of adsorbing metals into and out of a streambed and found that the penetration depth of possible pollutants approximates the bed form's wavelength. Packman and Brooks (1995) studied the same phenomenon for fine clay particles that may scavenge and carry pollutants and found that advection may transport these particles that are too fine to settle in the free flow into the sediment.

Huettel and Gust (1992) addressed advective transport under directed flows in the marine environment by demonstrating the effects of bioroughness on the interfacial solute exchange in permeable sediments. Bioroughness comprises biogenic sediment microtopography structures like e.g. burrows, mounds, half shells or benthic organisms resting on the sediment surface. It could be shown that under unidirectional flow, filtering rates in the order of 10 L m^2 d^{-1} occurred. A similar study was conducted by Hutchinson and Webster (1998), who studied the exchange of nonsorbing solutes between sediment and water by the interaction of pebbles half-buried in the sediment and boundary flow, that resulted in a filtering rate of 68 L m^2 d^{-1} for a natural coastal environment. More abundant features in sandy sediments are ripples. Their impact on advective transport of particles and solutes was studied by Huettel et al. (1996), who found that the pressure field developing around a ripple interacting with a flow ($u < 10$ cm s^{-1}) leads to transport of suspended particles into the upper 4 cm of a permeable sediment. Additionally, pore water from deeper sediment layers was dragged to the sediment surface at the downstream slope (Fig. 4).

These advective filtering of water through the sediment and the complex pore water flow pattern should also affect the sediment chemistry. Ziebis et al. (1996) measured that the oxygen penetration depth at the upstream foot of a *Callianassa* mud shrimp mound of 1 cm height increased 10-fold under a unidirectional flow. Moreover, oxygen-rich water penetrated the sediment at the downstream end of the mound whereas oxygen-depleted pore water from deeper sediment layers reached the sediment surface at the downstream end of the mound crest. Forster et al. (1996) demonstrated that advection could enhance the total oxygen utilisation of a sandy sediment. Whereas the filtering of oxic water through the sediment oxygenates significant volumes of sediment, the upwelling of anoxic pore water to the sediment surface leads to anoxic sediment volumes and horizontal oxygen concentration gradients. The biogeochemical reaction zones in permeable sediments were investigated by Huettel et al. (1998). These authors could show that in the oxic sediment volumes, nitrification and ferric iron precipitation occurred, whereas anoxic pore water could reach the sediment surface in the upwelling zones, thereby creating pathways for NH_4^+, Fe^{2+} and Mn^{2+} to the sediment surface.

Advective interfacial water exchange locally transfers suspended particles or phytoplankton from the boundary layer into the top centimetres of permeable sediments as shown by Huettel and Rusch (2000) and (Rusch 2000) in flume and field experiments.

1.3.4. Wave-driven interfacial exchange

Interchange processes between sediment and water can also be enhanced by surface gravity waves. Given a certain sediment permeability, the waves may drive interstitial flows that diverge under the wave crests and converge under the wave troughs. The diverging flow under the crests requires fluids to enter the sediment to maintain continuity and to leave the sediment under the troughs (Fig. 2), (Huettel and Webster 2001). This process was directly measured by Riedl et al. (1972) who introduced the term "subtidal pump". Based on the results, these authors presented a model to quantify the volume of water thus filtered through the sediment, with the conclusion that hydrostatic wave pumping could filter the complete ocean volume through the shelf sediments in only 14 ka. Rutgers van der Loeff (1981) described the same process as increased diffusivity in the upper 1-1.5 cm of sandy sediment under low to moderate wave action in a field study. However, merely periodic porewater motion is not a sufficient explanation for net transport of solutes across the sediment-water interface. Therefore the theory of wave pumping was extended by Harrison et al. (1983) with the concept of mechanical dispersion to explain net transport of solutes by periodic pore water motion. Mechanical dispersion requires that the direction of the pressure gradient rotates with time and is a function of the magnitude of the interstitial velocity and the sediment grain diameter. Harrison et al. (1983) concluded that dispersion behaves as a diffusive process that is many times more effective than molecular diffusion. The process is most effective with large sediment permeability, high wave amplitude and shallow water. A necessary condition for mechanical dispersion to be effective is that the scale of the vertical and horizontal porewater motions greatly exceeds the grain size of the sediment. Webster and Taylor (1992) numerically and experimentally studied the dispersal of clouds of particles through a highly idealised porous medium. They concluded that dispersion is able to enhance the solute transfer between the bed and overlying water and introduced the term rotational dispersion, since a key factor of their theory is that horizontal

and vertical pore water motions are out of phase with one another. Wave tank experiments showed good accordance with the numerical approach.

Malan and McLachlan (1991) carried out field measurements using benthic chambers with flexible membrane tops to allow for wave-induced interstitial water flow which showed that oxygen consumption and solute fluxes are positively correlated with wave action.

Surface gravity waves drive an oscillating flow at the sediment surface when the water depth is lower than half the wave's wavelength. Advective transport through the interaction of wave-induced oscillating boundary flow with sediment topography has received less attention than advective transport induced by unidirectional flows, although the effects of oscillating boundary layer flow driven by gravity waves on the sediment-water-interfacial fluxes of solutes in nature was already described by Webb and Theodor (1968). They injected dyed water into ripple troughs and crests of coarse sandy nearshore sediment at 3 m water depth and observed its reappearance at the ripple crests. This study was continued by Webb and Theodor (1972), who found that flow rate through the sediment depended on the height of the surface gravity waves and the permeability of the sediment. The accelerated flow above the ripple crests causes a lower dynamic pressure than in the ripple troughs thereby creating a pressure difference, which makes the existence of circulation cells in the sediment plausible. Shum (1992) presented a two-dimensional computational model calculating the trajectories of pore water particles under a rippled bed over one wave period with the result that the zone of advection extends to a few ripple heights below the ripple surface over a wide range of wave conditions and sediment characteristics. Additionally, the total exchange across the water-sediment interface, averaged over one wave period, is significantly higher across a rippled interface than across a flat bed. Based on these results and a similar model, Shum (1993) assessed the oxygen distribution in the porewater underneath a rippled surface under progressing waves: the oxygen concentration below a ripple trough could be many times higher than at the same depth below a crest and the concentration gradients in the horizontal could be in the same order of magnitude as those in the vertical.

Another wave-induced advective exchange process is the flushing of relict biostructures like empty worm burrows by waves (Webster 1992; Libelo et al. 1994).

1.3.5. Importance of advective transport in natural environments

Although Webb and Theodor (1968) described advective exchange driven by the interaction of oscillating boundary flow and sediment topography, the importance of advective exchange for the biogeochemical cycling of matter in the shelf environment was recognised only later. Previous studies on advective pore transport processes were reviewed and discussed by Shum and Sundby (1996) with respect to their role of organic matter processing in continental shelf sediments. These authors concluded that the classical one-dimensional approach developed for describing the distribution of pore water constituents and for measuring the related fluxes across the sediment-water interface could be inadequate for permeable shelf beds that permit pore water flows. These conclusions could be verified by and correspond with the findings of a number of field studies. Oldham and Lavery (1999) measured increased ammonium contents in the bottom waters of a shallow fetch-limited estuary correlated with increased hydrodynamic forcing. The increased nutrient fluxes were attributed to advective pore water release from the sediment.

Falter and Sansone (2000) could link the geochemical behaviour of reef flat permeable carbonate sand to hydrodynamic forcing by waves. Their results indicate that wave-driven advective exchange may transport oxygen down to sediment depths of 50 cm. With reduced hydrodynamic forcing, the deeper sediment strata became less oxic and accumulation of nitrate, nitrite and ammonium could be observed.

After whole core incubations of sandy sediments from the South Atlantic Bight continental shelf, Marinelli et al. (1998) inferred from pore water nutrient profiles that advective transport is likely to be an important process in promoting nutrient exchange in these sands. These results correspond with those of Jahnke et al. (2000) who measured in-situ nutrient, oxygen and inorganic carbon pore water profiles in benthic chambers on the Southeastern US shelf at water depths ranging from 14 to 40 m. These authors concluded that advective, non-diffusive transport contributes significantly to the overall benthic exchange. Advective transport has also been reported from a highly permeable sandflat, where it rapidly exchanged pore water with the overlying water down to 25 cm sediment depth on a time scale of hours (D'Andrea et al. 2002). Thus, these sandflats captured reactive organic particles and rapidly recycled nutrients.

All these findings indicate that sandy coastal and shelf sediments may play a more important role in the global cycling of organic carbon than was previously believed based on the low POC (particulate organic carbon) contents of these sandy beds. The decomposition and accumulation of particulate organic matter in the different sedimentary environments of the continental shelf were summarised by Huettel and Rusch (2000), (Fig. 5).

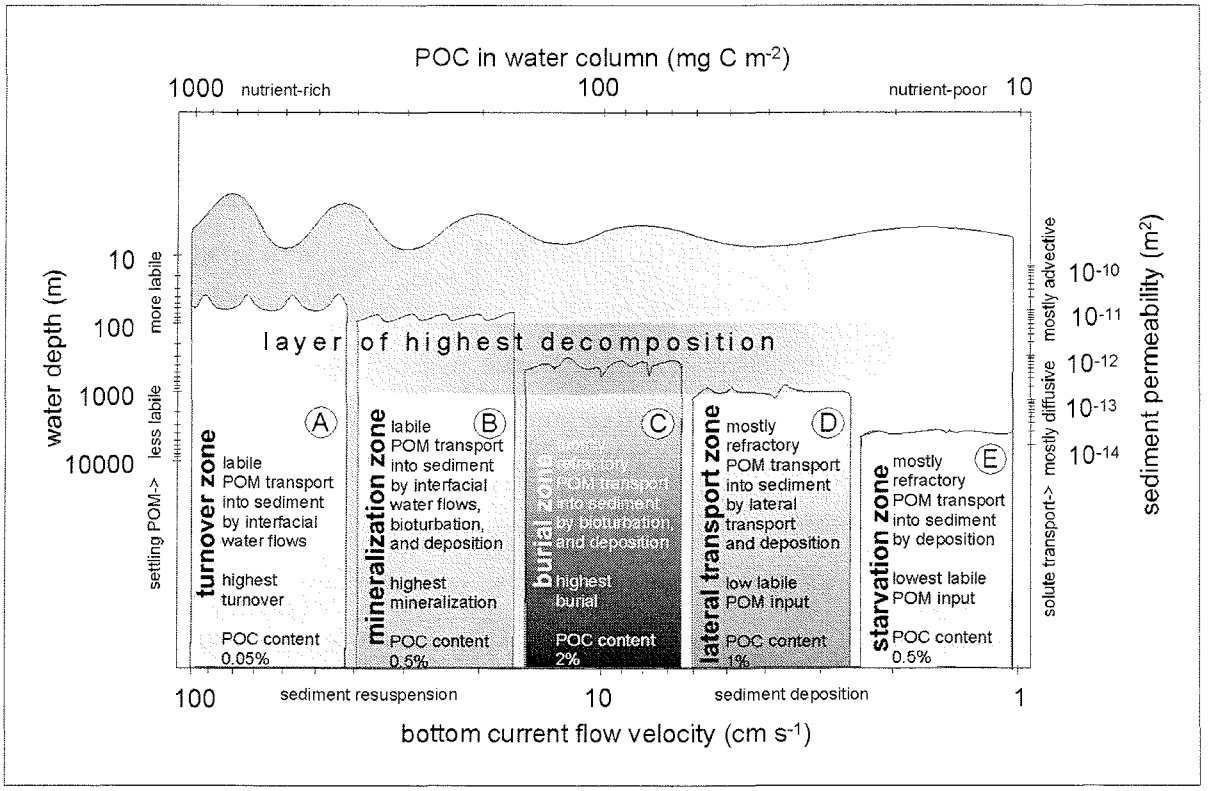

Fig. 5: A simplified scheme of the layer of accumulation and highest decomposition of sedimenting particulate organic matter demonstrating the increasing importance of sedimentary mineralisation in the shelf. The layer of highest decomposition gradually moves into the sediment with decreasing water depth.

(A) In the shallow shelf, wave and strong bottom currents cause frequent resuspension, keeping the sediment highly permeable but also suppressing bioturbation due to mechanical stress. Labile POM mixed down from the highly productive photic zone is transported deep into the sands by strong advective pore water flows. Burial of organic matter is nil due to rapid turnover promoted by the interfacial flows of oxygen-saturated water.

(B) Total sedimentary mineralisation peaks between the shallow non-accumulating shelf with highest turnover rates and the shelf slope with the highest burial rates. In this zone, sporadic resuspension keeps the sediment sufficiently permeable to permit limited advective transport, but the bottom currents are weaker and allow occasional settling of organic particles and an abundant macrofauna to grow. Hydrodynamical and

biological filtering and mixing mechanisms combine, which results in maximum uptake and decomposition rates of labile POM in the sediment

(C) The upper shelf slope receives mainly refractory organic material, and the slow bottom currents permit deposition of fine particles causing low sediment permeability. Ensuing lack of advective oxidation and reduced bioturbation promote anaerobic decomposition and highest burial rates.

(D) Below the upper shelf slope, POM input and the relative importance of the sediment for mineralisation gradually decreases. Downslope POM transport gains importance.

(E) Bacterial growth on sinking particulate organic matter peaks at 500-m water depth, Only 2-4% of surface water primary production reaches the sea floor at 4,500-m depth in the North Atlantic minimising the contribution of the sediment for its mineralisation.

Vertical extent of waves, sediment topography and layer of highest decomposition not to scale.

(from Huettel and Rusch, Limnology and Oceanography, Vol. 45(3), pp 534, 2000, © 2000 by the American Society of Limnology and Oceanography, with permission.)

1.4. Outline of the thesis

The main part of this work comprises four manuscripts, presented here as chapters. As these manuscripts will be peer reviewed, their final, published form might slightly differ from the chapters presented here.

Chapter 2:

Advective pore water exchange driven by surface gravity waves and its ecological implications

(accepted for publication in Limnology and Oceanography)

Advective pore water exchange from a permeable sediment driven by the interaction of sediment topography and oscillating boundary flow created by surface gravity waves, was assessed and quantified in wave tank experiments. Fluid exchange between sandy sediment and overlying water can increase 50-fold relative to the exchange by molecular diffusion. The ecological consequences for the wave-influenced continental shelf are discussed.

Chapter 3:

Rapid wave-driven advective pore water exchange in a permeable coastal sediment

(submitted to Journal of Sea Research 07.01.2003)

In order to demonstrate the applicability of the laboratory experiments presented in Chapter 2, in-situ measurements of pore water flow velocities in coastal sandy sediment were conducted in the Mediterranean Sea. A novel optode array technique was introduced that permitted direct pore water flow measurements using a fluorescent tracer. Advective transport exceeded transport by molecular diffusion by at least 3 orders of magnitude. The results showed that surface waves caused substantial water filtration through permeable sediments at water depths smaller than half the wavelength.

Chapter 4:

Oxygen dynamics in permeable sediments with wave-driven pore water exchange

(in preparation for submission to Limnology and Oceanography)

The results of a wave tank study on the effects of wave-driven advective transport on the in-sediment oxygen dynamics and its biogeochemical implications are presented. The key tool of this study was a planar optode that allowed direct 2-dimensional measurements of the oxygen distribution in the pore and overlying water. It could be shown that the advective exchange described in the previous chapters leads to a highly dynamic oxygen distribution in the sediments that had effects on pore water and sediment chemistry.

Chapter 5:

Hydrodynamical impact on biogeochemical processes in aquatic sediments

(accepted for publication in Hydrobiologia)

This chapter summarises the processes that control pathways and magnitude of material exchange in the surface layer of aquatic sediments. The effect of the various transport processes, especially advection, on the sediment biogeochemistry are summarised and discussed.

2. Advective pore water exchange driven by surface gravity waves and its ecological implications

(Limnology and Oceanography, 48(4), 2003, 1674-1684)

Elimar Precht and Markus Huettel

Max Planck Institute for marine Microbiology, Celsiusstrasse 1, D-28359 Bremen

Abstract

The effects of surface gravity waves on pore water release from permeable sediment (k = $1.3 - 1.8 \times 10^{-11}$ m^2) in shallow water were studied in a wave tank. Our tracer experiments demonstrate that shallow water waves can increase fluid exchange between sandy sediment and overlying water 50-fold relative to the exchange by molecular diffusion. The main driving force for this increased exchange are the pressure gradients generated by the interaction of oscillating boundary flows and sediment wave ripples. These gradients produce a pore water flow field with a regular pattern of intrusion and release zones that migrates with ripple propagation. The ensuing topography-related filtering rates in the wave tank ranged from 60 L m^{-2} d^{-1} to 590 L m^{-2} d^{-1} and exceeded the solute exchange rates caused by hydrostatic wave pumping (38 L m^{-2} d^{-1}) and initial molecular diffusion (corresponding to 10 to 12 L m^{-2} d^{-1}). Wave-induced filtration is ecologically relevant because permeable sandy sediments are very abundant on the continental margins and can be converted into effective filter systems suggesting that these sediments are sites for rapid mineralisation and recycling. We propose that the wave influenced continental shelf may be subdivided into two zones: a shallow zone (water depth < wavelength/2), where wave orbital motion at the sea floor creates ripples and causes topography related advective filtering and a deeper zone (wavelength/2 < water depth < wavelength), where wave pumping enhances interfacial exchange by hydrostatic pressure oscillations.

Acknowledgements

We thank Susanne Menger and Martina Alisch for assistance with the experiments, sampling and analyses, and Volker Meyer and Georg Herz for their help with the electronics and the flume set-up. We much appreciate the careful reviews of Jack Middelburg and one anonymous reviewer. We thank Bo Barker Jørgensen for support and interest in this work. The study was funded by the Max Planck Society (MPG).

Introduction

Physical and biological transport link the biogeochemical processes in water column and sediment. While molecular diffusion and locally also bioturbation are the major transport mechanisms in the cohesive, fine-grained deep-sea deposits, (Berner 1980; Aller 1982; Aller 2001), solute transport caused by pore water flows increases in importance in permeable sandy shelf sediments. Here, boundary layer flows interacting with sea bed topography induce pressure differences at the sediment-water interface, which lead to pore water motion in permeable sediments. Ensuing advective transport can exceed transport by molecular diffusion by several orders of magnitude (Huettel and Webster 2001).

In areas where water depth (d) is smaller than half the wavelength (λ) of the surface gravity waves, oscillating flows are generated at the sediment-water interface by the wave orbital water motion (e.g. Denny 1988, p.54). Webb and Theodor (1968, 1972) showed that such oscillating boundary flows could drive sediment-water-interfacial fluxes by injecting dyed water into coarse sandy near-shore sediment and observing its reappearance at the sediment surface. The trajectories of pore water particles under a rippled bed over one wave period were calculated by Shum (1992). His results suggest that the zone of advection extends several ripple heights below the sediment surface over a wide range of wave conditions and sediment characteristics. Indications that surface gravity waves may be relevant for the cycling of matter in shallow environments were reported by Oldham and Lavery (1999), who measured increased release of nutrient-rich pore water from estuarine sediment and attributed this enhancement to the effect of waves.

For pore water exchange driven by wave-related hydrostatic pressure oscillations, Riedl et al. (1972) introduced the term "subtidal pump". Based on field observations, these authors presented model calculations suggesting that the subtidal pump could filter the complete ocean volume in only 14 000 years. Rutgers van der Loeff (1981) described the same process as increased diffusivity in the upper 1-1.5 cm of intertidal sandy sediment under low to moderate wave action. In order to include the wave pumping in their in-situ flux measurements, Malan and McLachlan (1991) deployed benthic chambers with flexible membrane tops that revealed that oxygen consumption and solute fluxes are positively correlated with wave action. However, it is not obvious how circular motion of pore water within the sediment can cause net solute transport since the displacement through the wave

cycle guides the fluid back to its origin. To explain net transport, Harrison et al. (1983) included mechanical dispersion in the subtidal pump theory. In contrast to shear dispersion, the rotational dispersion caused by waves does not rely on molecular diffusion to be effective but requires that the direction of the pressure gradient rotates with time (Webster et al. 1996). The results of rotational dispersion are similar to those of diffusive processes, however, it can be many times more effective than molecular diffusion or shear dispersion as a transport mechanism.

These transport studies suggest that waves, by enhancing fluid exchange between sediment and overlying water, also affect the biogeochemical processes in permeable beds. Modelled oxygen distributions underneath a rippled surface exposed to progressing waves suggest that in permeable beds concentration gradients in the horizontal can be in the same order of magnitude as those in the vertical (Shum 1993). These findings demonstrate that the classical one-dimensional approach frequently used to describe the distribution of pore water constituents and for assessing the related fluxes across the sediment-water interface is inadequate for sandy permeable sea beds (Shum and Sundby 1996).

The potential relevance of wave-induced advective pore water exchange for metabolic processes in permeable shelf sands may be inferred from results obtained in flume studies addressing advective pore water exchange driven by unidirectional flows. These studies showed that advective interfacial fluid transport provides a rapid pathway for suspended organic particles and phytoplankton cells into permeable sediments (Huettel et al. 1996; Huettel and Rusch 2000). Simultaneously, oxygen can be transported advectively deep into the bed (Shum 1993; Ziebis et al. 1996), which enhances the mineralisation of this material (Forster et al. 1996). The advectively induced pore water flow field in the sediment generates a complex biogeochemical zonation with areas of enhanced nitrification or iron precipitation and vertical channels through which ammonium and reduced metals are transported to the sediment surface (Huettel et al. 1998).

The aim of the present study was to characterise and quantify the effects of surface gravity waves on fluid exchange between a sandy bed and the overlying water column, and to investigate the mechanisms leading to wave-induced interfacial exchanges. To achieve this, a set of laboratory wave tank experiments was conducted with sandy sediment stained with the conservative soluble tracer Rhodamine WT. The use of Rhodamine WT allowed

synchronous quantification of the interfacial flux and visualisation of the evolving pore water flow pattern.

Methods

Wave tank setup

Four experiments (referred to as Exp 1 through Exp 4) were carried out in a laboratory wave tank. The wave tank was of clear acrylic and had an open channel section of 520 cm length with rectangular cross-section (50 cm high, 47 cm wide). Two acrylic boxes ("upstream" box: 240 cm long, "downstream" box: 120 cm long, both 19 cm high and spanning the width of the channel) were placed into the open channel section, such that the opening between the two boxes enclosed a section of 120 cm length that could be filled with sediment (Fig. 1). Waves were generated at the upstream end of the wave tank with a paddle driven by an electric motor. The wave amplitude was controlled by the stroke of the eccentric, and the wave frequency could be adjusted via the motor speed. This set-up permitted the reproducible generation of sinusoidal waves of selected amplitude and frequency. At the downstream end of the wave tank, the dissipation of the waves was achieved by an artificial beach made of an acrylic wedge of 1 m length causing the waves to run up and break. In Exp 3 and 4, this wedge was additionally covered by a 10 cm thick mat of highly permeable plastic foam to maximise dissipation of the wave energy. The open channel section was sealed from the other parts of the wave tank and from the two inset acrylic boxes to prevent loss of tracer into those sections.

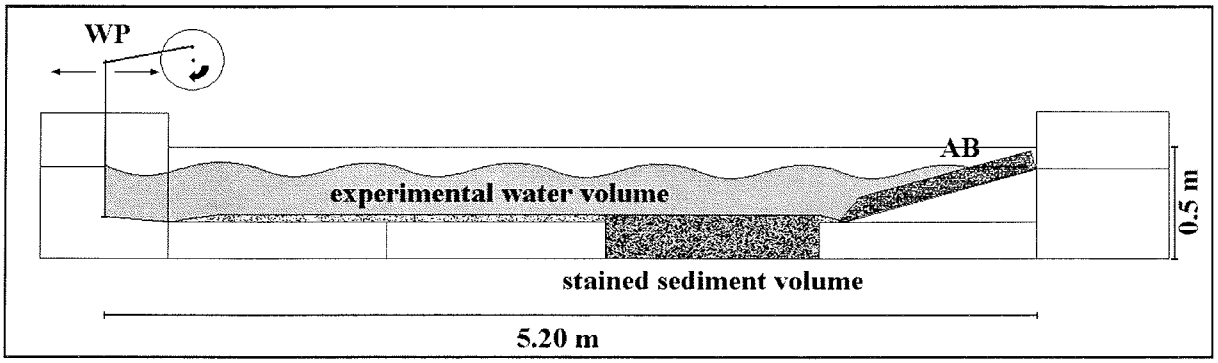

Fig. 1. The laboratory wave tank (dark grey: experimental water volume; WP: wave paddle; AB: artificial beach).

All experiments were conducted with propagating waves. Amplitudes, wavelengths and frequencies are listed in Table 1. Hydrodynamic conditions in Exp 3 and 4 were identical.

Table 1: Summary of experimental parameters. Permeabilities, porosities and tracer concentrations are initial values. Variability in initial permeability and porosity values are due to different degrees of compaction of the sediment.

Experiment	Exp 1	Exp 2	Exp 3	Exp 4	Diff 1	Diff 2
Start	14 Sep 1999	16 Sep 1999	11 Jul 2000	14 Nov 2000	22 Jun 1999	11 Jul 2000
End	15 Sep 1999	17 Sep 1999	12 Jul 2000	15 Nov 2000	24 Jun 1999	12 Jul 2000
Duration (h)	14.75	19.4	24	24	72	24
Sediment	quartz sand, 100-300 µm					
Permeability (m^2)	1.32E-11	1.32E-11	1.79E-11	1.82E-11	2.02E-11	1.75E-11
Porosity (Vol%)	36.6	36.9	37.3	38.1	38.25	37.7
Sediment depth (cm)	22	21.5	22	22	22	20.5
Water	Fresh, 19° C					
Tracer	Rhodamine WT		Brilliant Blue		Rhodamine WT	
Tracer conc. (µM)	40	39	21	5	47	19
Water depth (cm)	15	20	17	17	17	17
Wave	propagating			none		
Amplitude (cm)	8	9	6	6	--	--
Length (cm)	60	80	60	60	--	--
Frequency (Hz)	1.56	1.2	1.3	1.3	--	--

Sediment preparation and sampling

The experimental sediment was cleaned and sieved quartz sand originating from the Weser river estuary (Northern Germany) with a grain size distribution ranging from 100 µm to 300 µm. The dry sand was mixed with Rhodamine WT tracer solution giving it a pink appearance. The initial tracer concentrations for the respective experiments are listed in Table 1. The saturated pink sediment was inserted into the trough enclosed by the two acrylic boxes to produce a sediment layer of 25 cm (Exp 1) or 22 cm (Exp 2, 3, 4) depth with 141 dm^3 and 124 dm^3 volume, respectively. The two boxes in the open channel section were covered with 6 cm (Exp 1) or 3 cm (Exp 2, 3, 4) of unstained sand of identical grain size. The sediment was compacted by applying low frequency vibration, and the surface was carefully smoothed before each experiment to create an overall even surface with

uniform roughness in the open channel section. Ripple evolution occurred as response of the bed to the applied wave-action.

The use of Rhodamine WT as tracer to stain the sediments had two functions: Firstly, sequential water sampling during the experiments and subsequent analysis of the tracer content of the samples allowed the assessment of the flux of pore water from the sediment over time. Secondly, the red colour of Rhodamine WT allowed direct observation of the evolving pore water flow patterns in the sediment.

Directly before and after each wave tank experiment, sediment subcores of 2.6 cm diameter and 10 cm length were taken from the experimental sediment volume for porosity, permeability and tracer distribution analyses. Additionally, several surface sediment samples (1 cm in diameter, 2.5 cm long) were taken after Exp 3 and 4 using cut-off syringes. After carefully replacing the retrieved sediment volumes with equally stained sediment, the wave tank was filled with approximately 1750 L of fresh water. The water level in the channel was raised very slowly to minimise tracer release from the sediment. The water volume in the channel that could exchange with the sediment pore water amounted to 360 L in Exp 1 and 2 and 410 L in Exp 3 and 4. Table 1 gives an overview of the experimental parameters.

Diffusion experiments

Two sets of diffusion experiments (referred to as Diff 1 and Diff 2) were set up in three acrylic cylindrical chambers (19 cm inner diameter, 40 cm high) with stained sediment in order to assess diffusive release of tracer from the sediment. The experimental parameters are presented in Table 1. After compaction, sediment subcores were taken from each chamber and prepared for analysis of tracer content, permeability and porosity as described for the subcores from the wave tank. After the extracted sediment volumes had been replaced by stained sediment, the sediment surfaces were covered with a plastic foil and 4.25 L of fresh water were added to each chamber without mixing with the stained pore water. Then the plastic foils were removed, and the chambers were kept under stagnant conditions for the complete duration of the experiments. At regular time intervals, the water column of each chamber was gently mixed by 5 horizontal strokes with a spatula to homogenise tracer distribution, and water samples (3×2 cm^3) were taken and stored for

later analysis of their Rhodamine WT content. After the experiments, the chambers were carefully drained and a second set of sediment subcores was taken for analyses of tracer gradient over depth, permeability and porosity.

Analyses

The sediment subcores taken from the laboratory wave tank and the diffusion chambers were sectioned into 1 cm thick horizontal slices for pore water and porosity analysis. The porosity of the sediment samples of the respective cores was calculated from the wet and dry (after 48 h drying at 60°C) weights of the sediment slices.

Pore water extraction was achieved by centrifugation at 2900 **g** for 10 min at 10°C. The extracted pore water was analysed for its Rhodamine content by spectrophotometry (absorption at 556 nm) or fluorescence-spectrophotometry (excitation at 570 nm; emission at 556 nm). The absolute tracer concentrations of the analysed samples were calculated from the extinction coefficient for Rhodamine WT.

The sediment subcores used to assess the permeability were sealed after sampling and stored at 4°C until the measurements were carried out, usually within a few days. Permeability was assessed using a constant head permeameter (Klute and Dirksen 1986), and values for the dynamic viscosity η calculated after Krögel (1997).

During all experiments, water samples were collected at pre-set time intervals, with shortest intervals during the initial phase of the experiments. After starting the wave experiments, a tracer cloud developed over the stained sediment, which then dispersed over the entire volume of the open channel section. Our flux calculations therefore are based on the integrated dye content of the entire channel. Samples (3 $\times$ 5 ml) were taken at 6 representative positions from the experimental water volume and also from the sealed-off sections of the wave tank in order to assess tracer loss due to possible leakages into the sealed sections. The water samples were stored at 10°C and subsequently analysed for their tracer content to determine the flux of tracer between sediment and water.

Hydrodynamics were measured using a three-beam DANTEC™ LDA (Laser Doppler Anemometer) system in the backscatter mode during all experiments except Exp 4. This LDA technique allows three-dimensional measurements of the flow velocity in a spheroidal measuring volume as small as 70 µm in diameter. During Exp 3, two vertical

profiles (100 mm to 2 mm above the sediment) of the horizontal (u) and vertical (v) velocities were measured 150 min after start of the experiment above an unrippled section of the experimental sediment surface. In the water layer closer than 6 mm to the sediment-water interface, the LDA set-up only allowed the measurement of the u velocity component.

Results

Pore water flow pattern

The waves caused advective pore water exchange in the wave tank that exceeded the maximum diffusive exchange (based on exchange rate in the first hour) in the stagnant control by factor 8 to 54. This flux enhancement was mainly caused by pore water flows driven by oscillating boundary flows interacting with the wave-generated sediment ripples. The small flux enhancements prior to the development of the ripple topography revealed that the sinusoidal hydrostatic pressure oscillations due to the passage of the surface gravity waves ("wave pumping") had relatively little influence on the pore water exchange. Table 2 summarises the results of the wave tank and diffusion experiments.

Table 2: Summary of the experimental results.

Experiment:	Exp 1	Exp 2	Exp 3	Exp 4	Diff1	Diff2
Ripple length (cm)	3	3	2.5	2.5	--	--
Ripple height (cm)	0.7	0.7	0.5	0.5	--	--
Ripple height/length ratio	0.23	0.23	0.2	0.2	--	--
First ripples evolved (min)	15	5	10	20	--	--
Initial ripple evolution	complete	complete	half of the sediment surface	patchy	--	--
calculated washout depth (cm) / after (h)	2.6 / 14	3.0 / 17	3.1 / 24	3.2 / 24	0.8 / 24	0.7 / 24
calculated washout depth after 2 h (cm)	2.6	2.2	0.9	1	0.2	0.3
Tracer Exchange rate ($L\ m^{-2}d^{-1}$)	222	590	60	93	12 (1^{st} hour)	10 (1^{st} hour)

In the wave tank experiments, four phases could be distinguished after the initiation of the waves:

1. The Initial Phase with smooth sediment surface and moderate tracer release from the sediment. During this phase, diffusion, wave pumping (sensu Riedl et al. (1972)), and some advective release linked to small-scale topography elements remaining on the smoothed sediment surface drove the interfacial solute flux.
2. The Transitional Phase starting with the onset of ripple formation and ending when the entire sediment surface being covered with ripples. Within this period, the contribution of advective interfacial tracer exchange caused by ripple-flow interaction increased rapidly. At the end of this phase solute release rates reached their maximum.
3. The Flushing Phase during which the tracer was advectively washed from the upper sediment layer mainly due to oscillating flow – ripple interaction. Due to rapid tracer removal, its release rates decreased during this phase.
4. The final Equilibrium Phase during which the tracer release was limited by diffusion of tracer from deeper sediment layers into the flushed layer, with the concentration gradient not situated at the sediment-water interface, but at the lower limit of the washout zones.

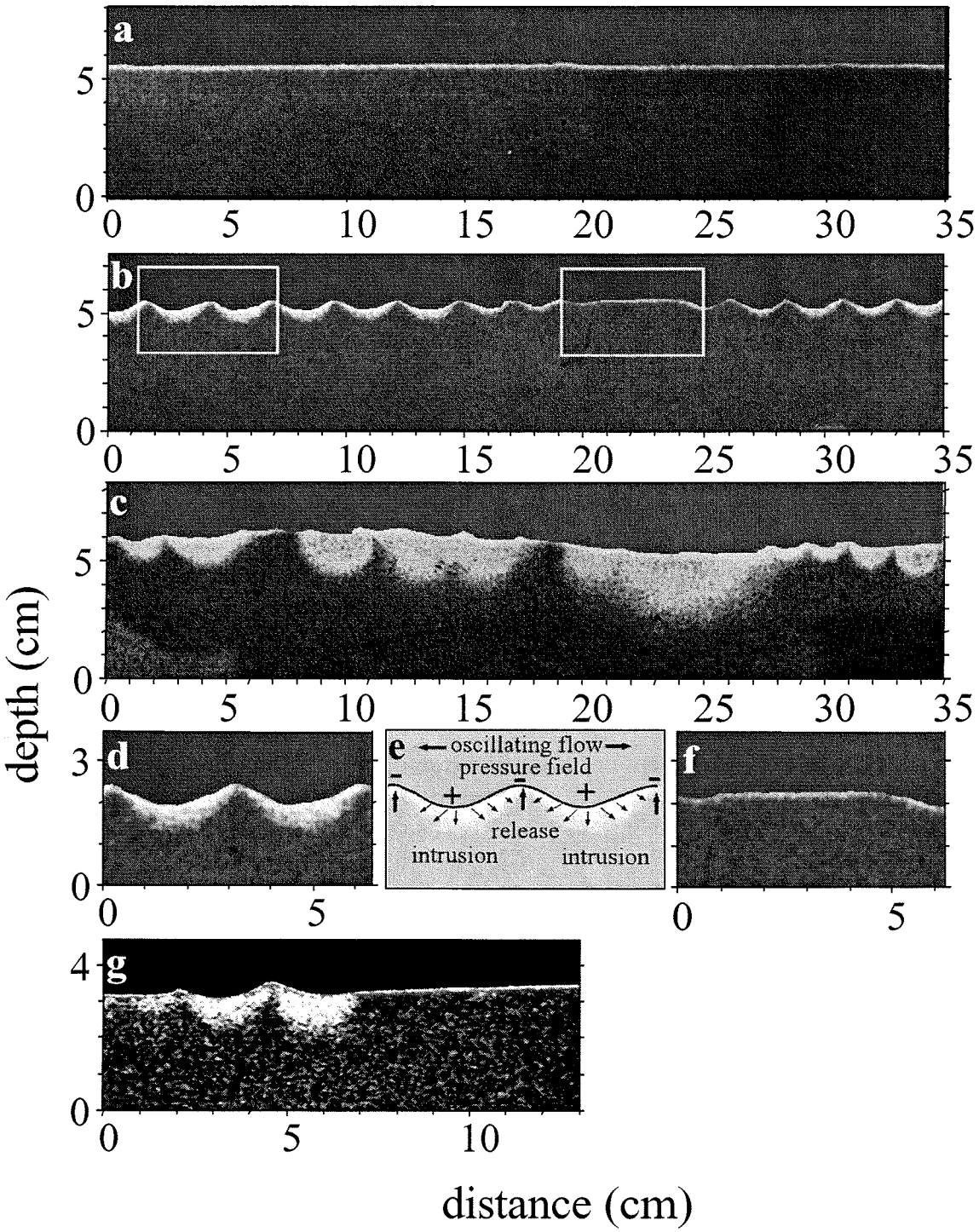

Fig. 2. Evolution of the washout pattern during Exp 3, dark areas of the sediment have high Rhodamine content; red and contrast digitally enhanced before changing to grey scale; a: before experiment; smooth sediment surface; b: after 20 min, boxes indicating sectors magnified in d and f; c: after 24 h; d: magnified from b, after 20 min; e: sketch of the pore water flow pattern and the current-induced pressure field; f: magnified from b, after 20 min; g: exceptional area after 23h where ripples did not form.

Fig. 2 a-c show the initial (2a) tracer distribution in the sediment and the distribution after 20 min (2b) and 24 h (2c) during Exp 3. Ripple formation started 10 min into the experiment.

During the Initial Phase, wave action removed the red dye from the upper 1-2 mm of the sediment, producing a thin, uniform washout layer. During ripple formation, light-coloured washout zones free of tracer formed rapidly in the ripple troughs, where water was forced into the sediment. This fluid intrusion was balanced by the release of pore water from confined upwelling zones at the ripple crests (Fig. 2b, 2d, 2e). This pore water flow pattern was firmly linked to the sediment ripples (Fig. 2d, 2f) and propagated with ripple migration. Later in the experiment, sediment bars (Rey et al. 1995) formed with wavelengths of ca. 30 cm and amplitudes of ca. 1 cm. Such bars are formed by resonance effects that exist in wave tanks due to partial wave reflection. Ripples were larger on the bar crests and smaller in the bar troughs. Intrusion and release zones linked to ripple and bar topographies combined to form larger irregular areas of down- and upwelling (Fig. 2c).

Fig. 2f shows an area of sediment surface that displayed no ripples until 23h after the start of Exp 3. This section permitted the direct comparison of tracer washout caused by hydrostatic wave pumping and topography-flow interaction. While areas with ripples were characterised by washout zones and pore water upwelling zones reaching the sediment surface, this smooth area displayed only a very thin uninterrupted surface layer depleted in tracer comparable to that observed during the initial phase of the experiment. This contrast reveals the dominance of the topography related pore water release.

As ripple formation did not take place in the same manner in all experiments, the release of tracer varied as well. In Exp 1 and Exp 2, ripples covered the complete experimental sediment surface after 45 min. This resulted in a pronounced peak of tracer release. In Exp. 2, tracer release increased sharply after 50 min and started to level out after 105 min (Fig. 3). The first derivative of tracer concentration over time yields the filtration rate (Fig. 3), which in Exp 2 peaked at 590 L m^{-2} d^{-1}. During the other experiments, the filtration rates ranged from 222 L m^{-2} d^{-1} (Exp 1) to 60 and 93 L m^{-2} d^{-1} (Exp 3 and 4, respectively).

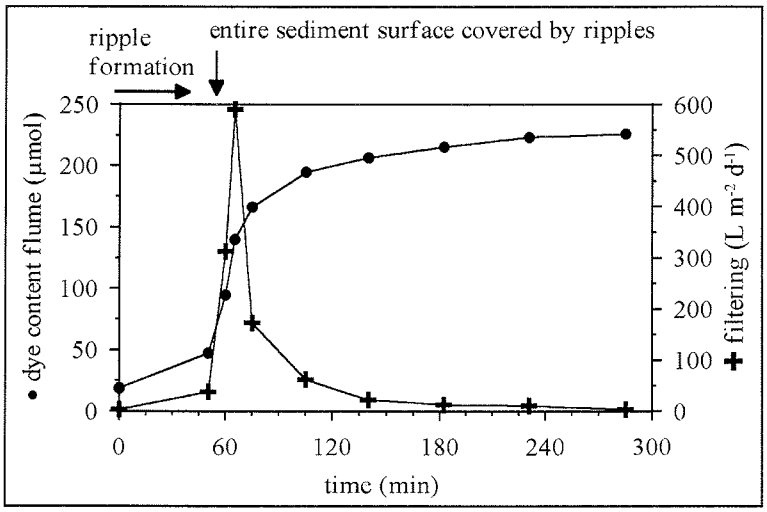

Fig. 3. Tracer release (solid circles) and derived filtering rates (crosses) during Exp 2.

In comparison, the tracer volume released by diffusion from the sediments under stagnant water columns during the first hour of the experiments corresponded to a fluid exchange of ca. 12 and 10 L m^{-2} d^{-1} for Diff 1 and Diff 2. All experiments are summarised in Fig. 4 that gives a picture of the sediment depths that theoretically had to be completely flushed of tracer to explain its concentration increase in the water column over time during the different experiments. This normalises tracer release for water volume, sediment surface area and porosity such that all experiments become directly comparable. Fig. 4 demonstrates that the four wave tank experiments showed a much stronger initial tracer release pulse from the sediment than the diffusion experiments under stagnant conditions. In all experiments, the high initial fluxes levelled out after a few hours and approached values in the order of the diffusive release because most of the tracer then was flushed from the upper sediment layer. Consequently, total tracer release rates at the end of all flume runs were similar. After 24 h, the total release of tracer from the sediment under waves still was 4 to 6 times higher than that under stagnant conditions and the final theoretical depth of complete flushing during all wave experiments was approximately 3 cm.

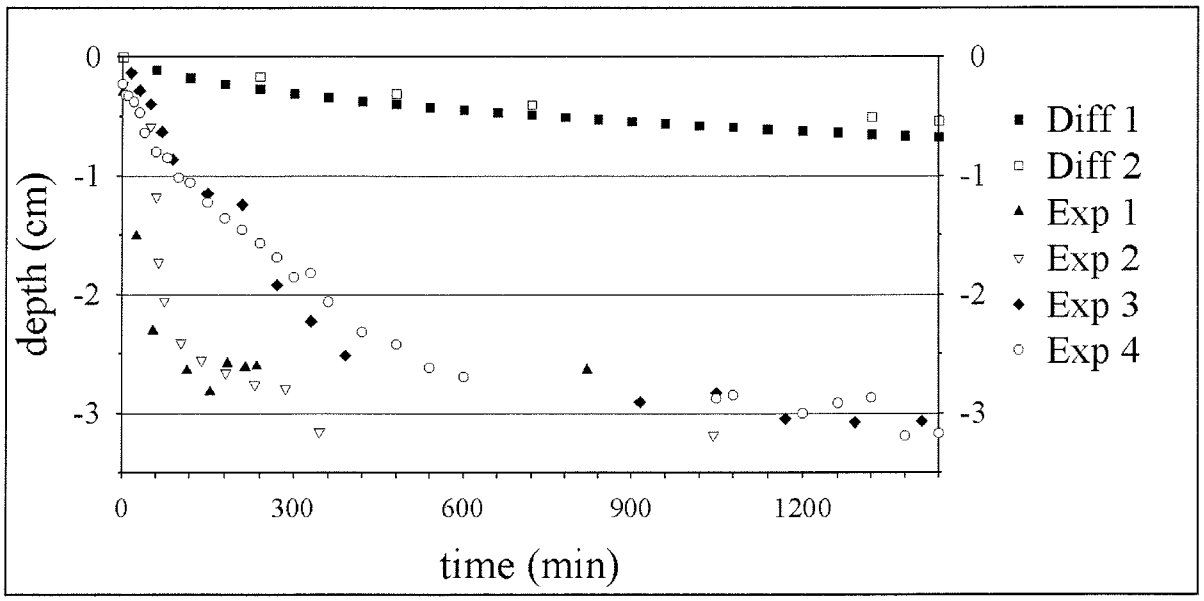

Fig. 4. Dye release during the wave experiments (Exp 1–4) and the control diffusion chambers (Diff 1: Brilliant Blue; Diff 2: Rhodamine WT) into the water expressed as theoretical sediment depths completely flushed free of dye - this form of presentation is independent of initial tracer concentrations, sediment surface area and experimental water volume. In reality, washout affected larger depths than this theoretical depth. The calculation assumes complete washout, however, observed horizontal dye concentration gradients in the sediment demonstrated that washout depths varied locally.

The analyses of the pore water from the sediment cores taken before and after the experiments quantified the vertical concentration gradients that had developed in the sediment. These gradients confirmed the theoretical washout depths inferred from the water samples as both methods yielded the same results. The initial tracer distributions showed homogeneous concentrations over all depths with little scatter (Fig. 5). The cores taken after Exp 3 and 4 revealed that the averaged release of tracer affected the sediment down to approximately 4 cm depth. This was 4 times higher than in the diffusive cores, where reduced tracer concentrations were detectable only down to 1 cm. The error bars reflect the horizontal variations of tracer concentration that characterised the washout zone between 1 cm and 3 cm sediment depth.

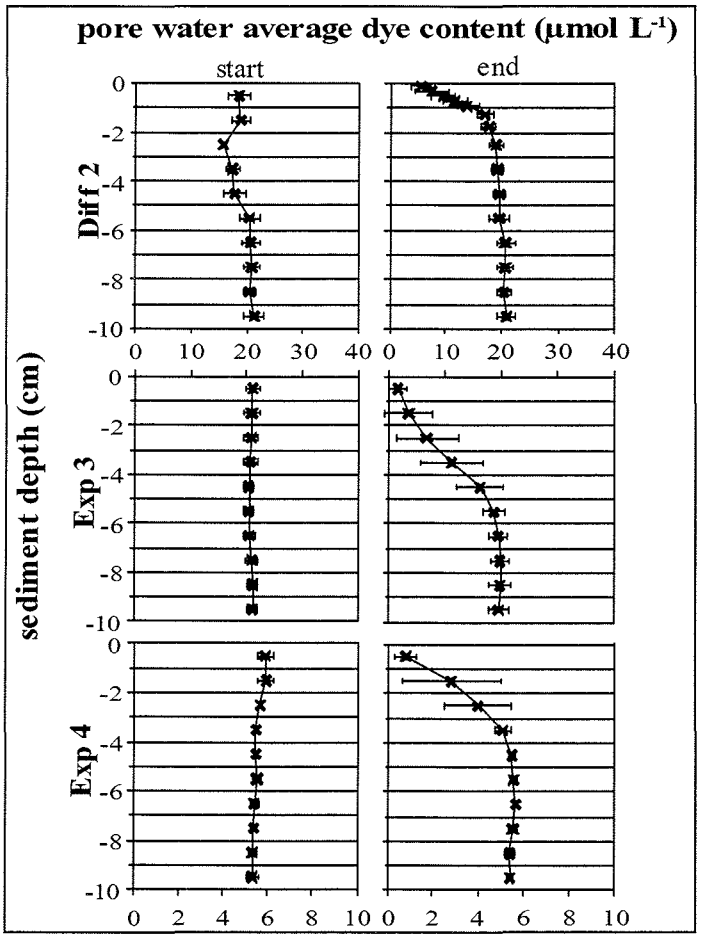

Fig. 5. Average sediment pore water dye concentration distributions over depth before and after Exp 3 & 4 (same wave settings) and Diff 2; left: before the experiment, right: after the experiment; error bars: standard deviation.

Hydrodynamics

The wavelengths (λ) of the propagating waves ranged from 60 cm to 80 cm and the water depths (d) from 15 cm to 20 cm. With d smaller than $\lambda/2$, oscillating water motion was present at the sediment-water interface.

Fig. 6 shows the mean maximal orbital velocities u_{max} and v_{max} for each depth measured over the smooth sediment surface at the beginning of Exp 3.

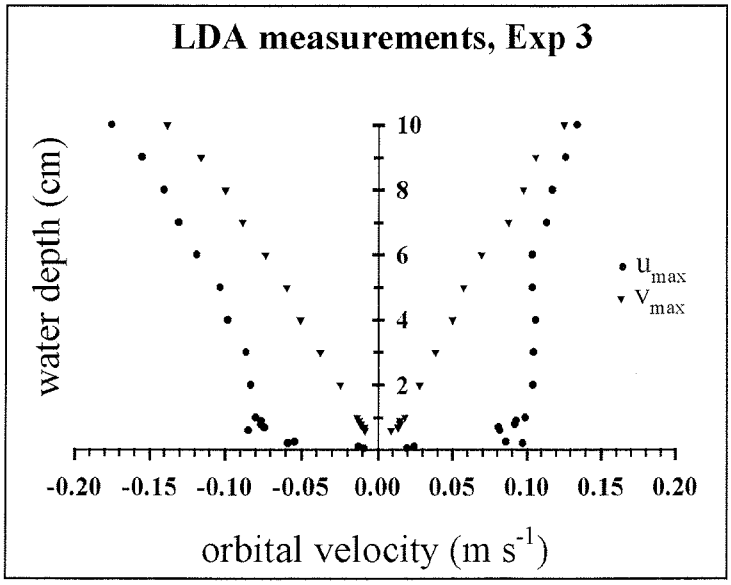

Fig. 6. Profiles of maximum orbital velocities measured with the Laser Doppler Anemometer (LDA) at the beginning of Exp 3 above unrippled experimental sediment surface; solid circles: maximum horizontal velocitiy (U), solid triangles: maximum vertical velocities (V). V values decrease linearly, U values non-linearly; between 0-cm and 0.6-cm above the sediment surface, the LDA set-up only allows for the measurement of the U velocity.

The maximum boundary shear stress can be calculated using the velocity gradient in the viscous sublayer:

$$\tau_{0m} = \rho\nu(\delta u/\delta z) \qquad (1)$$

with density ρ, dynamic viscosity ν, velocity in x-direction u and height over sediment z (Caldwell and Chriss 1979).

With an averaged maximum value of 0.1 m s^{-1} for δu for a δz of 0.1 cm, directly over the sediment surface, this results in $\tau_{0m} = 0.107$ N m^{-2}. Inferred from:

$$u_{*max} = (\tau_{0m}/\rho)^{1/2} \qquad (2)$$

the maximum shear velocity $u_{*max} = 0.01$ m s^{-1}. Assessing u_{*max} from a log velocity profile yields a similar result with $u_{*max} = 0.012$ m s^{-1}, which results in $\tau_{0m} = 0.148$ N m^{-2}.

Ripple formation

The shear velocity required to move a sediment particle of our sediment (calculated according to $u_* = 0.06\sqrt{(\rho_s-\rho_f)gD}$, with ρ_s = density of the sand grains, ρ_f = density of the fluid, g = gravitational acceleration, D = grain diameter (Hsü 1989)) was smaller and ranged from 0.0024 to 0.0042 m s^{-1}. Consequently, ripples started forming on parts of the sediment surface within the initial 20 min of all wave experiments (Table 2). Even though the sediment surface was carefully levelled and smoothed before the experiments started, a few small roughness elements of up to 1 mm height were still existent. Ripple formation started where small roughness elements were present. From the zones of initial ripple formation, the ripples spread over the entire experimental sediment area, which took 60 and 15 minutes in Exp 1 and Exp 2, respectively, and 8 to 10 hours in Exp 3 and Exp 4. The ripples migrated in the same direction as the waves propagated and their initial migration speed ranged between 2 to 3 cm h^{-1}.

Discussion

Advection and Wave pumping

Our experiments show that wave-induced oscillating flows interacting with sediment topography drive advective processes in a similar manner as in unidirectional flow as described e.g. by Savant et al. (1987), Thibodeaux and Boyle (1987) or Huettel and Gust (1992). Under oscillating flow, water is forced into the sediment at the ripple troughs and flanks and pore water emerges centred at the ripple crest as predicted by Shum's (1992) model calculations. According to Rutherford et al. (1995), the pressure perturbation along a sediment dune (= ripple) surface is a sinusoid with a wavelength equal to the dune wavelength. This could be confirmed in our experiments for the flow fields developing under oscillating flows, as washout was closely linked to ripple (and bar) wavelength. Likewise, applying mathematical models developed for the estimation of filtration rates caused by unidirectional flows to our settings, produce exchange rates that are close to those we measured in the wave experiments. Assuming that oscillating flows produce pressure gradients at protruding topography in a similar manner as unidirectional flows, the pressure perturbation at each ripple is estimated by:

$$p = 0.14\rho u^2(\delta/0.34d)^{3/8} \qquad (3)$$

for $\delta/H \leq 0.34$ with ripple height δ, water depth d, density ρ and mean current velocity u (Elliott 1990; Huettel and Webster 2001). For u we use the Root Mean Square value (RMS) of the oscillating horizontal velocity component that was 0.112 m s^{-1} at 10 cm water depth in Exp 3. From this pressure perturbation, the fluid exchange rate w_0 can be calculated according to:

$$w_0 = (2k/\rho\nu L_D)p \qquad (4)$$

with k, ν and L_D denoting permeability, kinematic viscosity and decay length (= the length scale of the ripple), respectively (Huettel and Webster 2001). Using the parameters and ripple dimensions of Exp 3, this gives a mean pressure perturbation of 1.11 Pa which yields a theoretical flushing rate of 116 L m^{-2} d^{-1}. The bars of 30 cm amplitude and 1 cm height would additionally contribute 12 L m^{-2} d^{-1} of filtration. The resulting total flushing rate of 128 L m^{-2} d^{-1} is in the same order of magnitude as the ones measured in our experiments.

It is clear that the wave generated flow – topography interaction addressed in this study only can cause filtration where the orbital motion reach the sea bed (depth <

wavelength/2). However, surface gravity waves cause filtration also beyond that depth due to the hydrostatic pressure oscillations they produce.

Riedl et al. (1972) observed pulsing of interstitial water linked to such pressure oscillations at the sea floor and introduced the term "subtidal pump". These authors estimated that, averaged over the global continental margin, the subtidal pump filters about 33 L m^{-2} d^{-1} through sandy shelf sediments. Mu et al. (1999) calculated a seepage of 15 L m^{-2} d^{-1} into and out of a flat sandy (md = 164 μm) seabed at 15 m water depth caused by wave-induced hydrostatic pressure oscillations (wave height = 1.5 m; length = 10 m, period = 6 s), which suggests a substantially smaller filtration rate than proposed by Riedl et al. (1972).

Our experimental set-up was not designed to quantify wave pumping, Nevertheless, the initial phase of Exp 2, when rippled surface topography was not yet developed, may indicate the magnitude of the effect of hydrostatic pressure oscillations on the pore water release (Fig. 2). During this phase we recorded a filtration rate of 38 L m^{-2} d^{-1}. This rate must be treated as a maximum estimate because in our flume experiments the ratio between sediment permeability and water depth was large relative to most areas in the shelf. However, as this rate is in the range of the findings of Mu et al. (1999) and Riedl et al. (1972), we use this value as an approximation for the effects of wave pumping. The comparison of this rate and the filtration rate caused by oscillating flow-topography interaction suggests that where wave orbital motion reaches the sea bed, oscillating flow-topography interaction is more effective for pore water exchange than wave pumping.

In our wave tank, exchange rates caused by oscillating flow-topography interaction reached up to 590 L m^{-2} d^{-1}. Because these calculations are based on the maximum observable pulse of tracer release from the sediment, the resulting estimates of the water volume filtered through the sediment by wave action are minimum values. This is because the pulse maximum depends on how fast the ripples are formed as shown by the delayed release of tracer during Exp 3 and 4, during which ripples initially formed on half the sediment surface (Exp 3) or patchy over the duration of several hours (Exp 4). It is likely that in those two experiments the final filtration rates with fully developed sediment topography were higher, but by that time an assessment of the effective filtration was

impossible since most of the tracer had already been washed from the upper sediment layers.

Oscillating flow-topography interaction caused a clear increase of the interfacial tracer flux relative to the controls with stagnant water, but how applicable are these results to natural environments? In shallow littoral regions, hydrodynamical settings almost identical to our flume settings may be found, and in such environments we can expect also similar effects on pore water exchange as those we observed in the laboratory. In-situ measurements by Precht and Huettel (see Chapter 3) in a littoral zone (70 cm water depth) with sands of comparable permeability revealed filtration rates very similar to those recorded in the wave tank. The visual observations of dye transport by Webb and Theodor (1968) confirm this transport process for a permeable rippled bed at 3 m depth. Similar observations could be made in a rippled carbonate sand bed at 18 m water depth off the East coast of Oahu (Huettel, unpublished data). Wave ripples on the sea bed are frequently found in areas with water depths less than 100 m (e.g. Cacchione et al. 1999; Ogston and Sternberg 1999). These ripples disclose that surface gravity waves generated substantial oscillating flows at these depths that were capable of moving sediment. Where the sediment is permeable enough, such flows will generate advective pore water exchange.

Natural environments

Large sections of the world's shelf areas display conditions that allow advective processes to occur: they are covered by permeable sandy sediments, display sediment topography in form of ripples and are reached by oscillating currents permanently or episodically. Waves dominate sediment dynamics in large shelf areas with the majority of sediment-transport occurring during times of energetic long period waves (e.g. Wiberg and Harris 1994; Harris and Wiberg 1997). The extension of the shelf areas affected by waves was numerically assessed by Harris and Coleman (1998) with the result that, e.g. in the North Atlantic, wave climate was such that quartz sands of 100 μm diameter would be mobilised down to a depth of 234 m at least once over a 3-year period. Wiberg and Harris (1994) showed the effects of water depth, wave height, wave period and sediment grain size on ripple formation. They calculated that orbital ripples could form at a water depth of 100 m with a wave period of 12 s, 4 m wave height and a sediment grain size of 250 μm.

Based on literature and our results, we suggest that the coastal and shelf seas can be divided into four depth zones that show different sediment-water interaction processes due to surface gravity waves (Fig. 7).

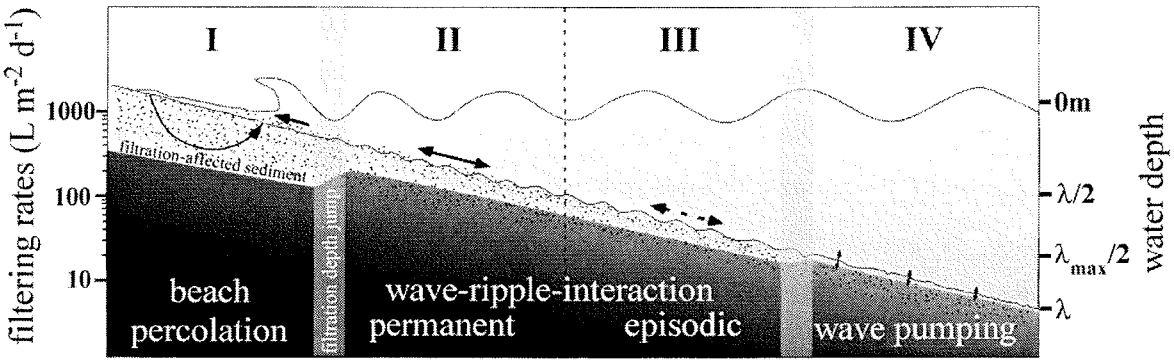

Fig. 7. Schematic overview of the different sediment-water interaction processes due to surface gravity waves in coastal and shelf environments (λ= wavelength):

I. Beach Zone: Beach percolation can lead to very high filtering rates in a zone of limited lateral extension. In lower parts of the beach, resuspension and high sediment mobility can lead to pore water release and POM burial.

II. Permanent Advection zone (water depth < $\lambda/2$), in which surface gravity waves permanently induce oscillating boundary flow that, by interacting with sediment ripples, lead to constant advective solute exchange. This advective flushing of the upper sediment layers leads to a relative thick oxygenated sediment layer and particle transport into the bed.

III. Episodic Advection Zone (water depth < $\lambda_{max}/2$), with episodic advection due to oscillating flow-sediment topography interaction, see Fig. 8 for details.

IV. Wave Pumping Zone ($\lambda/2$ < water depth < λ), where waves are only effective for the interfacial exchange due to pumping caused by hydrostatic pressure oscillations. In deeper areas, interfacial transport is governed by diffusion and bioirrigation.

The first and uppermost zone (not addressed in this study) is the beach, where the run-up of waves may cause filtering rates of up to 85 m^3 m^{-1} d^{-1} (McLachlan 1989), which equals, dependent on the lateral extension of the filtering zone, ca. 1000 L m^{-2} d^{-1}. The second zone comprises those shallow areas where the sediment is nearly permanently exposed to oscillating currents which cause filtration when interacting with bed topography. In the third zone, wave orbital motion reaches the seafloor only episodically, in the fourth zone never. In the latter zone, wave-induced hydrostatic pressure oscillations may enhance sediment-water fluid exchange. The lateral extension of these zones varies, in dependence of the shelf slope and the wave regime. With filtering rates of ca. 1000 L m^{-2} d^{-1} in beaches, 100 L m^{-2} d^{-1} caused by ripple-flow interaction, ca. 30 L m^{-2} d^{-1} by wave pumping (Riedl et al. 1972; Mu et al. 1999) and molecular diffusion equivalent to a fluid exchange rate of ca. 10 L m^{-2} d^{-1}, the ratio between the average rates caused by the four transport processes may be roughly 100:10:3:1.

The wave-induced filtering, thus, generally increases with decreasing water depth, and our study suggests that this increase is not steady but displays stepwise changes in its increase rates due to the dominance of different wave-driven exchange processes in the four depth zones (Fig. 7). This is most obvious at the interface of the sublittoral zone and the adjacent beach. However, the boundary between zones with and without wave ripples can be abrupt and sharp and we can expect a jump in the filtration rate between those areas as indicated by the sudden increase of flushing rate with evolving topography in our flume experiments. The changing magnitude of filtration rate with depth may have ecological consequences that are linked to the associated changes in transport rates of metabolites into and out of the sediment.

In the second zone, where waves have the strongest impact on the submerged seafloor, ripples are permanent features of the sediment surface and steady advection leads to complete and permanent flushing of the upper sediment layers, which therefore may be relatively rich in oxygen. Permanent advective transport of fine particles into the sediment and steady flushing of decomposition products from the bed may convert these areas into efficient biocatalytic filters (Huettel et al. 1998).

In our experiments, we measured strong initial pulses of solute release from the sandy sediment when ripples were formed. Such a scenario may take place in the third

zone, where surface gravity waves reach the sea floor only episodically. The nutrient pulses Oldham and Lavery (1999) measured in such an environment could be attributed to this effect. Fig. 8 proposes a sequence describing the solute fluxes across the sediment-water interface during an episodical storm event in the shallow sandy shelf environment.

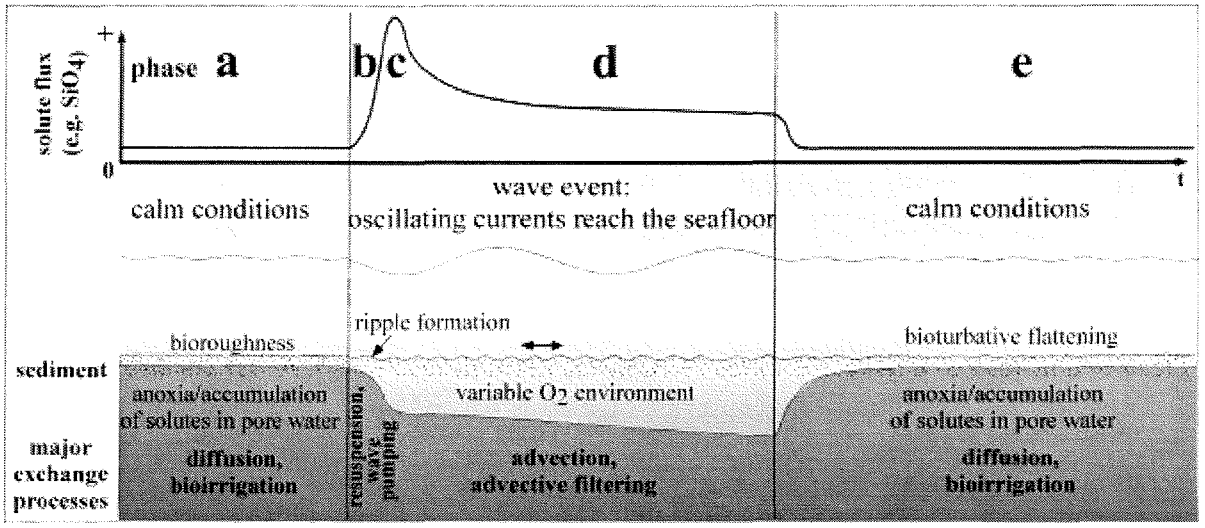

Fig. 8. Schematic overview of sediment water-interface processes in areas episodically affected by wave events.

a: (Calm Phase) in the absence of effective interfacial transport mechanisms, permeable sandy sediments, may accumulate solutes (e.g. Silicate) and small particles in their pore space.

b: (Wave Phase) at the beginning of a wave event, exchange between the permeable sediment and the overlying water may be driven by advection linked to oscillating flow interacting with sediment topography like e.g. bioroughness (Huettel and Gust 1992, Oldham and Lavery 1999) or existing relict ripples.

c: (Wave Phase) with continuing wave action, oscillating bottom currents generate sediment ripples. Boundary flow-ripple interaction causes advective filtering that exchanges the pore water of the upper sediment layer, therefore a maximum advective solute release takes place.

d: (Wave Phase) with continuing wave action and after the maximum solute flux, oxygen-rich water is being filtered through the sediment and mobile horizontal oxygen concentration gradients may develop (Shum 1993). Ensuing alternating exposure to variable redox conditions may result in more complete and rapid decomposition of organic material trapped in the upper sediment layer (Aller 1994). An equilibrium solute flux develops, and constant intrusion of oxygen-rich water into the sediment may increase overall oxygen penetration depth into the sediment.

e: (Calm Phase) after the wave event, the water exchange across the interface is reduced to its original low value, filtering is reduced, solute concentrations increase in the sediment and the former oxygen penetration depth is reinstated.

Applicability of experiments

Our experimental sediment had a grain size distribution ranging from 100 to 300 μm, which may be representative for the most common grain size on the continental shelves. E.g. Cacchione et al. (1999), Ogston and Sternberg (1999) describe shelf sands with a grain size distribution ranging between 125 μm and 250 μm and ripples with 9 cm wavelength at 60 m water depth. Additionally, large areas of the shelves are covered by coarser, more permeable sediments (e.g. Emery 1968; Marinelli et al. 1998; Black and Oldman 1999), where advective processes may be much stronger than observed in our flume experiments. The advective flux we observed during the experiments was mainly caused by the interaction of sediment topography and boundary layer flow. All topography evolved as the response of the bed to the hydrodynamic conditions during the respective experiments. No artificial roughness elements were placed or built on the sediment surface. Thus, the bed roughness was in equilibrium with the surface gravity waves and the observed solute flux is not exaggerated by e.g. oversized sediment topography.

However, under laboratory conditions, wave ripples may form that are different to those common in nature. Wiberg and Harris (1994) showed that most laboratory experiments produce orbital ripples with ripple spacing proportional to the wave orbital diameter, and this was also the case in our experiments. In nature, nearly all wave ripples belong to the anorbital or suborbital type and their wavelengths are proportional to sediment grain size rather than wave properties. For a natural environment, Wiberg and Harris (1994) predict a ripple spacing of approximately 10 cm for sand with a median grain size of 200 μm, which results in about 1/3 of the ripples per unit area than in our experiments. Even with only 1/3 of ripples per unit surface area and based on the maximum but conservative filtering rate of 590 L m^{-2} d^{-1} we recorded, this would result in a filtering rate of ca. 200 L m^{-2} d^{-1}.

We suggest that the numerical approaches developed to calculate advective filtering under unidirectional flow can be used to obtain conservative estimates of wave-induced advective exchange. We can estimate the magnitude and importance of these processes by applying these relationships on field data from previous studies. Cacchione et al. (1999) present data from the Eel continental shelf, situated at ca. 50 m water depth. Using values of 40 cm s^{-1} for u (120 cm over sediment), 9 cm ripple amplitude, 1.1 cm ripple height

(calculated with a ripple steepness of 0.12 (Wiberg and Harris 1994)) and 1.5×10^{-11} m^2 permeability (assumed to be similar to this study because of the similar grain size), we obtain a filtering rate of 103 L m^{-2} d^{-1}. Li and Amos (1999) conducted a field study on the Nova Scotia shelf at 56 m water depth. With a maximal wave-induced u = 25 cm s^{-1} (50 cm over sediment); ripple amplitude L_D = 9 cm; (calculated) ripple height δ= 1.1 cm and an assumed permeability of $1.5 \times 10^{-11} m^2$, we calculate 68 L m^{-2} d^{-1} of advective filtering during single events, whereas during calmer periods with bottom currents below 10 cm s^{-1}, calculated filtering is reduced to 11 L m^{-2} d^{-1}. Based on these calculations and our experimental findings, we conclude that 50 to 100 L m^{-2} d^{-1} is a moderate value for advective filtering in permeable shelf sediments exposed to oscillating flow. Sediments only episodically reached by waves may display similar filtering rates but only during storm events. In these beds, however, wave pumping by hydrostatic pressure oscillations may constantly enhance solute release.

The ecological relevance of wave-induced filtration is linked to the high load of organic matter commonly present in near-shore waters. In contrast to continuous pore water advection caused by constant unidirectional flow, wave-induced pore water exchange is characterised by pulsing flow due to the constant acceleration and deceleration of the boundary current. These pulsing flows can transport particulate matter efficiently through the pore space, thereby enhancing the filtration capacity of the bed. Surface gravity waves convert the sand sediments ubiquitous in the shallow shelf into effective filter systems suggesting that these beds are sites for rapid mineralisation and recycling.

3. Rapid wave-driven advective pore water exchange in a permeable coastal sediment

(submitted to Journal of Sea Research)

Elimar Precht and Markus Huettel

Max Planck Institute for Marine Microbiology, Celsiusstrasse 1, D-28359 Bremen

Abstract

In this study we present in-situ measurements of pore water flow velocities in a coastal sandy sediment (permeability=3.65×10^{-10} m^2). The advective pore water flows were driven by the interaction of oscillating boundary flows with sediment wave ripples, (amplitude=7 cm, wavelength=30 to 50 cm). The measurements were carried out in the Mediterranean Sea at 50 to 70 cm water depth during a phase of very low wave energy (max. wave amplitude=10 cm). A novel optode technique is introduced that permits direct pore water flow measurements using a fluorescent tracer. Near the sediment surface (0.5 cm depth) pore water reached velocities of up to 40 cm h^{-1}. Thus, advective transport exceeded transport by molecular diffusion by at least 3 orders of magnitude. Based on the pore water velocity measurements and ripple spacing, we calculate that 140 L m^{-2} d^{-1} are filtered through the sediment. Pore water visualisation experiments revealed a flow field with intrusion of water in the ripple troughs and pore water release at the ripple crests. The wave driven water flow through the sediment, thus, was directly linked to the wave-generated sediment topography, and its spatial dimensions. These results show that surface waves cause water filtration through permeable sediments at water depths smaller than half the wavelength. We conclude that surface gravity waves constitute a dominant hydromechanical process that converts large areas of the continental shelves into expansive filter systems. Surface gravity waves thereby could affect suspended particle concentration and cycling of matter in the shelf.

Key Words: permeable sediment, coastal sand, advection, in-situ optode, pore water flow velocity measurements, surface gravity waves.

Acknowledgements

We thank Prof. B.B. Jørgensen for his interest and support in this work. We especially would like to acknowledge H. Røy for his help and constructive ideas during fieldwork. We appreciate the co-operation of F. Janssen and C. Wild before and during the measurement campaign. J. Jensen is thanked for assistance during fieldwork, M. Alisch for nutrient analyses, and V. Meyer, P. Färber and G. Herz for their help with the electronics. This study was funded by the Max Planck Society (MPG).

Introduction

In permeable sandy sediments that are common in coastal and shelf environments (de Haas et al. 2002), interaction of boundary layer flow and sediment topography can drive interstitial pore water flows. Such advective transport may be an important link between sediment and water column processes and could affect coastal and shelf biogeochemical cycling as it can exceed transport by molecular diffusion by several orders of magnitude (Huettel and Webster 2001).

Webb and Theodor (1968) observed that under moderate wave conditions dyed water injected into a coarse sandy nearshore sediment was drawn to the sediment surface in a matter of minutes. These authors concluded that surface gravity waves were the driving force behind this process, as density driven and biological processes could be ruled out. Shum (1992) used a two-dimensional numerical approach to calculate the trajectories of pore water particles under a rippled bed over one wave period. The results indicated that the zone of advection extended to a few ripple heights below the ripple surface over a wide range of wave conditions and sediment characteristics. Advective exchange driven by surface gravity waves was quantified in a series of laboratory wave tank experiments by Precht and Huettel (Chapter 2). These authors also showed that wave-induced pore water exchange increased sharply at the temporal transition from a smooth to a rough sediment surface when ripples were generated by the oscillating boundary flows.

The term "subtidal pump" for the exchange between sediment and water column driven by wave-related hydrostatic pressure oscillations was introduced by Riedl et al. (1972). These authors used in-situ data to calculate the amount of water forced through the bed and concluded that the subtidal pump could filter the global ocean volume through the shelf sediments in ca. 14 000 years. Rutgers van der Loeff (1981) described the effect of wave pumping in intertidal flats and concluded that observed increased solute flux was caused by pore water exchange driven by waves. In order to explain net transport of solutes by periodic interstitial motion, the concept of mechanical dispersion was added to the subtidal pump theory (Harrison et al. 1983). In a numerical and experimental approach, Webster and Taylor (1992) showed that dispersion driven by surface gravity waves was able to enhance the solute transfer between sediment bed and overlying water and introduced the term rotational dispersion. Precht and Huettel (Chapter 2) proposed that

wave-driven exchange at water depths < wavelength/2 caused by oscillating flow-sediment topography interaction may exceed the effects of wave-pumping at least by a factor of 3.

These wave-induced transport processes may cause characteristic changes in the biogeochemical zonation of permeable sediments. Shum's (1993) model calculations indicate that the oxygen distribution in the pore water underneath a rippled surface under progressing waves can display horizontal concentration gradients that may be of the same order of magnitude as those in the vertical direction.

Advective exchange processes driven by unidirectional near-bottom flows have been studied in more detail than exchange driven by oscillating currents. Thibodeaux and Boyle (1987) and Savant et al. (1987) investigated the flow patterns in permeable sediment generated by obstructions on the sediment surface. Advective solute exchange was studied and quantified for a streambed with bedforms and nonsorbing solutes (Elliott and Brooks 1997a; Elliott and Brooks 1997b); a rippled bed and adsorbing metals (Eylers et al. 1995); biogenic sediment structures and nonsorbing solutes (Huettel and Gust 1992) and solid obstacle-boundary flow interactions (Hutchinson and Webster 1998). The biogeochemical implications of advection were examined by Ziebis et al., (1996) for oxygen penetration depth, and by Huettel et al. (1998) for biogeochemical reaction zones in permeable sediments. With interfacial water exchange, suspended particles (Huettel et al. 1996) or phytoplankton (Huettel and Rusch 2000) locally can be transferred from the boundary layer into the top centimetres of permeable sediments. Thus, the classical one-dimensional approach developed for describing the distribution of pore water constituents and for measuring the related fluxes across the sediment-water interface is inadequate for permeable shelf beds that permit pore water flows (Shum and Sundby 1996).

The aim of the present study was to quantify wave-induced pore water velocities in-situ in order to assess the magnitude of advective fluid exchange.

Methods

Study site

The measurements were carried out in October 2001 in shallow-water sediments of Campese Bay at the western coast of the Island of Giglio. Giglio is part of the Tuscany Archipelago in the Mediterranean Sea off the western coast of Italy, approximately 150 km north-west of Rome at 42° 20' N, 10° 52' E (Fig. 1). The tidal regime is microtidal as in the whole Mediterranean Sea.

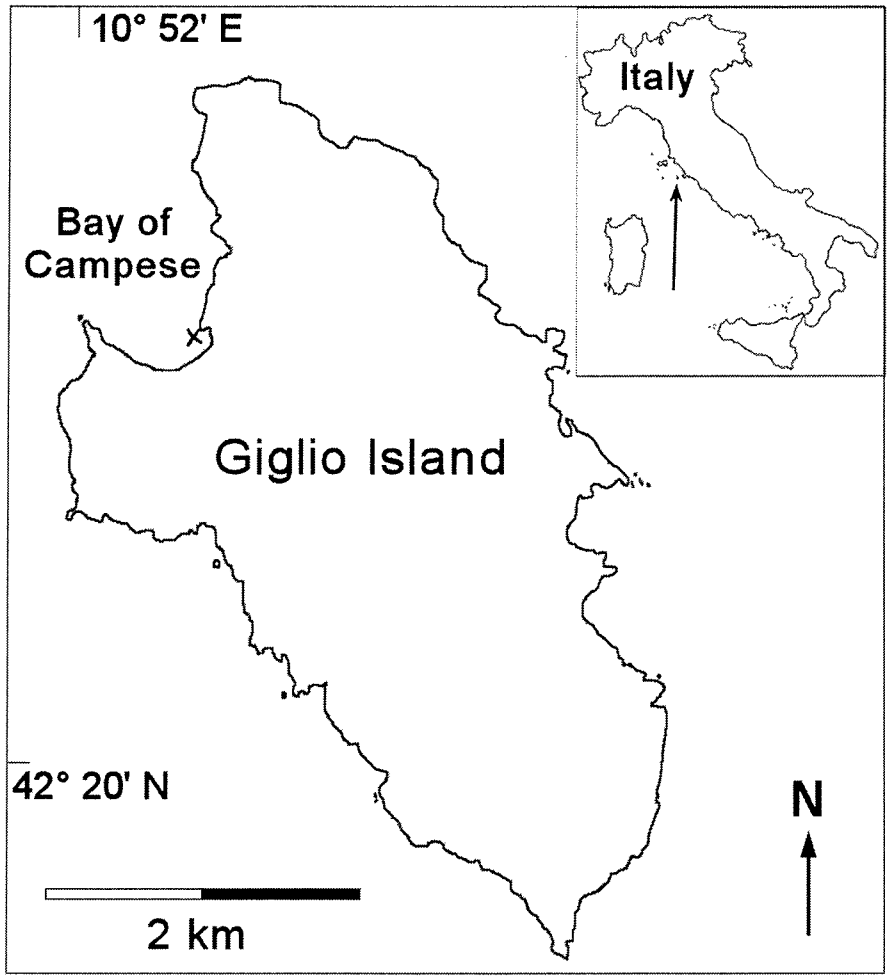

Fig. 1: Bay of Campese, x indicating study site.

The beach and sublittoral of Campese Bay consist of permeable medium sand with a high content of Pyrite grains as iron ore was mined on Giglio and washed and loaded in Campese Bay until ca. 1950. In the shallow (< 10 m) areas of the bay, surface gravity waves produce coast-parallel wave ripples, while in the deeper regions mounds created by

the burrowing activity of the mud shrimp *Calianassa truncata* are the main topographical features (Ziebis et al. 1996). Due to the calm weather conditions prior to the measurement campaign, the *Calianassa* activities had largely destroyed the regular wave ripple pattern in the areas deeper than 2 m. Salinity during the measurement period was 39, water temperature ca. 2°C and weather conditions were calm with wind velocities of 2 to 5 m s^{-1}. The measurements were carried out in sediment at 50 to 70 cm water depth. This shallow depth was chosen as only small waves were present. Symmetric wave ripples dominated the sediment topography at the study site with amplitudes between 6 and 8 cm and wavelengths between 30 and 50 cm. Although rolling sand grains could be observed at the ripple crests, the ripples as such remained stationary during the measurements.

The grain size distributions in the sediment surface layer (0-5 cm) at the ripple troughs and crests were different, with median values of 370 µm and 500 µm for the crests and troughs, respectively. The higher median value for the troughs was mainly due to a thin surface layer of gravel (max. diameter: ca. 1 cm) that had accumulated in the troughs. This had no significant influence on permeability and porosity, which were 3.65×10^{-10} m^2 (sd=1.64×10^{-10}, n=4) and 36.9 % (sd=1.35, n=10), regardless of where the sediment cores for these measurements were taken.

Water column hydrodynamics

The wave heights were measured with a pole fitted with a scale that was anchored in the sediment at the study site. Water currents were measured using an Acoustic Doppler Velocimeter (Nortek). The ADV technique allows 3 component current measurements in a small measuring volume located ca. 10 cm below the sensor. Two time series of triplicate flow measurements were carried out; one set above a ripple crest, one above a trough. The downwards measuring ADV sensor was attached to a custom-built aluminium frame with a transverse system permitting to move the measuring volume vertically to predefined specific depths (27, 15, 5 cm and 30, 19, 5 cm above the sediment surface at crest and trough, respectively). Flow velocities were recorded at each measuring point for 1000 s with a sampling frequency of 25 Hz.

Pore water flow measurements

The measurements of the pore water flow velocities where carried out by injecting 2 ml of fluorescent dye into the sediment and subsequently following the movement of the dye cloud through the sediment with optical sensors. The dye was a Fluorescein solution (100 mg L^{-1}) with a density attuned to the local seawater by addition of NaCl until neutral buoyancy.

The principle of detection of a fluorescent solution with optical fibres is similar to that of oxygen measurements with optodes as laid out by Klimant et al. (1995). For Fluorescein concentration measurements, blue light (λ=470nm) is emitted through an optical fibre into the measuring medium where the light causes excitation of the Fluorescein. The resulting fluorescence signal is transferred back through the same optical fibre, and the intensity is measured after passage through a green interference filter (λ=519nm) with a photo-multiplier tube (PMT). The intensity of the signal is linearly proportional to the Fluorescein concentration within the range of the dye concentrations employed (F. Janssen, unpubl. data). A custom-built fibre optical switch with 7 channels allowed connecting 6 optical fibres for fluorescence measurements and one internal reference. The electronics were housed in a sealed titanium cylinder, and power was supplied by a submergible 24 V battery. The cylinder containing the electronics and the battery were placed onto the sediment 3 m away from the actual measuring site ensuring no interference with the measurements. Prior to the measurements, thermal equilibrium of the electronics with the surrounding water was allowed, as the PMT gain is temperature sensitive. A cable connection allowed the direct surveillance of the measured data with a laptop computer on the beach.

The optical fibres (Radiall; fibre diameter=140 μm), were stripped of their outer elastic plastic coating but retained their inner plastic cladding for protection resulting in a sensor tip diameter of < 1 mm. The ends of the fibres were cut straight to achieve an optimal compromise between sturdiness and signal strength.

The fluorescence sensors were fixed in an array that was constructed from mesh wire (mesh width 1.25 cm). This set-up allowed aligning the sensors in a "comb" with 1.25 cm vertical distance between the sensor tips (Fig. 2). A hypodermic needle was attached to the array 2.5 cm below and parallel with the lowest sensor tip. The end of the needle was

vertically aligned with the sensor tips. The shaft of the needle was connected with tubing to a syringe that permitted release of a defined tracer volume through the buried open end of the needle. With this set-up, the optical sensors and the hypodermic needle could be placed at fixed and known positions in the sediment covering a distance of 8.75 cm. For the measurements, the array was positioned vertically in the centre of the ripple crests parallel to the ripple geometry. The uppermost fluorescence sensor was ca. 1 mm below the sediment surface at the ripple crests so that the dye was injected ca. 8.8 cm below the sediment surface. Inserting the sensor array into the ripple was done manually by partially removing the ripple, pressing the array horizontally into an undisturbed part of the ripple and rebuilding the ripple where it had been disturbed. Thus all measurements were carried out in undisturbed parts of the ripples. After injection of Fluorescein, the passage of the dye cloud past the optical sensors could be recorded in the measurements. Four successful measurements of dye migration in the sediment were carried out, two of them with three successive dye injections. The bulk flow velocity of the pore water could then be inferred from the time between the passages of the Fluorescein concentration maxima at the individual optical sensors.

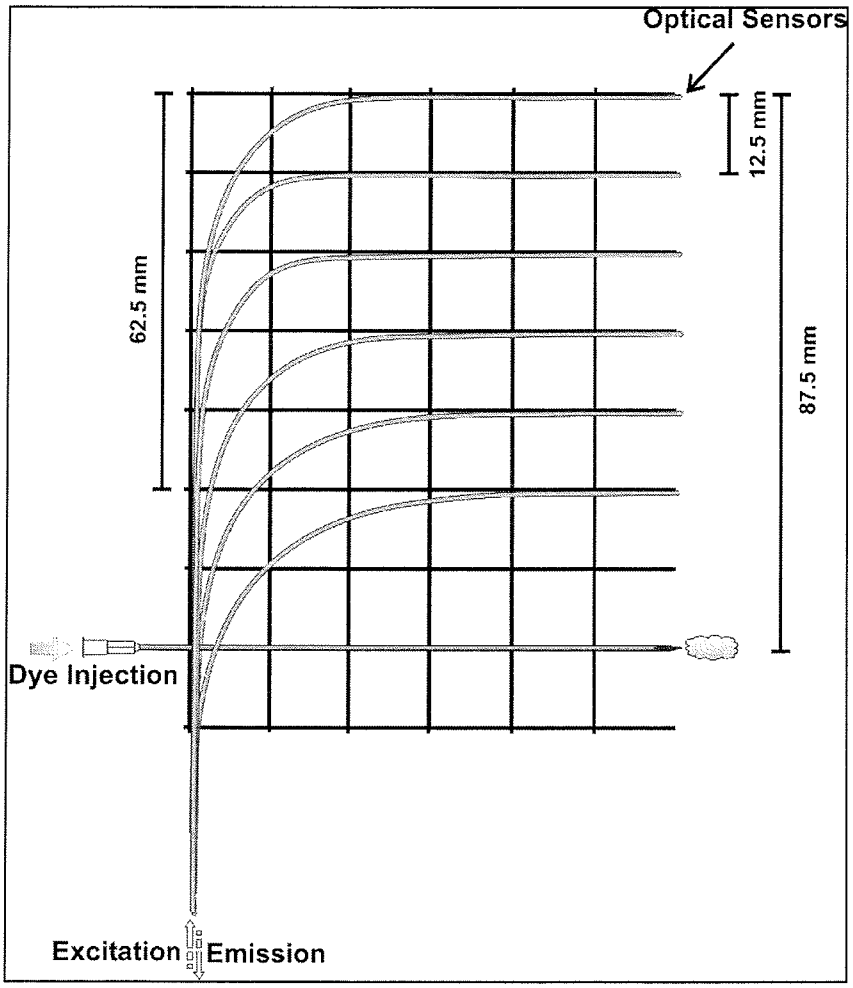

Fig. 2: Sketch of the set-up of the optical sensors: grey are the optical fibres, black the mesh wire framework.

Pore water flow visualisation

The pore water flows could be visualised in situ with a simple technique: a 20 cm wide and 30 cm long transparent polycarbonate plate (6mm thick) was carefully pushed vertically into the sediment perpendicular to the ripples and thus aligned with the main boundary flow. By removing the sediment on one side of the plate, the cross-section of the ripple became visible. The plate had silicone-sealed holes (0.5 cm in diameter) drilled at regular intervals in a rectangular grid pattern. Through these holes dye could be injected into the sediment with a hypodermic needle, and additionally these holes served as reference points. The dyes employed for these pore water flow visualisations were neutrally buoyant and thermally equilibrated Rhodamine or Fluorescein solutions. The movement and development of the dye cloud in the sediment could be observed visually through the

transparent sheet and for quantitative analyses was recorded with an underwater digital camera. The camera was attached to a custom-built aluminium frame anchored in the sediment and photographs were taken at regular time intervals.

Sediment Characteristics and Pore Water Analyses

At the study site, 3 sediment samples were taken at ripple crests and 3 in the ripple troughs. Each sample consisted of surface sediment (top 5 cm of the sediment) and comprised about 500 g of dry material, which was used to assess grain size distributions using a column of 8 sieves.

To assess the porosity, 5 + 5 sediment cores (diameter: 2.6 cm, length: 3.3 to 9 cm) were taken at ripple troughs and crests. Supernatant water was carefully removed, and the cores were sealed and stored for transport. The porosities of the respective cores were calculated from the wet and dry (after drying at 50°C until constant weight) weights and corrected for salinity.

For permeability measurements, 4 sediment cores (diameter: 2.6 cm, length between 8.5 and 13.7 cm) were taken at both, ripple crests and ripple troughs. Measurements were done directly after sampling with a constant head permeameter (Klute and Dirksen 1986).

For nutrient analyses, pore water was extracted using a steel pore water sampler with a perforated pointed tip filled with filter material. 3 × 3 samples were taken 10, 20 and 30 cm below both, ripple troughs and crests (ca. 4 to 5 ml each). According to the measured porosities, pore water was extracted from a sediment volume of ca. 13.5 cm^3, which means a vertical resolution of ca. 3 cm assuming a spherical shape of the extracted water volume. These 18 pore water samples and 3 open water samples were preserved with 0.1 ml of $HgCl_{2\ sat.}$ solution directly after retrieval, sealed and stored for nutrient analysis. The samples were diluted by factor 3 and analysed spectrophotometrically for NO_3^-, NO_2^-, NH_4^+, PO_4^{3-} and $Si(OH)_4$ with a Scalar 5-canal Continuous-Flow-Auto-Analyser. The chemistry of the underlying reactions is described in Grasshoff et al. (1999). Pore water salinity was measured in the same samples.

Sediment temperature measurements were carried out with temperature loggers (HOBO, resolution=0.7°C) at various sediment depths down to 20 cm.

Results

Flow measurements in the water column

Wave conditions during the entire measurement period were calm with wave amplitudes not exceeding 10 cm. A power spectrum analysis of the ADV data revealed a distinct peak at 0.18 Hz, implying a main wave period of 5.5 s. Wave amplitude was 6 cm during the ADV measurements, and this wave action was not strong enough to induce ripple migration. Only motion of very few sand grains at the ripple crests could be observed. An excerpt representative for the measurements and the conditions during the study period is shown in Fig. 3. The dominant water motion 27 cm above the ripple crest was the horizontal oscillation perpendicular to the crests with maximum velocities of 30 and –30 cm s^{-1}, whereas maximum vertical velocities reached 10 cm s^{-1} and –10 cm s^{-1}. The averaged orbital velocities were 9.8 cm s^{-1} and 9.2 cm s^{-1} at 27 cm and 15 cm above the ripple crests, respectively. The RMS values for the main horizontal velocity component at these depths were 9.7 and 8.5 cm s^{-1}, respectively.

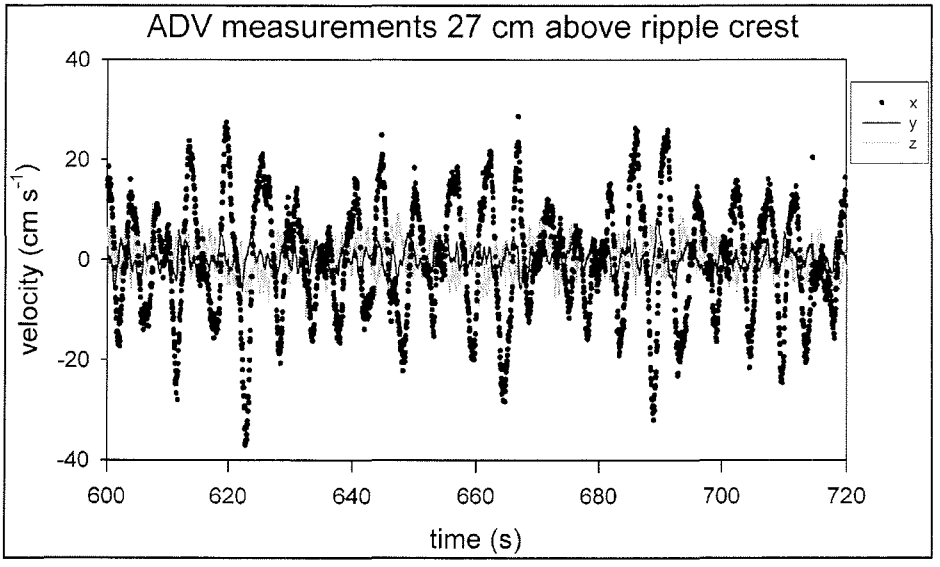

Fig.3: Excerpt from one of the ADV measurements.

Pore water flow field

The motion of the pore water tracer in the sediment could directly be observed trough the transparent panes inserted into the sand bed. Tracer injection at different locations under the ripple revealed the local pore water flow pattern, and the sum of all observations gave an image of the pore water flow field.

After injection of a dye cloud (2.5 cm diameter) directly underneath the ripple crest at 6 cm sediment depth, the dye migrated vertically upwards and finally emerged from the sediment at the ripple crest. The upwelling dye cloud became horizontally compressed and vertically elongated on its path to the ripple crest. (Fig. 4a).

Injection of dye to 1 cm sediment depth into the land- and seaward slopes of the ripples resulted in sideways dye movement along a curved path towards the ripple crest, where it finally emerged from the sediment (Fig. 4b).

Injection of dye into the centre of a ripple trough showed the dye cloud propagating downwards and simultaneously being stretched towards the ripple crests, with the first dye release at the ripple crest after 30 min (Fig. 4c).

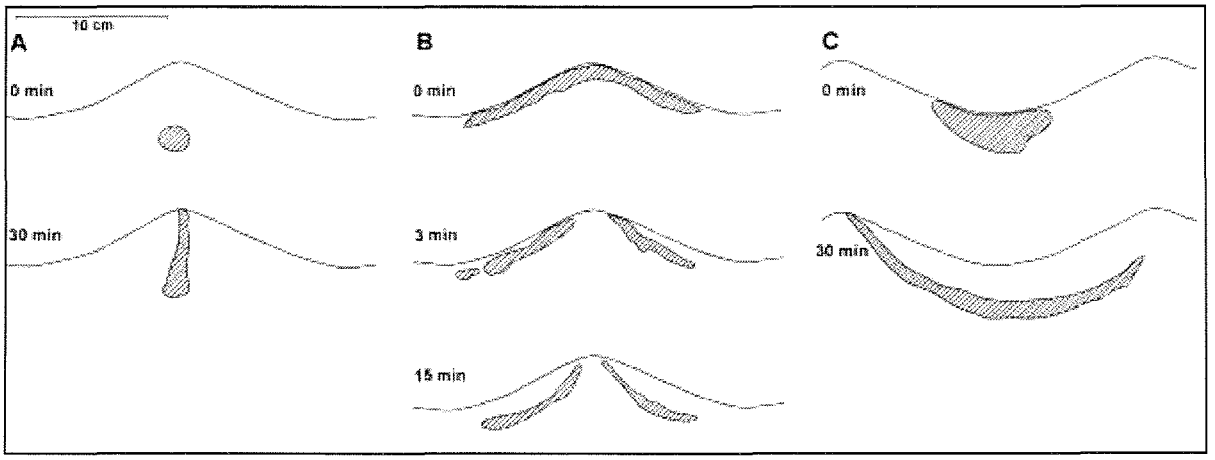

Fig. 4a-c: Sketch summarising the results of the pore water flow field dye experiments.

The pore water flow field that could be reconstructed from these observations is schematically depicted in Fig. 5. Water is entering the sediment in the ripple troughs and at the ripple flanks and leaves the sediment centred at the ripple crests. This pattern evolves as the average of the two pore water flow fields that would evolve under unidirectional flows

in opposing directions. The seawater penetrating into the sediment close to the ripple crest follows a short path to the ripple crest and passes the sediment relatively fast and close to the sediment surface. Water penetrating in the centre of the troughs reaches deeper zones of the sediment, but all filtered water leaves the sediment through the emergence zone, a band comprising the central area of the ripple crest. Using the pore water flow field images, the lengths of the pore water pathways could be estimated, which, in the upper 10 cm of the sediment, ranged from 10 to 31 cm (average: 17.5 cm).

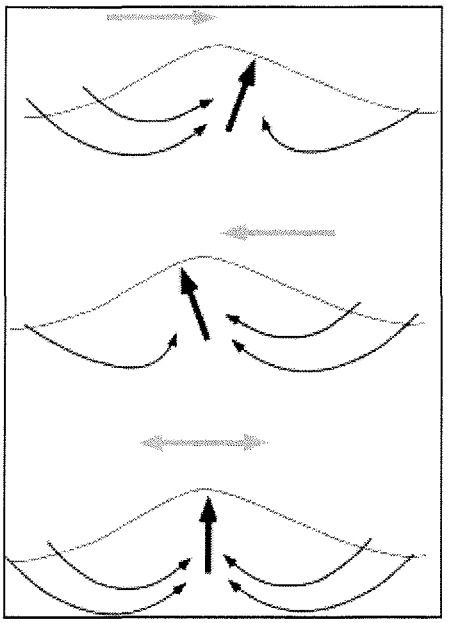

Fig. 5: Schematic overview of pore water flow field driven by oscillating flow interacting with a sediment ripple. Top and centre show the pore water flow field that would develop under steady unidirectional flow in opposing directions; the bottom drawing shows the averaged pore water flow field under oscillating flow as induced by surface gravity waves.

Pore water velocity

The pore water velocity measurements were conducted in the upwelling zone along a vertical line directly underneath the ripple crests. In all measurements, the tracer cloud passed by the optical sensors and created distinct peaks in the sensor signal. This is presented in Fig. 6, which shows the results of an experiment with three sequential dye injections.

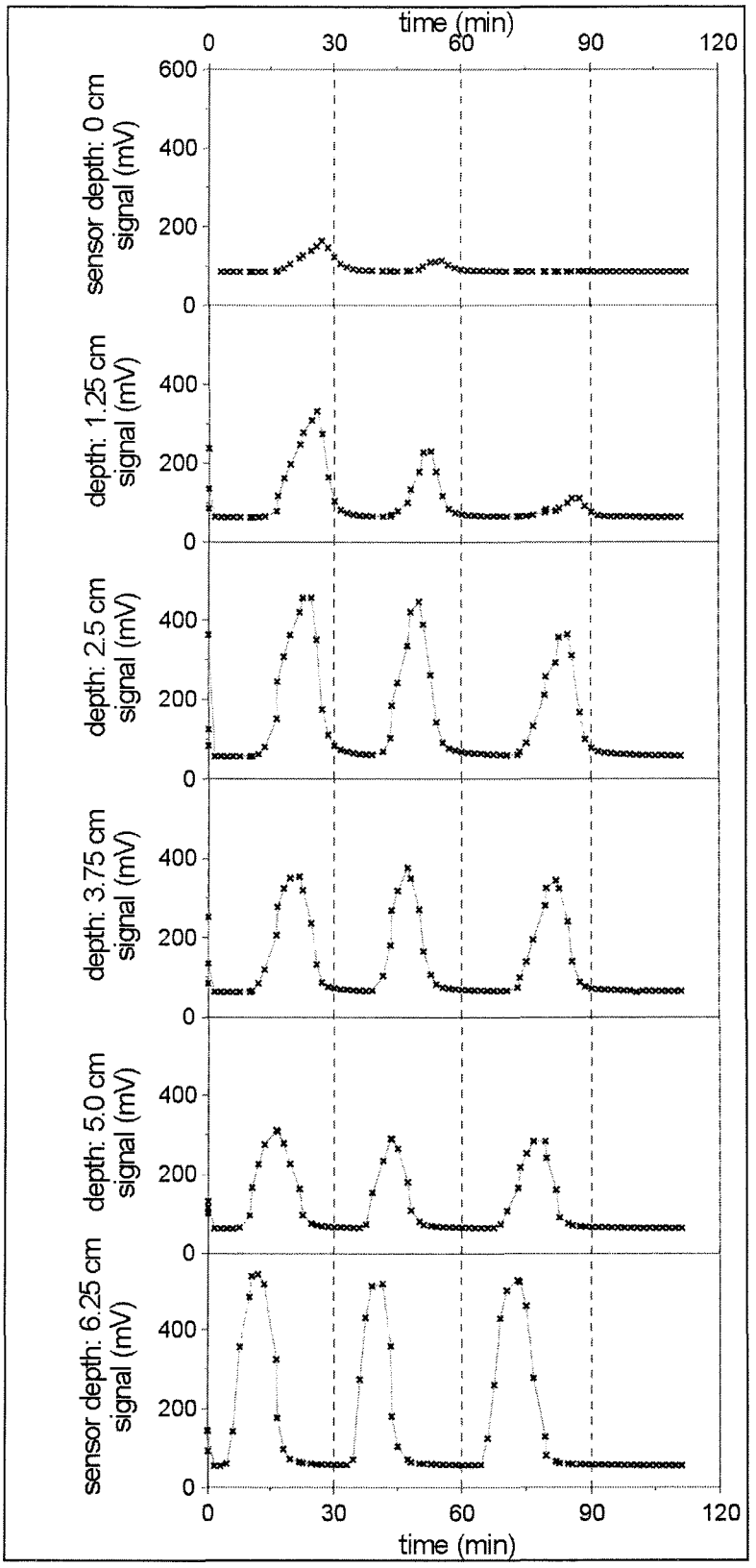

Fig. 6: Result of pore water velocity measurements: example with 3 successive dye injections passing the sensors on their path to the ripple crest.

The results of all other experiments looked similar. The matrix-averaged pore water velocity is the bulk velocity at which the tracer cloud moves through the sediment. It can be calculated from the distance of the signal peaks. The upward bulk velocity between 0 and 6.25 cm depth averaged over all valid measurements was 26 cm h^{-1} (sd=16.2, n=36). Fig. 7 shows a plot of the averaged vertical pore water velocities versus depth. It can be seen that the velocity decreased with depth with values ranging from 40 cm h^{-1} between the uppermost sensors to 15 cm h^{-1} between the lowest sensors.

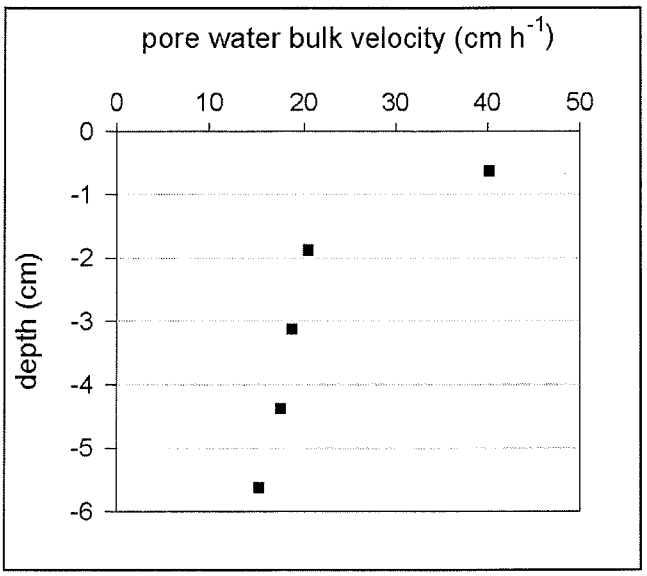

Fig. 7: Upward pore water velocity underneath ripple crest at various depths.

Pore water characteristics

The nutrient concentrations did not change significantly over the investigated sediment depth of 30 cm and were not significantly different from the nutrient concentration in the overlying water except for silicate. No accumulation of NO_3^-, NO_2^-, NH_4^+ or PO_4^{3-} in these layers could be detected. $Si(OH)_4$ was detectable with 11 µM (sd=4, n=18) in the pore water and 2.4 µM (sd=0.12, n=4) in the water column. The pore water solute concentrations were very low with measured concentrations of NO_3^-, NO_2^-, NH_4^+ and PO_4^{3-} around or below the detection limit of 0.3 µM in the pore water and water column samples.

Pore water salinity was ca. 39 and uniform over depth in the upper 30 cm of the sediments. Likewise, sediment temperature was 21.5°C down to 20 cm and showed no significant variations at the resolution of the sensors.

Discussion

In this study, we present direct in-situ measurements of interstitial flow velocities in permeable coastal sediment. The measurements reveal that even very weak wave action can produce rapid and effective pore water exchange in shallow permeable beds. In the sediments investigated, pore water velocities of almost 1 cm min^{-1} were reached near the sediment water interface.

The new optode technique proved to be a useful method for measuring the pore water velocities in-situ without disturbing the sediment structure. The optodes were embedded in the sediments such that pore water flow velocities were measured only in undisturbed sections of the ripples, and the thin optodes did not create additional pathways for pore water. A possible local sediment compaction caused by the optode insertion would reduce sediment permeability and therefore lower pore water flow velocities. While pore water velocities could be determined from the passage of concentration peaks by the sensor tips, a quantitative analysis of the dye concentration in the pore space was not possible. The strength of the fluorescence signals was not only dependent on the dye concentrations but also on the pore space geometry in front of the optical sensor, possible mechanical damage to the sensor tip or fouling. Efforts to calibrate the sensors in-situ to obtain quantitative data on dye concentrations were unsuccessful, which did not affect pore water velocity measurements but excluded assessment of phenomena like e.g. dispersion. Moreover, it can be inferred from Fig. 6 that the intensity of the fluorescence signals decreased at the upper measuring ports. This is probably due to the sensor array not being perfectly aligned with the pathway of the dye cloud. The dye cloud, which gets narrowed on its path to the sediment surface, then passes the upper sensors not centrally causing a weaker signal.

The transparent acrylic plates inserted into the sediment for pore water visualisation were more likely to affect the results as sections of the plates sticking out of the sediment could obstruct the flow. While this effect could be minimised by placing the plates perpendicular to the main direction of the oscillating flows, wall effects that may reduce the pore water velocity near the plate could not be excluded. Nevertheless, this technique produced reproducible results that were consistent with the optode measurements and the findings of previous studies suggesting that the artefacts linked to the wall effect were relatively small.

Pore water flows in permeable beds can be caused by a number of different processes, and in the following we discuss how these processes may have affected our observations. Interstitial water motion close to the swash zone can be linked to beach drainage after swash run up (Riedl and Machan 1972). Waves running up the beach could theoretically cause pore water motion as far away from the beach as where our measurements were carried out. This beach groundwater ideally flows on curved pathways through the beach back into the sea (Longuet-Higgins 1983; Li et al. 1999). On a larger time scale, also tidal dynamics may drive beach drainage (Nielsen 1990). Neither process could explain the observed flow pattern within the ripple. Furthermore, the swash zone only spanned a few centimetres during the measurements and as the study site is microtidal.

Density-driven convection due to salinity or temperature differences is another possible mechanism to drive interstitial flows (Webster et al. 1996; Rocha 2000). As the salinity measurements in the upper 30 cm of the sediment and the temperature measurements in the upper 20 cm showed no variability, this mechanism can be ruled out as driving force for the pore water flow patterns observed in this study.

The recorded pattern of water entering the sediment in the ripple troughs and emerging the sediment at the ripple crests supports the observations of Webb and Theodor (1968) and the model calculations by Shum (1992). In contrast to unidirectional flows that cause upwelling of fluid under the downstream slope of sediment ripples (Huettel and Gust 1992; Huettel et al. 1996), wave-induced oscillating flows can produce a symmetric pore water flow pattern relative to the sediment ripples as the strength of the flow is similar in both directions (Fig. 5). The water penetrating on both sides of the ripple and the acceleration of the pore water close to the sediment surface result in a narrowing and focusing of the centrally upwelling pore fluid. This flow field characteristic reduces mixing of the pore water moving from deeper sediment layers towards the surface.

With the measured averaged pore water velocity of 26 cm h^{-1} under the ripple crests (upper 6.2 cm), solutes in the pore water can effectively be transported over a distance of 1 cm in less than 3 minutes. The time it would take a solute to travel this distance by molecular diffusion can be approximated by $t=z^2 / 2D$ with t, z and D denoting time (s), distance (cm) and diffusion coefficient in water (cm^2 s^{-1}), respectively. The span of

biogeochemically relevant D values for ions, gasses and molecules in water ranges from 0.4 to 2×10^{-5} cm^2 s^{-1} (Jørgensen 2001). For oxygen in seawater with a salinity of 39 and a temperature of 22° C, the diffusion coefficient is 2.07×10^{-5} cm^2 s^{-1} (Li and Gregory 1974). In the sediment, the tortuosity of 2.99 (Boudreau 1996) has to be taken into account to assess the sediment's effective diffusion coefficient, which is, calculated after Boudreau (1996), 2.55×10^{-6} cm^2 s^{-1}. Using these values in above equation shows that diffusive transport of oxygen would need ca. 54 hours to overcome the distance of 1 cm in our sediment. Advective oxygen transport in our sediments due to the wave-topography interaction thus is more than three orders of magnitude faster than transport by diffusion alone.

A tortuosity of ca. 3 implies that the actual velocity of water flowing through the sediment's pore space is three times faster than the bulk velocity of a several centimeter wide solute cloud moving through the sediment. Under the ripple crest, this matrix-averaged velocity ranged from 40 cm h^{-1} close to the surface to 15 cm h^{-1} between 6.2 and 5 cm depth. The typical directional swimming velocity of a bacterium lies in the order of 2 μm s^{-1} (Jørgensen 2001), which equals ca. 1 cm h^{-1}. This value is 45 to 120 times lower than the interstitial velocities we measured corrected for tortuosity, which may explain why more than 90% of the bacterial cells in surface layers of permeable sea beds are attached to the mineral grains (Rusch et al. 2001).

The upward pore water velocity under the ripple crests can be used to assess the filtering rates of water through the sediment because the only areas where pore water was released from the sediment were the ripple crests.

With an average distance of 40 cm between neighbouring ripple crests, the total length of ripple crest per m^2 of sediment surface at our study site was approximately 250 cm. Multiplied with the averaged pore water upwelling velocity of 26 cm h^{-1} underneath the ripple crests, an average width of the release zone of 2.5 cm and the porosity of 36.9 %, this results in a filtering rate of ca. 140 L m^{-2} d^{-1}.

Advective filtering leads to enhanced transfer of suspended particles (Huettel et al. 1996) or phytoplankton (Huettel and Rusch 2000) into the sediment. During the measurement campaign, the particulate organic carbon (POC) content in the water column

of Campese Bay was approximately 0.4 mg C L^{-1} dry mass (C. Wild, unpubl. data). Assuming complete filtering of the particulate matter in the sediment, the filtering rate we assessed suggests that at the study site ca. 50 mg m^{-2} d^{-1} particulate organic carbon could be carried into the sediment by this wave-induced exchange process. This is in the same range as the findings of Durrieu De Madron et al. (2000) who found between 16 and 24 mg m^{-2} d^{-1} particulate organic carbon deposition on the shelf of the Gulf of Lion in the Mediterranean. Canfield and Teske (1996) calculated a median carbon oxidation rate of 164 mg m^{-2} d^{-1} for modern coastal sediments in water depths < 200 m from the findings of 60 studies. As 87.5 to 97 % of the carbon deposited at the seafloor is decomposed (Berger et al. 1989) our values are in the same order of magnitude but smaller, which can be attributed to the oligotrophic conditions in the Mediterranean.

Approximately 0.120 km^2 of Campese Bay have water depths shallower than 10 m. Assuming a filtering rate of 140 L m^{-2} d^{-1}, this section of the bay could filter ca. 6×10^6 m^3 a^{-1} of water through its sediments.

Impact of pore water flow on sediment chemistry

The rapid advective pore water exchange in the upper sediment layers is reflected in the pore water nutrient profiles. Only $Si(OH)_4$ displayed slightly elevated values in the sediment compared to the overlying water. This may be due to relatively large amounts of biogenic silicates (sponge spiculae, radiolarian shells, diatom shells) being filtered through, trapped and dissolving in the sediment.

In combination with the uniform pore water salinity and sediment temperatures, these findings indicate that at least the upper 30 cm of the sediment were completely and constantly flushed, linking pore water concentrations tightly to the solute concentrations in the overlying water column. Constant flushing of the sediment causes at least the upper 20 to 30 cm of the sediment to be in thermal equilibrium with the overlying water.

If the upper sediment layers are not completely flushed, anoxic pore water can be drawn to the sediment surface if the biogeochemical processes consumed all free oxygen in the deeper sediment layers. Assuming that all oxygen was stripped from the water filtered through the bed, the filtration volume of 140 L m^2 d^{-1} would produce an oxygen flux of ca. 30 mmol m^2 d^{-1} (with 0.217 mmol O_2 L^{-1} at 22°C and salinity=39 (Garcia and Gordon

1992)). Horizontal oxygen concentration gradients then develop in the upper sediment layers that are as steep as the vertical gradients providing ecological niches for organisms that profit from such gradients (e.g. metal oxidisers, (Huettel et al. 1998)).

The present study was carried out under hydrodynamic conditions under which the ripples were stationary. Stronger hydrodynamic forcing causes sediment ripples to migrate, and pore water is then released on one and trapped on the other side of the ripple (Elliott and Brooks 1997a). The magnitude of this process is negligible compared to advective pore water movement when the pore water velocity exceeds the bedform velocity (Elliott and Brooks 1997a). Traykovski et al. (1999) state after field observations on migrating wave ripples that these bedforms only move a few cm per hour (on the continental shelf at 11 m water depth; sediment median grain size=400 µm, ripple wavelengths typically 10 to 100 cm). With the pore water velocities we measured, this indicates that the pore water extrusion zone at the ripple crests could follow ripple migration. If the pore water that is drawn to the sediment surface by advection is anoxic, this entails that a vertical anoxic zone moves horizontally through the sediment, thereby exposing sediment alternately to oxic and anoxic conditions. Such a scenario can lead to the release of metals (Fe, Mn) and phosphate bound to iron from the flushed sediment layers.

Comparison with other studies

To our knowledge, very few studies dealt with in-situ measurements of wave-induced transport processes. Webb and Theodor (1968) worked at 3 m water depth under waves producing stronger bottom boundary flow than in this study. The sediment at their study site was coarser (median ca. 1000 µm) and thus more permeable. Calculations of filtering rates based on their estimates for pore water velocity (average 130 cm h^{-1}) underneath the ripple crests results in an averaged filtering rate of ca. 300 L m^{-2} d^{-1} (assuming a conservative release area width of 2 cm and a porosity of 37 %). This value is larger than our findings, due to the different wave and sediment characteristics, but lies well in the range of this study.

Compared to the findings of Riedl et al. (1972), who investigated wave pumping on the North Carolina Shelf, our results suggest a filtering rate that is 3 to 4 times larger and deeper penetration of the advective flows into the sea bed. The sediments Riedl et al.,

(1972) examined were slightly finer (250 to 177 μm mean grain diameter) but this may have been partly compensated by the stronger wave action that was present during their field experiments. The magnitude of the filtration rates we calculated from the in-situ measurements is also supported by wave tank experiments of Precht and Huettel (Chapter 2), which were carried out with a finer, less permeable sediment and smaller ripples than in Campese Bay but resulted in a filtering rate larger or in the same range as in this study (60 to 590 L m^{-2} d^{-1}).

The relevance of the wave-induced filtering may also be assessed by comparison with the effect of unidirectional boundary flows that are common in coastal and shelf environments. Interstitial flow induced by unidirectional currents was studied in the laboratory by Savant et al., (1987). These authors employed sand with a mean particle diameter of 370 μm, and a flow of 20 cm s^{-1} over ripples of 5 cm height and 50 cm wavelength. Thus, the physical parameters were comparable to those we found at our study site. These authors observed porewater flow velocities between 3.2 cm h^{-1} and 26.3 cm h^{-1}, and we measured values between 15.2 cm h^{-1} and 40.2 cm h^{-1}. This demonstrates that advective porewater motion induced by oscillating and unidirectional flow lie in the same order of magnitude.

The filtering rates calculated from measurements can be compared to the rates derived from the analytical model of Elliott (1990) that gives the pressure perturbation p created by a sediment ripple interacting with unidirectional flow as:

$$p = 0.14\rho u^2(\delta/0.34H)^{3/8} \qquad (1)$$

For $\delta/H \leq 0.34$ and with ρ, u, δ and H denoting density, mean current velocity, ripple height and water depth, respectively. From the pressure perturbation, the flow volume per area can be calculated:

$$w_0 = (2k/\rho\nu L_D)p \qquad (2)$$

With k, ν, and L_D denoting permeability, kinematic viscosity and decay length (= the length scale of the ripple), respectively (Huettel and Webster 2001). Using the measured values (u_{RMS}=0.09 m s^{-1}; δ=0.07 m; k=3.65 × 10^{-10} m^2; L_D=0.33 m and ν=1.024 × 10^{-6} m^2 s^{-1} (calculated after Krögel (1997)), this results in a mean pressure perturbation of 1.05 Pa, which yields a theoretical flushing rate of 191 L m^{-2} d^{-1}. This is in good agreement with our measured values.

The findings of previous studies on the magnitude of solute transport driven by different processes in the sediment are summarised in Fig. 8.

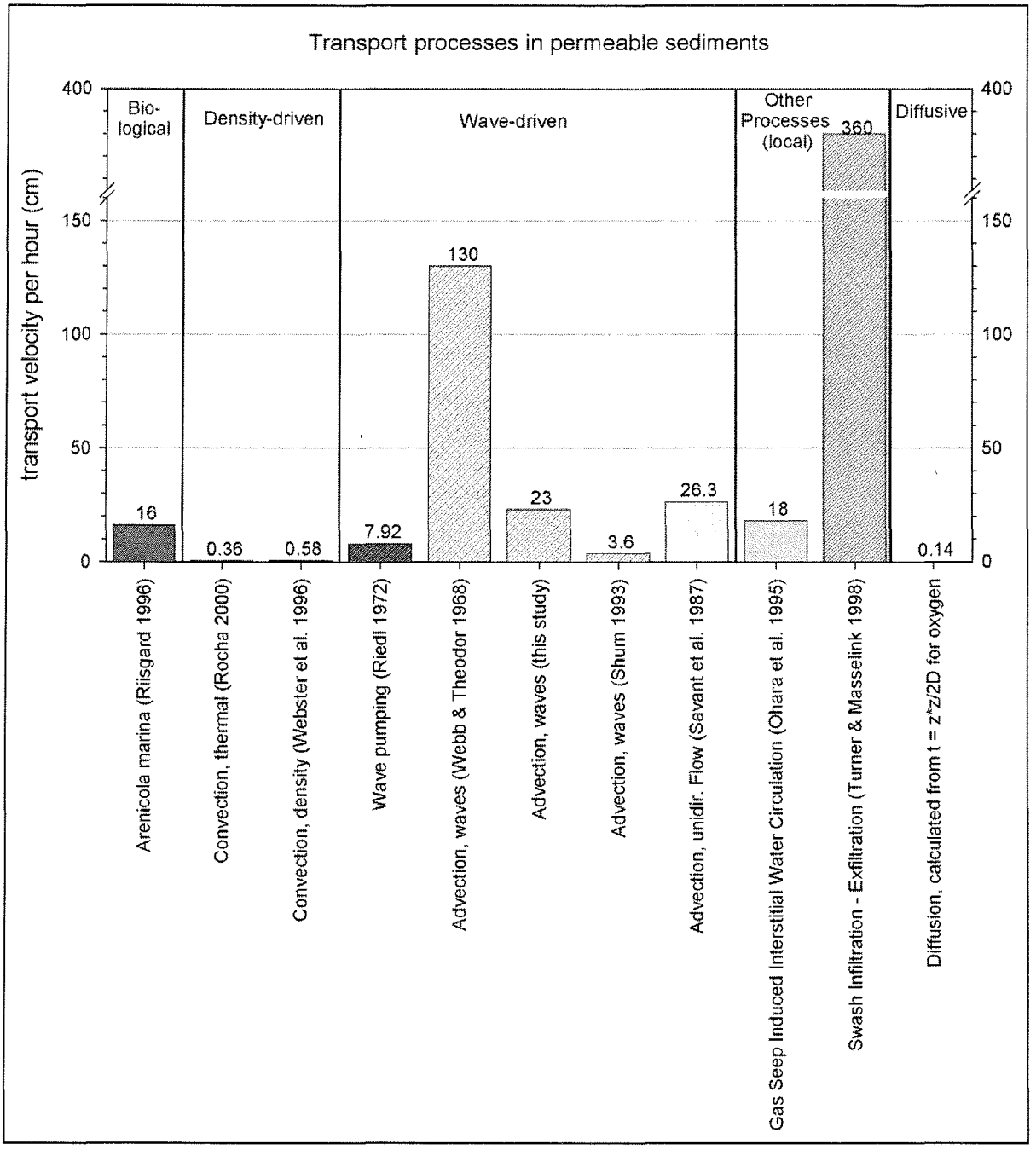

Fig. 8 Comparison of transport velocities in permeable sediments driven by different processes.

Fig. 9 shows the ensuing filtering rates of water through permeable sediments and reveals that wave-driven advective pore water flow and filtering substantially exceed the

magnitude of other wave-driven transport processes, with the exception of swash in- and exfiltration. The latter, however, has only a very limited spatial extent. The pore water velocities under unidirectional flow are very much comparable to those we found in this study, so it is likely that filtering rates can reach higher values than those that were reported so far.

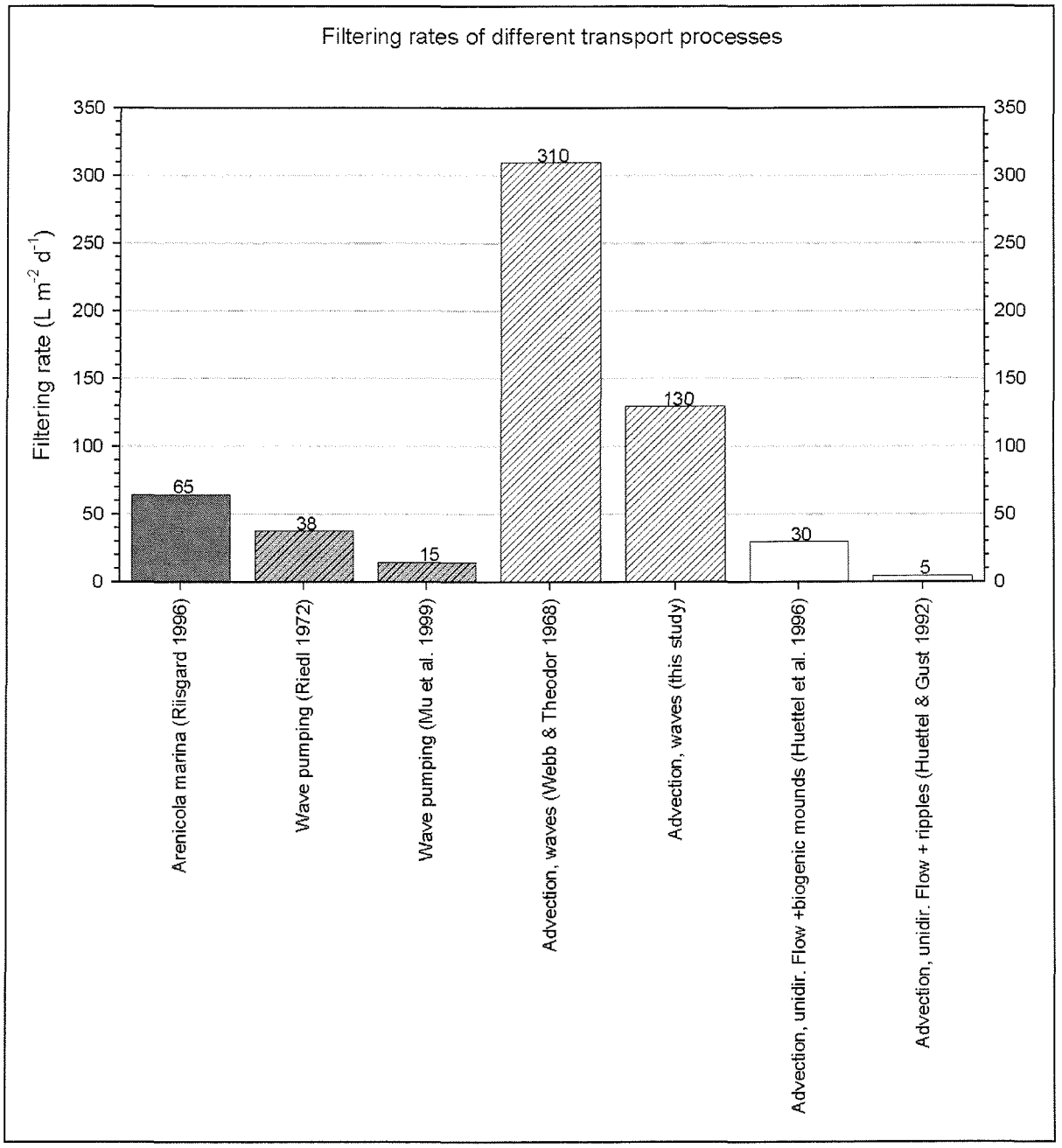

Fig. 9: Comparison of filtering rates through permeable sediments driven by different processes.

Applicability of data on a broader scale

In this study, we describe advective pore water exchange driven by the interaction of oscillating boundary flow with sediment topography rather than wave-related hydrostatic pressure oscillations. Webb and Theodor (1968) showed that these processes also occur in slightly deeper water. Wave-driven advection can take place in extended areas of the global shelves covered with permeable sediments where water depth < wavelength/2 where oscillating currents are generated at the seafloor which then interact with the sediment topography. The magnitude of the advective pore water exchange depends on sediment permeability, bed topography and near-bottom flow velocities.

Many of the sediments of the global shelf seas consist of coarse-grained relict sediments (Emery 1968) and a wealth of studies has described the abundance of sands and wave ripples on the continental shelves for a variety of study sites and water depths (e.g. Cacchione et al. 1999; Li and Amos 1999). The study of Black and Oldman (1999) carried out on the Australian and New Zealand Shelf showed that the sediment parameters at our study site can also be found in deeper shelf areas. These authors describe a 20 km wide zone between 20 and 45 m water depth with grain sizes of 300 to 900 µm and ripple wavelengths ranging from 30 to 100 cm, which is close to or larger than the values we found in Campese Bay. The similar sediment characteristics indicate that the hydrodynamic forcing at the seabed may be comparable at both study sites, suggesting that the magnitude of probable advective processes would also be similar. Taking the 20 km wide zone between 20 and 45 m water depth into account and assuming a filtering rate of 140 L m^{-2} d^{-1}, each 1 km of shelf could filter slightly more than 1 km^3 a^{-1} of water through its sediments in this zone alone. This value is considerably larger than the value of 0.419 km^3 a^{-1} of filtering by wave pumping that Riedl et al. (1972) assume for 1 km of an averaged global shelf transect from the beach to the 200 m isobath. This indicates that wave-driven advection is an important mechanism for the interfacial exchange of water, solutes and suspended particles in shallow shelf and coastal environments.

We conclude that for a given sandy coastal sediment with typical permeability, the bulk pore water velocities due to wave-driven advection we measured in-situ lie in the same order of magnitude (several cm h^{-1}) as those driven by advection due to unidirectional flows. The observed wave-driven advection was at least 3 orders of magnitude faster at our

study site than solute transfer by diffusion would have been. In shallow coastal environments, the pore water velocities and filtering rates caused by wave induced oscillating boundary flows interacting with sediment topography substantially exceed other wave-driven transport processes. The ecological significance of the filtration caused by wave - sediment topography - interaction is the efficient transport of organic substances and electron acceptors into the sands, thereby increasing the contribution of permeable sediments in the coastal mineralisation of matter.

Future research should attempt to assess pore water velocities under variable wave conditions, water depths and sediment characteristics in order to quantify the contribution of wave-related sediment filtration to the coastal cycles of matter.

4. Oxygen dynamics in permeable sediments with wave-driven pore water exchange

(in preparation for submission to Limnology and Oceanography)

Elimar Precht, Ulrich Franke, Lubos Polerecky and Markus Huettel

Max Planck Institute for marine Microbiology, Celsiusstrasse 1, D-28359 Bremen

Abstract

The effects of advective pore water exchange driven by shallow water waves on the oxygen distribution in a permeable ($k = 3.28\times10^{-12}$ to 4.85×10^{-11} m^2) natural sediment were studied with a planar oxygen optode in a wave tank. Our experiments demonstrate that advective pore water flow driven by the interaction of sediment topography and oscillating boundary flow changes the spatial and temporal oxygen distribution in the upper sediment layer. Oxygenated water intruding in the ripple troughs and deep anoxic pore water drawn to the surface under the ripple crests create an undulating oxic-anoxic boundary within the upper sediment layer mirroring the topographical features of the sediment bed. Magnitudes of pore water flow and sedimentary oxygen consumption determine the spatial dimensions of the oxic zones. In organic-rich coastal sediments, like the one we used, anoxic upwelling zones under ripple crests can reach the surface, thereby separating the oxic sediment areas of neighbouring ripple troughs. Horizontal oxygen concentration gradients develop that are in the same order of magnitude as in the vertical. The optode showed that migrating wave ripples are trailed by their pore flow field alternately exposing flushed sediment volumes to oxic and anoxic pore water until the ripple movement is too rapid (experimental threshold ≈ 20 cm h^{-1}) for the pore water to follow. Rapid ripple migration, thus, produces a continuous oxic surface layer that inhibits the release of reduced substances from the bed, which under slowly moving ripples is possible through the anoxic vertical upwelling zones. Swift, dramatic changes in oxygen concentration in the upper layers of permeable seabeds due to surface gravity waves challenge sedimentary organisms and affect organic matter mineralisation in the bed.

Acknowledgements

Hans Røy is thanked for initial discussions, helpful comments and help during fieldwork. We thank Susanne Menger and Martina Alisch for assistance with the experiments, sampling and analyses, and Volker Meyer and Georg Herz for their help with the electronics and the flume set-up. For assistance with the planar oxygen optodes, Gerhard Holst and Björn Grunwald are acknowledged. Bo Barker Jørgensen is thanked for support and interest in this work. The study was funded by the Max Planck Society (MPG).

Introduction

The dominant boundary layer flows in shallow marine environments are those generated by surface gravity waves. This dominance is reflected by the presence of wave ripples that structure large areas of shallow sandy seabeds that are abundant in coastal, estuarine and shelf environments. These sediments are permeable and thus allow interstitial water motion; therefore pressure differences at the sediment-water interface may drive interfacial solute transport. This advective transport can exceed transport by molecular diffusion by several orders of magnitude (Huettel and Webster 2001). In contrast to this, the major transport mechanisms in fine-grained muddy sediments are molecular diffusion and locally bioturbation (Berner 1980; Aller 1982).

Increased fluid exchange between sediment and overlying water affects the oxygen dynamics of permeable sediments and therefore also affects biogeochemical processes. Booij et al. (1991) showed in benthic chamber experiments that oxygen-rich water can be advected vertically into sandy sediment, which increased the oxygen penetration depth in the sediment as a function of the flow velocity of the overlying water. Advective in-sediment oxygen dynamics due to unidirectional boundary flow interacting with sediment topography were studied by Ziebis et al. (1996). Oxygen is transported rapidly and effectively into deeper sediment layers and may thus enhance mineralisation of organic matter (Forster et al. 1996). This organic matter may be transferred from the boundary layer into the top centimetres of the sediments as suspended particles or phytoplankton by advection (Huettel et al. 1996; Huettel and Rusch 2000). As further consequence of these processes, advective pore water flow can generate a complex biogeochemical zonation in the sediment with areas of enhanced nitrification or iron precipitation and vertical channels through which ammonium and reduced metals are transported to the sediment surface (Huettel et. al. 1998).

Surface gravity waves produce oscillating flows at the sediment-water interface by the wave orbital water motion (e.g. Denny 1988, p.54) in areas with a water depth shallower than half the wavelength of the waves. The ability of such oscillating boundary flows to drive pore water flow was shown by Webb and Theodor (1968, 1972) by injecting dyed water into coarse sandy near-shore sediment and observing its reappearance at the sediment surface. Shum (1992) calculated the pore water motion under a rippled bed over

one wave period with a two-dimensional computational model showing that the zone of advection extends several ripple heights below the ripple surface over a wide range of wave conditions and sediment characteristics. These transport studies suggest that waves, by enhancing advective fluid exchange between sediment and overlying water, also affect the biogeochemical processes in permeable beds similarly as unidirectional flows. Oxygen distributions underneath a rippled surface exposed to progressing waves modelled by Shum (1993) revealed that in permeable beds oxygen concentration gradients in the horizontal can be in the same order of magnitude as those in the vertical. In a wave tank study quantifying the wave-induced advective interfacial exchange, Precht and Huettel (Chapter 2) showed that horizontal tracer concentration gradients may be migrating with sediment topography (ripple) propagation. These authors suggested that this might be of significance for sediment oxygen dynamics as sediments might alternately be exposed to changing oxygen concentrations. These findings demonstrate that the classical one-dimensional approach frequently used to describe the distribution of pore water constituents and for measuring the related fluxes across the sediment-water interface is inadequate for sandy permeable sea beds (Shum and Sundby 1996).

The aim of the present study is to elucidate the effects of advection driven by oscillating boundary flow interacting with mobile sediment topography on the oxygen dynamics of natural sediment. To achieve this, experiments were carried out in natural sandy sediment in a laboratory wave tank with a planar oxygen optode.

Material and Methods

Sediment and Sediment preparation

The sediment employed in this study was collected on an intertidal flat in Königshafen Bay at Sylt Island in the German North Sea (55°02'N, 08°26'E) in February 2001 at a temperature of 4°C. Sediment was sampled in two layers: first, the top 2 cm of the surface sediment were collected, then the bulk sediment was retrieved down to 20 cm depth. These sediments were stored and transported separately and were combined again in the laboratory wave tank within 24 h of sampling. The wave tank was filled with approx. 1750 L of artificial seawater (instant sea) with a salinity of 31 and kept at a constant temperature of 17 °C.

The sediment surface was levelled by the foraging activity of a small *Carcinus maenas* crab, which also eliminated the initial abundant of *Hydrobia ulvae* mud snails. The sediment was left then under a constant recirculating unidirectional flow of ca. 5 cm s^{-1} for 12 months to regain a quasi-natural balance. In-fauna consisted mostly of oligochaetes of the Tubificidae family living in the upper 2 cm of the sediment. No nourishment was added to the wave tank during the first months of the set-up to prevent accumulation of nutrients. Starting 8 weeks before and during the experiments, Wakame algae powder (ground to a particle size between 125 and 250 µm) equivalent to an input of 1 g m^{-2} was added biweekly by suspending the material and evenly distributing it in the wave tank.

Sediment analyses

At the sediment sampling site, sediment cores (2.6 cm diameter, 12 cm long) were taken for measurement of in-situ permeability and porosity. Three representative sediment samples were additionally taken for grain size analyses. Before and after the experiments, sediment cores (2.6 cm diameter) were taken in the wave tank for analyses of permeability (ca 12 cm long), porosity (10 cm long) and grain size distribution (10 cm). Additionally, grain sizes and permeability of the upper 2.5 cm of the sediment were assessed.

For porosity and pore water analysis, the sediment subcores taken in-situ and from the laboratory wave tank were sectioned into 1 cm thick horizontal slices. Porosity averaged over depth, as calculated from wet and dry (after drying until constant weight at 60°C) weights of the sediment slices, was 37.1 % (sd 2.0, n = 10) in-situ, 34.0 % (sd 2.3, n = 20) before the experiments, and 36.2 % (sd 3.8, n = 30) after the experiments. The

sediment subcores used to assess the permeability were sealed after sampling and stored at 4°C until the measurements were carried out within a few days. Permeability was assessed using the constant head method (Klute and Dirksen 1986) directly on the retrieved sediment cores. Values for density and dynamic viscosity were calculated after Krögel (1997). In-situ sediment permeability was 7.55×10^{-12} m^2 (sd = 1.40×10^{-12} m^2; n = 4) and wave tank permeability 3.28×10^{-12} m^2 (sd = 0.75×10^{-12} m^2; n = 2), with higher permeability of the surface sediment (upper 2.5 cm) of 4.85×10^{-11} m^2 (sd = 0.42×10^{-12} m^2; n = 3). In-situ grain size distribution was determined by desalination, drying and sieving with a set of 8 sieves. The median grain size of the sediment was 180 μm.

Wave tank set-up

The laboratory wave tank used in this study was made of clear acrylic and had an open channel section of 520 cm length with rectangular cross-section (50 cm high, 47 cm wide). Two acrylic boxes were put into the open channel section as placeholders ("upstream" box: 240 cm long, "downstream" box: 120 cm long, both 19 cm high and spanning the entire width of the channel) such that the gap between the two boxes had a width of 120 cm that could be filled with sediment (Fig. 1). Filled with a sediment layer of 22 cm depth this amounted to a sediment volume of 124 dm^3. The placeholders in the open channel section were covered with 3 cm of sediment to create an overall even surface with uniform roughness throughout the open channel section. Initially, the sediment surface was level and all subsequent ripple formation was the response of the bed to the applied wave-action. Waves were generated at the upstream end of the wave tank with a paddle driven by an electric motor, controlling wave amplitude by the stroke of the eccentric and wave frequency via motor speed. This set-up permitted reproducible generation of sinusoidal waves of selected amplitude and frequency. At the downstream end of the wave tank, the dissipation of the waves was achieved by an artificial beach made of an acrylic plate of 1 m length covered by a 10 cm thick mat of highly permeable plastic foam causing the waves to run up and break.

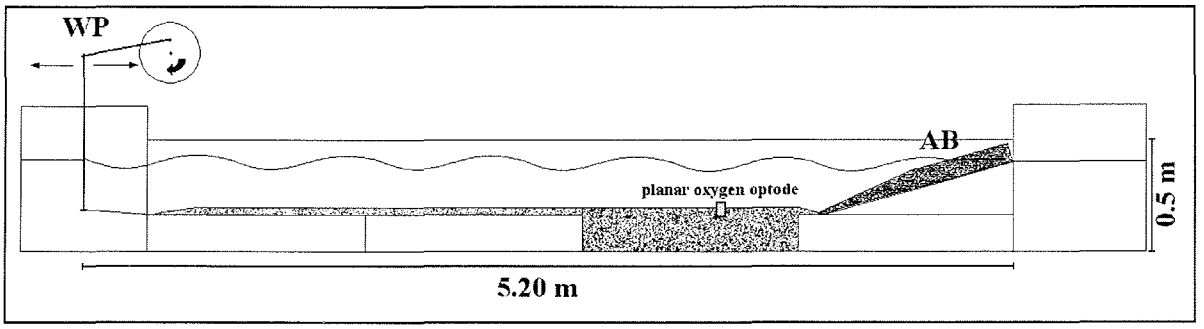

Fig. 1: the wave tank set-up; WP = wave paddle, AB = artificial beach.

Hydrodynamics

The hydrodynamic conditions in the wave tank were measured using a three-beam DANTEC™ LDA (Laser Doppler Anemometer) system in the backscatter mode. This LDA technique allows three-dimensional measurements of the flow velocity in a spheroidal measuring volume 600 μm long and 70 μm in diameter. During the experiments, vertical velocity profiles (120 mm to 0.5 mm above the sediment) of the horizontal and vertical velocities were measured above unrippled sections of the experimental sediment surface. In the water layer closer than 6 mm to the sediment-water interface, the LDA set-up only allowed the measurement of the horizontal velocity component. During the experiments in which ripples formed, the root mean square values of the horizontal velocity (U_{RMS}) 12 cm above the sediment surface ranged from 0.12 m s^{-1} to 0.14 m s^{-1}. In the experiments with flow not sufficient to initiate sediment mobilisation, the U_{RMS} was around 0.06 m s^{-1}.

Oxygen measurements

The 2-dimensional oxygen distribution was measured with a planar semi-transparent oxygen optode (3.7 cm wide, 5.7 cm high) glued to the inside wall of the wave tank such that 2.7 cm of the optode were above and 3 cm were below the sediment-water interface. The optical oxygen measurement is based on the dynamics of collisional quenching of the luminescence of an indicator by oxygen (Kautsky 1939). The planar sensing foils consisted of 2 layers: a transparent polyester support foil (125μm thick, Goodfellow, Bad Nauheim, Germany) and a sensing layer. The luminescent oxygen indicator of the optode, platinum(II) meso - tetra (pentafluorophenyl) porphyrin (Pt-PFP) (Porphyrin Products, Logan, USA), was immobilised in a polystyrene matrix (Sigma-Aldrich, Weinheim, Germany). To increase the amount of excitation light within the sensing layer, titanium

dioxide (TiO_2) particles (< 5µm, Aldrich, Weinheim, Germany) were added. These particles do not interfere with the quenching but enhance the signal by scattering. Therefore they increase the output luminescence signal on the expense of loosing a clear view of the structure behind the sensor (Klimant and Wolfbeis 1995). The thickness of the semi-transparent sensing layer was approximately 30 µm, resulting in an overall thickness of the planar optode of 155 µm.

The O_2-distribution measurements were conducted by the specially developed modular luminescence lifetime imaging system MOLLI as described by Holst et al. (1998) and Holst and Grunwald (2001). The planar optode was illuminated by blue (λ_{max} = 475 nm) excitation light of light emitting diodes (LED's, HLMP-CB 15, Agilent, USA) and the luminescence (λ_{max} = 647 nm) emitted by the optode was filtered with a red optical filter (80 % transmission at ≥ 620 nm; Deep Golden Amber, LEE-Filters, U.K.) to remove most of the reflected excitation light. The luminescence images of the planar optode were recorded using a CCD Camera (SensiCam, Optosens, Germany) with a resolution of 640 × 480 pixels. The images covered an area of 24 × 19 mm^2. Taking the thickness of the sensing layer (30 µm) and the spatial resolution of the imaging system into account, the spatial resolution of the oxygen images was 40 × 40 μm^2 $pixel^{-1}$. In order to determine the distribution of oxygen concentrations, the 2D luminescence lifetime distributions were evaluated by the so-called rapid lifetime determination (RLD) method (Woods et al. 1984; Ballew and Demas 1989; Liebsch et al. 2000). Further image processing was carried out with a custom-made computer program (Holst and Grunwald 2001). The planar optode was calibrated before and after the experiments by recording images corresponding to 0% and 100 % air saturation. The measured luminescence lifetime distributions were converted into oxygen concentration values by a modified two component model of the Stern-Volmer equation (Klimant et al. 1995; Holst and Grunwald 2001). The accuracy of the used oxygen optode is approx. ± 1% at 100% and ± 0.15% at 0% air saturation (Liebsch et al. 2000).

Sediment topography

The sediment relief in front of the planar optode had to be assessed simultaneously with the oxygen measurements. This was achieved by a CCD camera positioned on the side of the wave tank opposite to the planar optode. The camera field of vision covered the area of the planar optode and was fixed slightly elevated in a 10° downward angle so that the sediment

topography not directly in front of the optode did not obstruct vision (Fig. 2). The camera was triggered simultaneously with the diodes that emitted the excitation light for the oxygen measurements. Thus, the obtained images showed the planar optode with the background light of the diodes and partly darkened by the respective sediment relief. The sediment relief was assessed from these images with an edge-detecting algorithm using the transition between dark and light regions of the image corresponding to the sediment surface relief. With 3 fluorescent marking points, the horizontally mirrored image of the sediment surface relief and oxygen distribution images could be precisely aligned. The sediment relief line was superimposed to the oxygen distribution images in a batch conversion routine. Time sequences of the resulting composite images were combined to produce animations of the oxygen dynamics in the sediment simultaneously showing the changes of the sediment relief.

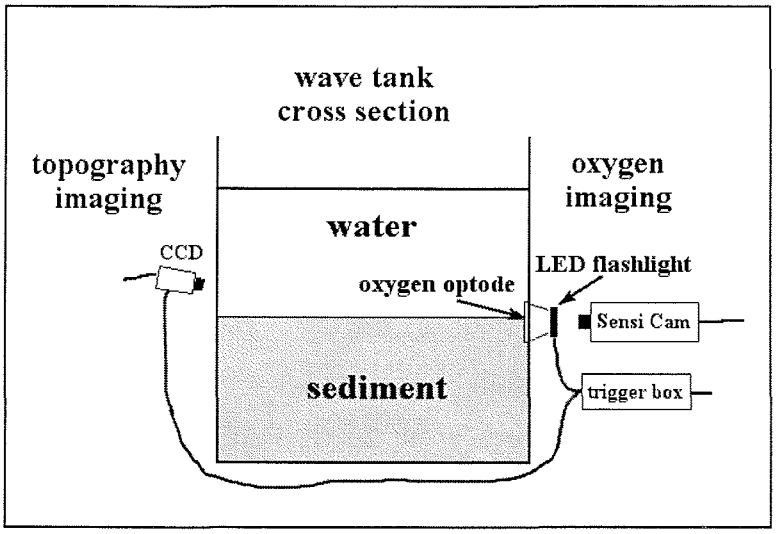

Fig. 2: Side view of the set-up for the simultaneous oxygen and surface topography imaging, in the wave tank.

Experiments

To assess pore water velocities and pore water flow pattern under typical wave conditions, an experiment was carried out with waves equivalent to those in Exp 2, 5, 6 and 7 (Table 1). Prior to the experiment, the sediment surface was levelled. After the waves were switched on, ripples formed (wavelength = 2.5 cm, amplitude = 0.5 cm), and Rhodamine WT solution was injected into the sediment at various locations adjacent to the transparent wave tank wall next to the planar optode, ripple troughs and crests included. The

development of the dye clouds in the sediment was recorded in high-resolution photographs taken at distinct time intervals (15 or 60 s). From the dye migration, the pore water velocity could be assessed.

Seven successful wave tank oxygen dynamics experiments were conducted between April and June 2002. All experiments were carried out with surface gravity waves of variable lengths and heights. The bed was smoothed before the experimental runs, and no artificial roughness elements were placed on the sediment surface. Exceptions were Exp 3 and 4, which were carried out with the remaining sediment topography of the previous experiment to test the case of identical sediment topography and decreased flow velocities. During all experiments, oxygen images measured by the planar optode together with the sediment relief images were recorded. The experimental parameters relevant to the different experimental settings are listed in Table 1.

Table 1: Experimental parameters.

Experiment	Exp 1	Exp 2	Exp 3	Exp 4	Exp 5	Exp 6	Exp 7
date	16-May-02	16-May-02	27-May-02	30-May-02	05-Jun-02	26-Jun-02	08-Jul-02
duration (h)	4.5	15	1.5	3.5	26	5	36
water							
temperature (°C)	17	17	17	17	17	17	17
salinity	31	31	31	31	31	31	31
waves							
wave height (cm)	8	8	7	3	8	8	8
wave length (cm)	80	70	80	120	70	70	70
period (s)	0.75	0.75	0.8	1	0.75	0.75	0.75
type	shoaling	shoaling	sinusoidal	sinusoidal	shoaling	shoaling	shoaling
flume							
water depth (cm)	20	17	17	17	17	16.5	17
Sediment depth (cm)	20	20	20	20	20	20	20
measurements							
planar optode	Yes	Yes	Yes	Yes	Yes	Yes	Yes
sediment relief	Yes	Yes	Yes	Yes	Yes	Yes	Yes
LDA	No	Yes	No	Yes	No	No	Yes
ripples							
sediment surface	flattened	flattened	existing topography	existing topography	flattened	existing topography	flattened
first ripples (min)	15	15	0	0	15	0	15

Results

Pore water velocity

Figure 3 shows the directions of pore water movement with the corresponding velocities assessed from the measurements of the injected dye clouds. Water enters the sediment at the ripple troughs and leaves it at the ripple crests. Pore water velocities are higher closer to the sediment and lie in the range of cm h^{-1}.

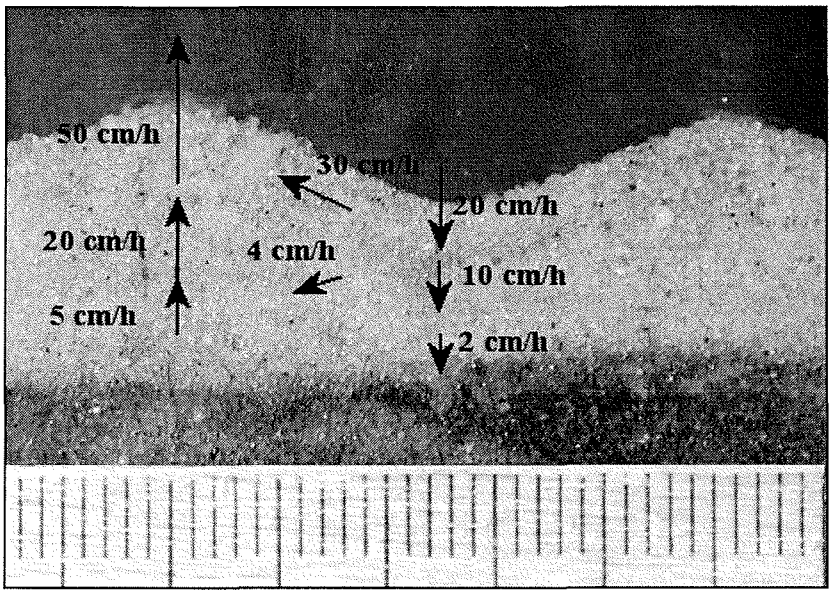

Fig. 3: Summary of pore water velocity measurements conducted with soluble tracer. The arrows indicate the observed pore water directions and are not to scale. The mm scale of the image is shown at the bottom.

Oxygen measurements

The average oxygen penetration depth into the sediment under stagnant conditions without waves was approx. 3 mm. This oxygen distribution governed predominantly by molecular diffusion was only locally altered by bioirrigation by oligochaetes (Fig. 4).

After the waves were switched on, but prior to the formation of sediment ripples, the oxygen penetration depth slowly increased to 5 mm in about 80 min (Fig. 5). This effect may be attributed to advection associated with small-scale surface roughness or wave pumping. However, we could not detect any pumping effects in the form of a pulsing of oxic or anoxic pore water, even when using the highest possible temporal resolution achievable by the MOLLI system (1 Hz).

Figures 4 and 5 show non-saturation oxygen values in the water column. This is an effect that occurs when large anoxic areas are imaged by the oxygen optode. Due to reflections of

the luminescent light within the acrylic wave tank wall, anoxic regions of the studied area affect the measurements in neighbouring oxic regions. Although a reverse influence also takes place, the former one is more pronounced because of the stronger luminescence intensity generated within anoxic regions. This effect lowers the spatial resolution of the obtained oxygen images, but on a lower spatial scale than required to observe the principles of the processes studied here.

After ripples formed in front of the planar optode, the interaction of oscillating boundary flow and sediment topography induced advective pore water flow. This pore water flow caused changes in the oxygen distribution in the sediment that could be recorded with the optode. Upwelling of anoxic pore water from lower sediment layers led to an oxygen-depleted zone underneath the ripple crests. In the ripple troughs, oxygen-rich water from the water column was forced into the sediment generating oxygenated zones in the sediment reaching a maximum depth of 1 cm (wave amplitude = 8 cm, wavelength = 80 cm, ripple amplitude = 0.4 cm, ripple wavelength = 2.9 cm). Thus, the pore water flows produced an oxygen distribution pattern reflecting the structure of the ripple topography with alternating oxic and anoxic zones associated with ripple troughs and crests, respectively (Fig. 6).

This oxygen distribution led to horizontal oxygen concentration gradients underneath the ripple that were comparable to the vertical ones (Fig. 7).

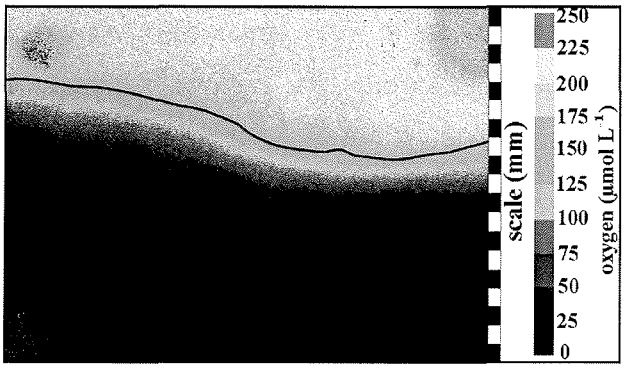

Fig. 4: Oxygen image under stagnant conditions without waves (Exp 3). The black line indicates the sediment surface relief.

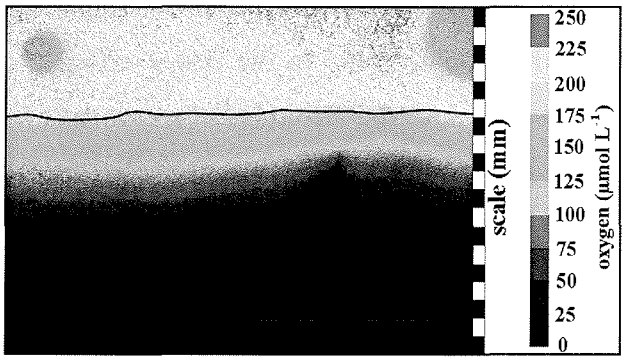

Fig. 5: Oxygen image demonstrating an increased oxygen penetration depth under oscillating flow in the absence of sediment topography (Exp 6). The black line indicates the sediment surface relief.

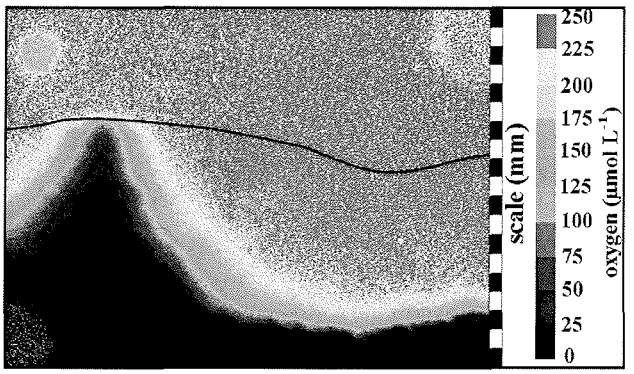

Fig. 6: Image of oxygen distribution linked to a stationary sediment ripple under oscillating flow (Exp 1). The black line indicates the sediment surface relief.

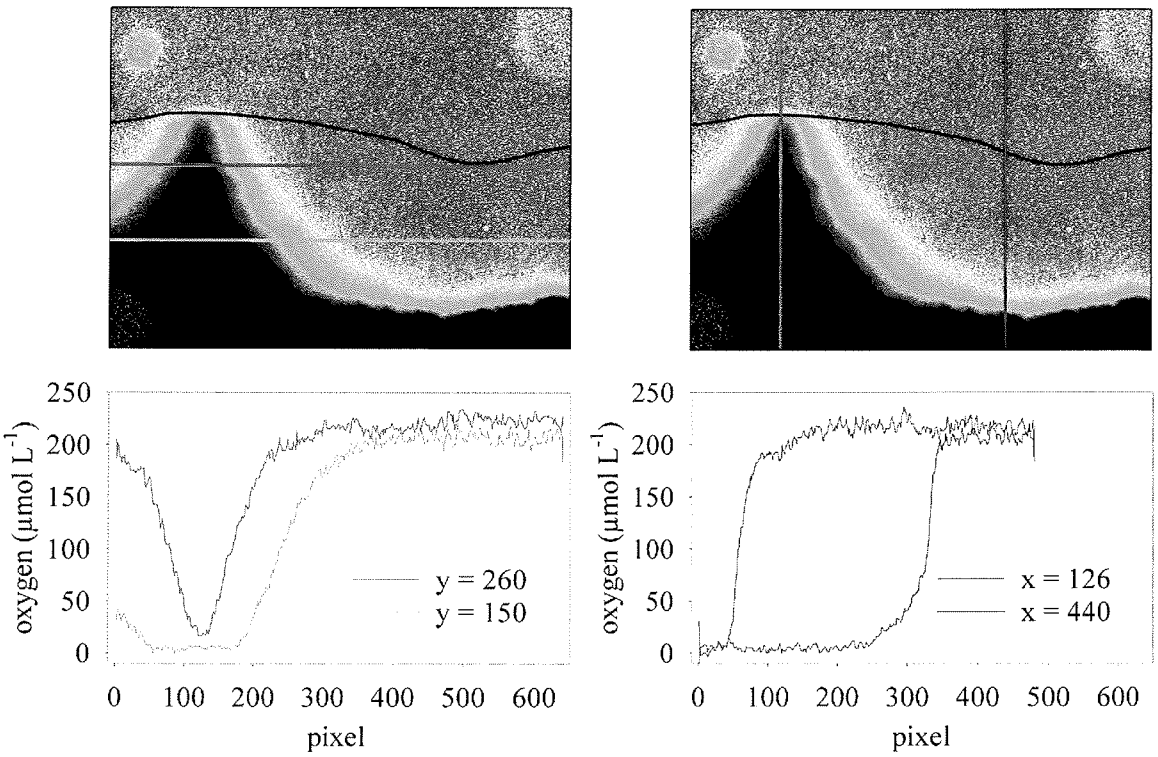

Fig. 7: Horizontal (left) and vertical (right) oxygen concentration gradients extracted from optode image underneath a stationary ripple under oscillating flow (Exp 1). The black lines indicate the sediment surface relief; the coloured lines show the extracted profiles. Scale and colour code see Fig. 6.

In the experiments with existing sediment ripples in front of the optode and flow that was not strong enough to initiate further sediment movement, it could be observed that the final oxygen distributions in the sediment were similar regardless of the hydrodynamic forcing. With decreasing wave energy, the time needed to reach the final equilibrium was increased (from 46 min in Exp 3 to 216 min in Exp 4), showing that the pore water flow pattern is dependent on the sediment topography, whereas the pore water velocity is dependent on the magnitude of the hydrodynamic forcing.

In the case of sediment ripples migrating in front of the planar optode, the pore water flow field and the associated oxygen distribution migrated with the ripples, alternately exposing sediment to oxic and anoxic conditions. This is shown in Fig. 8 presenting a series of oxygen distribution patterns under slowly migrating ripples.

The effect of sediment being alternately exposed to variable oxygen concentrations is depicted in Fig. 9, showing oxygen profiles extracted from the same vertical row of pixels

of the 2-dimensional oxygen images as a function of time. Figure 9 demonstrates how an initial equilibrium phase (75 min) was succeeded by a phase with ripple migration causing pronounced oxygen changes in the sediment. The redox conditions at one single vertical profile in this case changed 6 times from anoxic to oxic within 90 min.

In the case of faster migrating ripples, the upwelling zones start to lag behind the ripple crest and show only oxygen depletion but not completely anoxic conditions. This is the case when the ripples migrate at rates between 10 and 20 cm h^{-1} (Fig. 10). When the ripple migration velocity exceeds the pore water flow velocity (experimental threshold ≈ 20 cm h^{-1}), it was observed that the anoxic zone underneath the ripple crest becomes completely detached from the ripple topography, leading to a thick, uninterrupted oxygenated sediment surface layer (Fig. 11).

After the waves were switched off, the effect of oxygen consumption of the sediment could be observed with the optode. The zone of oxygen-depletion in the sediment slowly moved upwards until oxygen distributions reached the pre-experimental state with a homogenous oxygen penetration depth of about 3 mm. Without pore water flow, the oxygen distribution was governed by oxygen consumption and molecular diffusion. The oxygen consumption rates of the sediment at specific depths could be calculated by extracting time series of oxygen values (averaged over 10 × 10 pixels) from the 2-dimensional oxygen distribution images at selected sediment depths recorded after the waves had been switched off. The maximum measured respiration rate for the deeper sediment layers was approx. 1.3 µmol L^{-1} min^{-1} (Fig. 12).

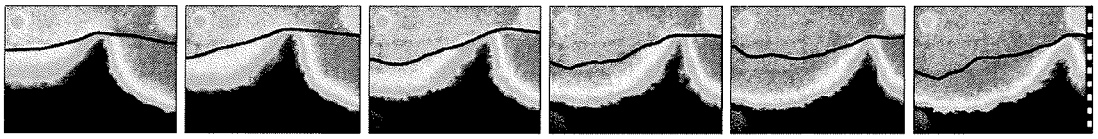

Fig. 8: Time-series of images of oxygen distributions under a slowly migrating ripple with a fully developed mobile upwelling zone. Colour code see Fig. 4, 5 or 6. (image interval: 1 min; Exp 6).

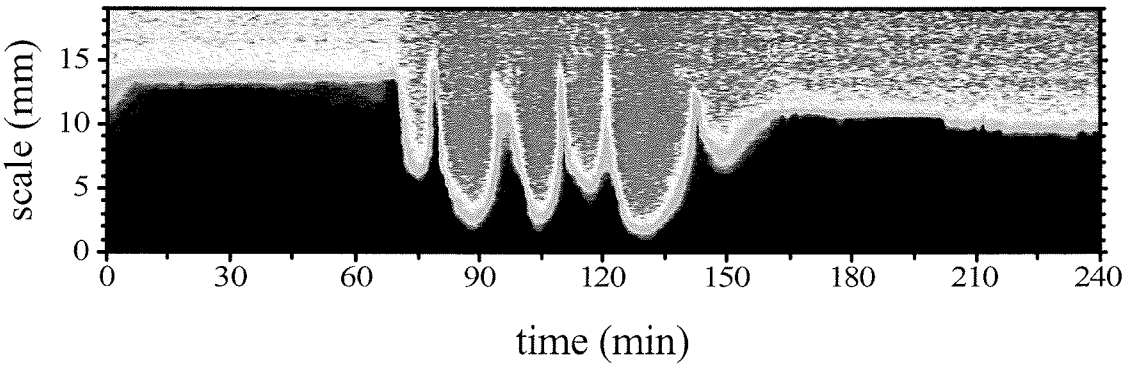

Fig. 9: An example of a time-series oxygen profile extracted from one selected vertical row of pixels of the planar optode images, revealing a temporal exposure of the sediment to redox oscillations. Colour code see Fig. 4, 5 or 6 (Exp 6).

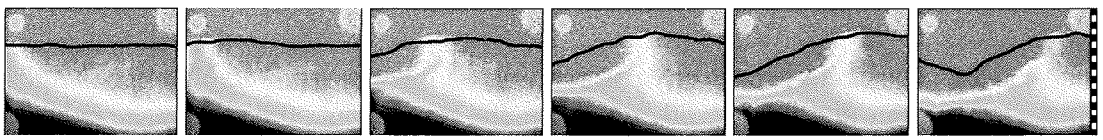

Fig. 10: A time-series of oxygen distributions under a migrating ripple with an upwelling zone lagging behind the ripple crest. Colour code see Fig. 4, 5 or 6 (image interval: 2 min; Exp 2).

Fig. 11: A time-series of oxygen distributions under a fast migrating ripple with no upwelling zone linked to ripple crests. Colour code see Fig. 4, 5 or 6 (image interval: 2 min; Exp 2).

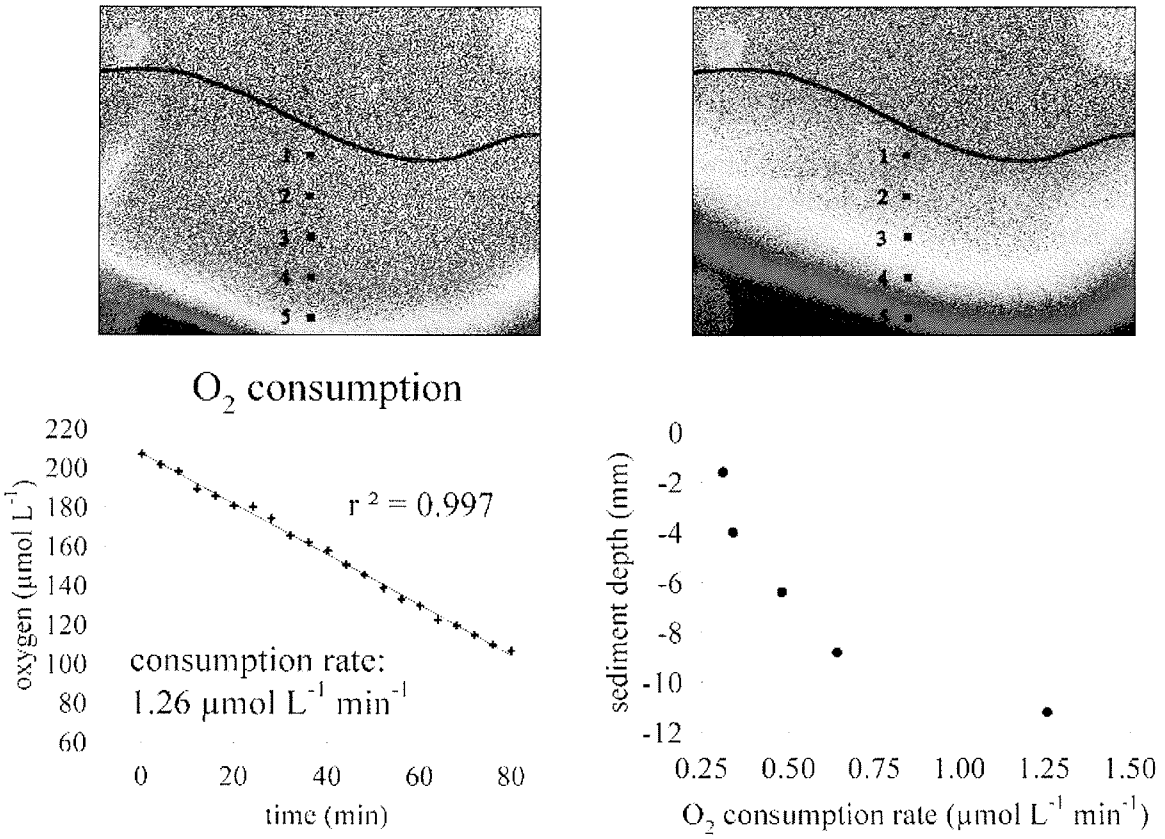

Fig. 12: Upper left: optode image of oxygen distribution directly after Exp 1; upper right: optode image of oxygen distribution 80 min after the experiment; the 5 squares indicate areas of 10 ×10 pixels over which the oxygen consumption rates were calculated; lower left: plot of oxygen concentration at area 5 over time and inferred oxygen consumption rate; lower right: plot of the oxygen concentration rates as a function of depth. Scale and colour code see Fig. 4, 5 and 6.

Discussion

We showed in a previous study that the interaction of wave-generated oscillating boundary flows and ripple topography produces zones of up- and downwelling of pore water in permeable sands that propagate with ripple migration (Precht and Huettel, Chapter 2). These finding suggested that waves can produce a complex and dynamic oxygen distribution in sandy sea beds that would strongly influence benthic organisms and sediment biogeochemistry.

Here we demonstrate that wave-driven advective pore water flow associated with sediment wave ripples creates a pattern of sediment zones where oxygen-rich water is forced into the bed alternating with zones where anoxic pore water is drawn to the surface. The spatial and temporal distribution of these zones is closely related to the ripple topography and its changes. Because the oxygen distribution under such a rippled surface changes mainly in two dimensions, the planar oxygen optode technique proved to be a powerful tool to investigate the two-dimensional distribution and dynamics of the oxygen distribution at the spatial and temporal scales of the pore water flow field.

While sediment permeability, ripple height and spacing, and magnitude of boundary currents control the advective pore water flow directions, velocities, and penetration depths (Huettel and Webster 2001), the penetration of oxygen additionally depends on the consumption rates in the flushed sediment layers. The oxygen distribution pattern we observed, thus, is a complex result of oxygen injection into specific areas with ensuing directed oxygen transport along lines of equal pressure, and sedimentary oxygen consumption characterised by a vertical gradient with higher rates in the deeper layers. The waves transformed the smooth sediment with a thin continuous oxygenated surface layer into a rippled bed with a thick oxygenated layer interrupted by anoxic zones of upwelling deep pore water. Consequently horizontal oxygen concentration gradients developed in the sediment of the same order of magnitude as the vertical gradients, as has been predicted by Shum (1993).

The advective oxygen transport in our sediments due to the wave-topography interaction was more than one order of magnitude faster than transport by diffusion (with our settings 0.13 cm in one hour) explaining the relatively deep oxygen penetration into a sediment with oxygen consumption rates of 0.33 to 1.26 $\mu mol\ L^{-1}\ min^{-1}$. In permeable sediments with a

homogenous permeability, the vertical extension of the pore water flow field equals approximately the ripple wavelengths (Rutherford et al. 1995). The maximum oxygen penetration depth we could observe in the ripple troughs was 14 mm, which corresponds to 18 mm below the flat sediment surface. With ripple wavelengths between 25 and 30 mm, the oxygen penetration depth we observed was slightly lower than the sediment depth theoretically affected by advection demonstrating the dominance of oxygen injection over oxygen consumption although our sediment had consumption rates common in shelf sediments. Due to this dominance, pore water flushing caused by the interaction of oscillating boundary flows and ripple topography increased the oxic sediment volume more than 3-fold in our experiments compared to the situation with stagnant water column and diffusive transport only.

The sharp boundaries of the dye patterns in our previous wave tank experiments (Precht and Huettel, Chapter 2) revealed that the pore water drawn to the surface under the ripple crest mixes very little with pore water of adjacent sediment zones. The fluid basically flows to the surface along streamlines that do not cross except the mixing caused by dispersion in the porous medium. Because the pore water ascends from different biogeochemical reaction zones, a pattern develops with upwelling flows that differ in their solute inventories. These pore water flows focus and narrow approaching the ripple crest where fluid of different composition (and residence time in the sediment) emerges through narrow bands paralleling the crests (Fig. 13). With increasing distance from the centre zone, these "emergence bands" release pore water from lesser and lesser depths and with shorter residence times in the sediment. As revealed by the oxygen concentration pattern under the stationary ripple (Fig. 6) this produces bands of distinctly different geochemical characteristics at the sediment surface which may be reflected e.g. by bands of different iron precipitates (Huettel et al. 1998). Micro-organisms like e.g. sulphide oxidisers, denitrifiers or iron oxidisers may profit from such patterns and the steep concentration gradients they produce (Fig. 7). While the central upwelling zone may carry refractory DOM, Fe^{2+} and ammonia to the surface, "outer" zones may release more labile DOM and NO_3^- resulting from the enhanced organic matter decomposition and nitrification in the ripple slopes.

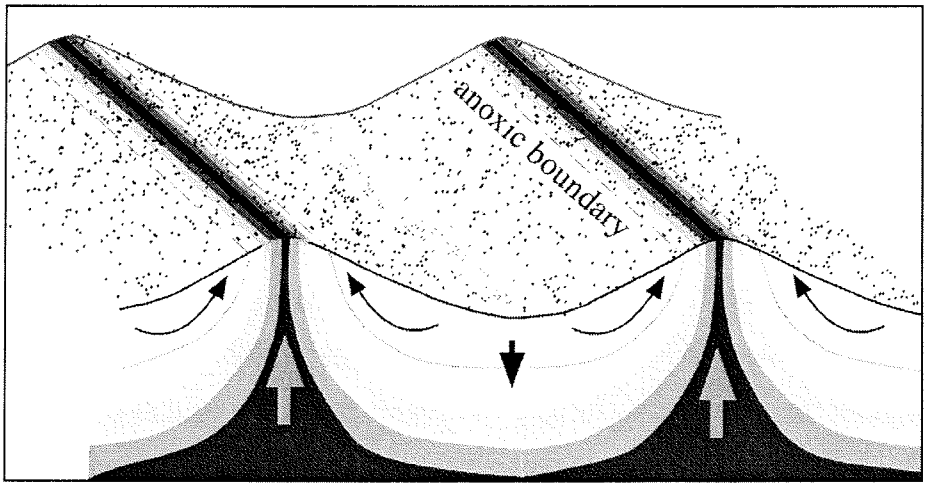

Fig. 13: Schematic drawing of the biogeochemical reaction zones underneath stationary ripples created by wave-induced advective pore water flow. In the center of the release areas, pore water from the deepest reaction zones emerges while at the outer edges of these areas, pore water leaves the sediment that resided shorter in the sediment and therefore has different solute content.

The situation in the ripple troughs is different because no solutes can be released from this area as molecular diffusion cannot counteract the water flow into the sediment. This implies that flux out of rippled permeable sediments averaged over larger areas only occurs through a fraction of the actual sediment surface area that is confined to the ripple crests. In our experiments, the total width of the upwelling zone at the ripple crest was between 6 and 8 mm, while the sediment band separating these zones was approximately 20 to 24 mm wide. This resulted in a ratio of uptake to release area of about 3, while the volume flow through both areas is the same for reasons of mass balance (which explains why the upwelling pore water flow reaches higher velocities than the downwelling flows, Fig. 3). As the width of the upwelling zone linked to each ripple should be proportional to the ripple wavelength, we conservatively estimate that also in natural environments the flux from a permeable sediment into the water column occurs only in < 30 % of the actual sediment surface areas in sea beds where advective exchange is effective. This demonstrates how tightly the fluxes into and from permeable seabeds are linked to surface topography. The same sediment exposed to the same boundary layer flows can show very different fluxes if large waves or biological activity produced new topography. Likewise, bioturbation can reduce fluxes by destroying ripple topography.

Oxygen consumption in the sediment counteracts the vertical oxygen penetration in the ripple troughs. High oxygen consumption decreases the depth down to which the sediment turns oxic by advective flushing and widens the width of the anoxic zones at the ripple crests. Where oxygen consumption rates are low, the complete sediment surface layer may be oxygenated after some time because oxygen consumption in deeper sediment layers is not sufficiently high to replenish anoxic pore water. We could observe in the wave tank that the oxygen consumption 10 mm below the sediment surface was about 4 times higher than 4 mm below the sediment surface. This reflects the effect of intense flushing of the upper layer that had promoted the rapid degradation of the labile organic matter.

Natural environments

The impact of wave action and bottom currents on interfacial pore water exchange was studied on an intertidal North Sea sandflat by Rutgers van der Loeff (1981). An increased apparent diffusivity in the upper 1.5 cm of the sandy sediments was measured. Measurements of pore water oxygen profiles in the North Sea by Lohse et al. (1996) revealed that the effective oxygen diffusion coefficients the surface layers of sandy sediments could be > 100 times higher than the molecular diffusion coefficients, which was attributed to turbulent diffusion driven by near-bottom currents. Moreover, Webb and Theodor (1968) and Precht and Huettel (Chapter 3) observed that wave driven advective pore water flow is a natural process occurring in nearshore environments. As the processes studied here are caused by the interaction of boundary flows and topography, it may be argued that in spite of small wavelength and shallow water depth, the laboratory results are applicable to natural permeable sediments affected by waves.

Sandy sediments are abundant in the global continental shelf environment (Emery 1968; de Haas et al. 2002) and sands like our experimental sediment with a median grain size of 180 μm are common on the shelf (e.g. Cacchione et al. (1999); Ogston and Sternberg (1999) describe shelf sands with a grain size ranging from 125 μm and 250 μm and ripples of 9 cm wavelength at 60 m water depth). The oxygen consumption rates in the deeper layers of our wave tank sediment were 1.26 μmol L^{-1} min^{-1}, which is relatively low but close to values measured by Epping and Helder (1997) for sandy sediments of the Northern Adriatic shelf (approx. 2 μmol L^{-1} min^{-1}).

Previous studies have shown that wave-induced boundary flows may reach the sediment surface in large areas of the global continental shelf down to > 100 m (Wiberg and Harris 1994; Harris and Wiberg 2001). The extent of the shelf areas affected by waves was numerically assessed by Harris and Coleman (1998): e.g. in large areas of the Southern North Sea, wave-induced flow exceeds the mobilisation threshold for quartz sands of 100 µm diameter 10 to 50 % of the time.

However, the wave ripples that formed during our experiments were of the orbital type (Wiberg and Harris 1994) with wavelengths between 2.5 and 3 cm. Under natural conditions, mainly anorbital ripples with comparable heights but longer wavelengths (ca. 9 cm for a sediment of our grain size) are formed. This suggests that in nature wave driven pore water advection affects greater sediment depths than in our experiments, given that the permeability of the sediment is sufficiently high. As the pore water flow velocities decrease with depth, the oxic water entering the sediment in the ripple troughs will be de-oxygenated by oxygen consumption due to the longer residence time in the sediment. Therefore, it is unlikely that the sediment depth affected by advective transport equals the actual sediment depth that is exposed to oxygen through advective flushing. Nevertheless, larger ripple spacing means that the sediment depth from which material can be released is increased. Thus, a storm event may affect sediment water exchange and penetration depth of advective pore flows much longer than its actual duration because it produces or enhances ripple topography. After a storm, this "memory effect" may increase sedimentary biological and biogeochemical activity due to higher particle filtration and oxygen penetration associated with the "new" topography.

The observed oxygen dynamics are of biogeochemical relevance and have an impact on the in-sediment ecology. Our study revealed 4 different scenarios of advective interfacial exchange caused by waves in dependence of the existence and mobility of the sediment topography (Fig. 14):

(I) Sediment without significant topography

Development of a continuous oxidised sediment surface layer, with slightly increased oxygen penetration depth due to small-scale advection and possibly wave pumping. Additional solute release caused by molecular diffusion and bioirrigation. The sediment is redox sealed, meaning that reduced substances that precipitate or are adsorbed under oxic conditions (e.g. Fe^{2+}) cannot penetrate from deeper, anoxic sediment layers to the surface.

(II) Sediment surface with stationary ripples

Vertically alternating oxic and anoxic surface layer with the oxygen penetration depth locally increased by nearly an order of magnitude. The flushed sediment volume compared to stagnant conditions increases more than 3-fold. Anoxic boundaries at the ripple crests may confine meiofauna to the sediment volume underneath the ripple troughs. Development of geochemical zonation at the ripple crests; upwelling of pore water from deeper sediment layers creates anoxic channels to the surface through which reduced substances can be released to the water column.

(III) Sediment surface with ripples moving slower than pore water

The flushed sediment volume relative to stagnant conditions increases more than 3-fold and is comparable with (II). Mobile pore water upwelling zones alternately exposing sediment volumes to oxic and anoxic conditions enhance organic matter degradation in the upper sediment layer due to associated redox oscillations (Aller 1994). Anoxic upwellings passing through oxic zones leach precipitates from the sediment. Mobile vertical anoxic zones may chase infauna and select for a bacterial community that is tolerant to oxygen and anoxic conditions. Sulphide oxidisers that depend on oxygen or that can store nitrate like Beggiatoa (Jørgensen and Des Marais 1990) or Thioploca (Fossing et al. 1995; Huettel et al. 1996) may profit from alternating pore water down- and upwelling.

(IV) Sediment with ripples moving faster than pore water

Upwelling of pore water too slow to follow ripples. Establishment of a continuous oxic layer creates a redox sealed sediment with an undulating oxic-anoxic interface. Largest sediment volume flushed by oxygen-rich water (more than 6-fold increased to stagnant conditions). Intensive mixing of upwelling and downwelling pore water within the sediment may cause layers with increased precipitation of redox-sensitive substances (e.g. the common ferric iron coatings on surface layer sands).

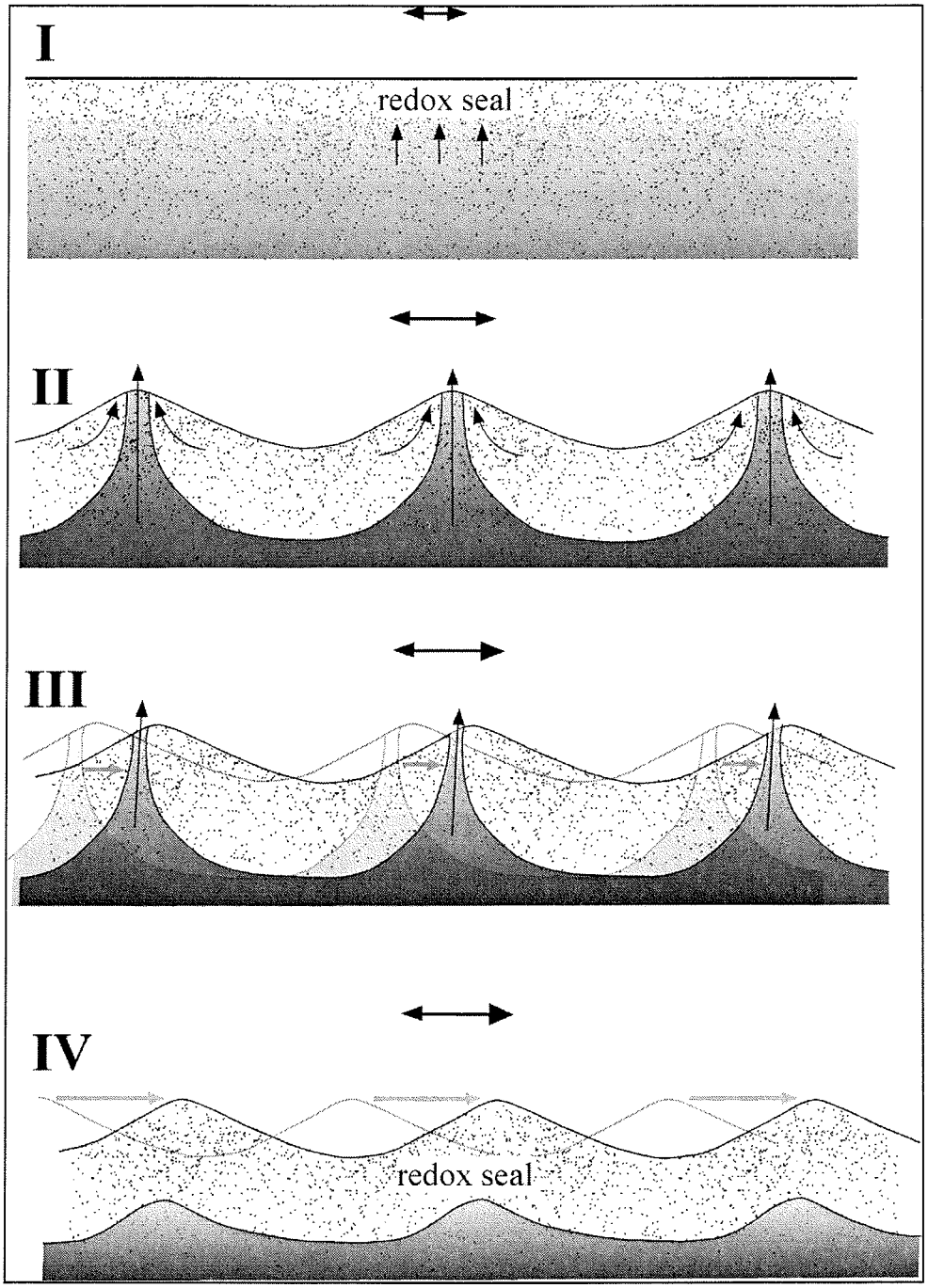

Fig. 14: (I): no sediment topography, oscillating flow; (II) stationary ripples; (III) ripples moving slower than pore water; (IV), ripples moving faster than pore water; for further details see text.

Between scenario III and IV, there is a gradual transition. In our experiments, when the ripples propagated at velocities < 10 cm h^{-1}, the upwelling zones were fully developed with anoxic conditions in the centres (III). With ripple propagation > 20 cm h^{-1}, the upwelling zone became detached from the ripple crest (IV). With pore water velocities between circa 10 and 20 cm h^{-1}, the upwelling zone trailed behind the ripple crest and could only be observed as a zone of slight oxygen depletion. Therefore, ripple migration velocity defines not only how long a sediment volume is exposed to anoxic conditions but also the degree of anoxia. This has implications on what substances can be "leached" from the sediment due to the passage of an oxygen depleted or oxic zone (applicable to Fe, Mn, NO_3, NH_4, PO_4, and possibly to heavy metals like Pb, Cd or Hg).

Doucette et al. (2002) measured the migration rates of wave ripples 45 m offshore with ripple wavelengths and sediment grain sizes comparable to those in our study. They observed averaged ripple migration rates of 55 cm h^{-1}, which would mean that at least in the highly mobile nearshore environment, scenario (IV) of a redox sealed sediment with completely oxic surface layer occurs. Migration rates of larger wave ripples (ripple wavelengths typically 10 to 100 cm; sediment median grain size=400 μm) were measured by Traykovski et al. (1999) at 11 m water depth and it was found that these bedforms moved at speeds between 1 and 3 cm h^{-1}. These values show that in natural environments, all the scenarios we postulate can occur.

As we demonstrated in this study, anoxic conditions can migrate through the sediment at velocities of up to 10 cm h^{-1}, which exceeds the typical directional swimming speeds of bacteria (ca. 1 cm h^{-1}, Jørgensen (2001)). Therefore, bacteria living in highly mobile sandy sediment need to be tolerant to redox oscillations. The relatively high pore water velocities in the sediment surface layer may be a reason why more than 90% of the bacteria in such permeable sands are attached to the grains (Rusch et al. 2001).

We conclude that surface gravity waves can control oxygen transport and distribution in shallow permeable sediments. Because this influence is affected by the formation of sediment wave ripples and associated advective pore water flows, the regularity of the ripple topography is reflected in the oxygen distribution pattern in the upper sediment layer with alternating zones of oxic and anoxic sediment. However, the fluxes into the sediment are confined to different and larger surface areas than the fluxes out of the sediment, a

separation that can generate a regular pattern of extremely different biogeochemical zones at the surface. The tight link between topography and pore water flow fields makes this distribution pattern highly dynamic as ripples migrate or change their shape. Through the persistence of ripples after a storm event, this "memory effect" of the sea bed may control sediment metabolism long time after such an event due to advective exchange caused by the interaction of boundary flows (e.g. tidal flows) and relict topography.

5. Hydrodynamical impact on biogeochemical processes in aquatic sediments

(Hydrobiologia, in press)

Markus Huettel, Hans Røy, Elimar Precht and Sandra Ehrenhauß

Max Planck Institute for Marine Microbiology, Celsiusstr. 1, 28359 Bremen

Abstract

Boundary layer flow characteristics and sediment permeability control pathways and magnitude of material exchange in the surface layer of aquatic sediments. In fine-grained cohesive beds, bottom currents and sediment microtopography shape the diffusive boundary layer and locally produce areas where the interfacial solute fluxes are increased or reduced. Where sediment permeabilities exceed 10^{-12} m^2, advective pore water flows driven by boundary flow-topography interaction dominate the sediment-water exchange of matter, with transport rates that exceed those of molecular diffusion by two orders of magnitude and more. The curved paths of the advective pore flows through the surface layers of such sandy beds generate complex three-dimensional biogeochemical patterns with extreme spatial and temporal variability ranging from millimeters to decimeters and seconds to seasons. High filtration rates, a bacterial community firmly attached to the mineral grains, rapidly changing biogeochemical zonations and winnowing of the sediment surface layers by frequent resuspension convert these beds into effective biocatalytical filter systems.

Key Words: Boundary flow, sediment, permeability, solute flux, mineralization.

Acknowledgements

This work was supported by the Max Planck Society and by the Danish Research Agency (stipend for Hans Røy).

Transport mechanisms at the sediment-water interface

In shallow aquatic environments, the sediment bed is the most important site for accumulation, storage and biogeochemical transformation of organic matter and contaminants (Wainright et al. 1992; Canfield et al. 1993; Villar et al. 1999). The extent to which the sedimentary processes are linked to the overlying water column is determined by transport mechanisms that carry particulate and dissolved substances into and out of the bed (Berner 1976; VanRees et al. 1996). In most aquatic environments, the most important transport processes are molecular diffusion, gravitational settling, bioturbation and bioirrigation, pore water advection and burial due to lateral sediment transport (Aller 1982; Shum and Sundby 1996; Vaughn and Hakenkamp 2001). All these mechanisms are strongly affected by boundary layer flows making water currents, surface gravity waves and turbulence dominant factors controlling benthic-pelagic coupling.

Boundary flows and diffusive sediment-water exchange

Where the boundary flows are weak, fine-grained sediments can accumulate producing deposits with organic matter and solute concentrations that exceed those in the overlying water column by far (Berner 1980; Ignatieva 1996). Due to the resulting concentration gradients and the relatively low hydraulic conductivity of these deposits, molecular diffusion in such beds usually is the most important mechanism for the transport of dissolved substances across the sediment-water interface. In such environments, the boundary layer hydrodynamics govern the biogeochemistry of the sediment surface layers by controlling the solute concentration gradients at the sediment water interface (Jørgensen 1994; Golosov and Ignatieva 1999). These gradients are not only shaped by the characteristics of the boundary layer flow (e.g. laminar or turbulent) but also by the interaction of the flow with the microtopography of the sediment. (Jørgensen and Des Marais 1990) observed the compression and dilatation of oxygen concentration isolines due to locally accelerating or decelerating contour flows at microtopography of a microbial mat. In their recent microscale studies of oxygen distribution at the surface of a silty bioturbated sediment, (Røy et al. 2002) demonstrated that flow-microtopography interaction affects also the diffusive boundary layer and oxygen flux in fine-grained marine sediments. At sub-millimetre scale, the sediment surface appears as a three-dimensional structure where the

concentration gradients that loosely follow the topography support fluxes not only in vertical but also in horizontal direction (Fig. 1). A one-dimensional measuring approach may underestimate oxygen flux in such settings by 5 to 15% revealing the importance of flow, topography and the ensuing three-dimensional nature of the sediment water exchange.

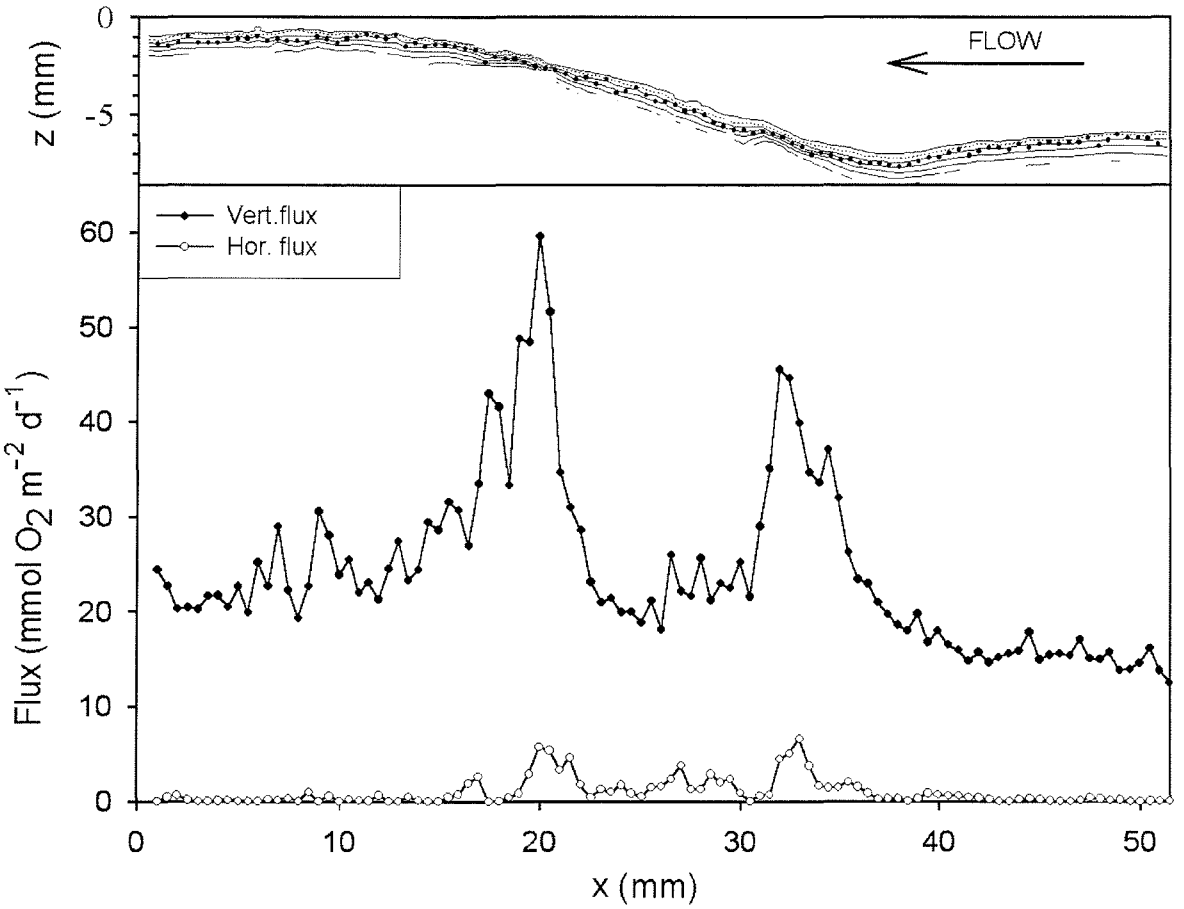

Fig. 1. Upper pane: Cross-section of a fine grained sediment that was inhabited by oligochaetes (interface indicated by dotted line) and the oxygen concentration isolines that are shaped by the interaction of the microtopography, hotspots and boundary layer flow. The isolines were derived from oxygen profiles measured with a microsensor at a spatial resolution of 250 μm and 100 μm in horizontal and vertical direction, respectively. The isolines reveal compression of the diffusive boundary layer (DBL) and enhanced oxygen flux at microtopography and two hotspots (at x = 20 mm and x = 32 mm, lower pane). The latter were caused by fresh faecal pellets deposited on the surface by oligochaetes. The elevated flux between 10 and 30 mm relative to the flux between 40 and 50 mm can be attributed to the compression of the DBL due to the hydrodynamical compression of the DBL. Median grain size 6.3 μm, permeability $k = 1.5 \times 10^{-13}$ m^2, porosity = 0.8, organic content = 2.9%, shear velocity $u^* = 0.09$ cm s^{-1}.

Advective filtering in permeable sediments exposed to flow

The importance of boundary flows for the metabolic activities in the sediment increases with increasing intensity of the flow near the sediment-water interface (Berninger and Huettel 1997; Migne and Davoult 1998). In river and shallow coastal environments, strong bottom currents frequently resuspend and winnow the sediment resulting in coarse-grained beds with relatively high hydraulic conductivities and low content of organic matter (Li and Amos 1999). Nevertheless, such sediments can have oxygen consumption rates similar to those recorded for fine-grained beds rich in organic matter suggesting that these beds efficiently mineralize organic material originating from the overlying water column (Andersen and Helder 1987; Lohse et al. 1996). However, strong currents and turbulence exceeding the settling velocities of organic matter and fine particles by far require other processes than gravitational settling for the uptake of such substances into the sediments. The boundary layer hydrodynamics again are the key factor controlling the transfer of matter into these sediments. In such high-energy environments, advective pore water flows and lateral sediment transport control the transfer of matter into the permeable bed.

Interfacial advective flows are driven by small lateral pressure gradients (ca. 1-3 Pa cm^{-1}) that result from the interaction of unidirectional or oscillating boundary layer flows with sediment topography (Huettel and Gust 1992). Obstruction of the flow by protruding structures causes local increase of pressure that forces water and suspended particles into porous sediments, while the acceleration of flow when passing over these protrusions results in a pressure decrease that draws pore water from the sediment (Savant et al. 1987; Thibodeaux and Boyle 1987; Huettel et al. 1996) (Fig. 2). In typical coastal settings this transport reaches to approximately 15 cm sediment depths. Because there is no river or sea bed that is perfectly smooth, all natural sediments with a permeability exceeding 10^{-12} m^2 function as effective filter systems when exposed to boundary layer flow.

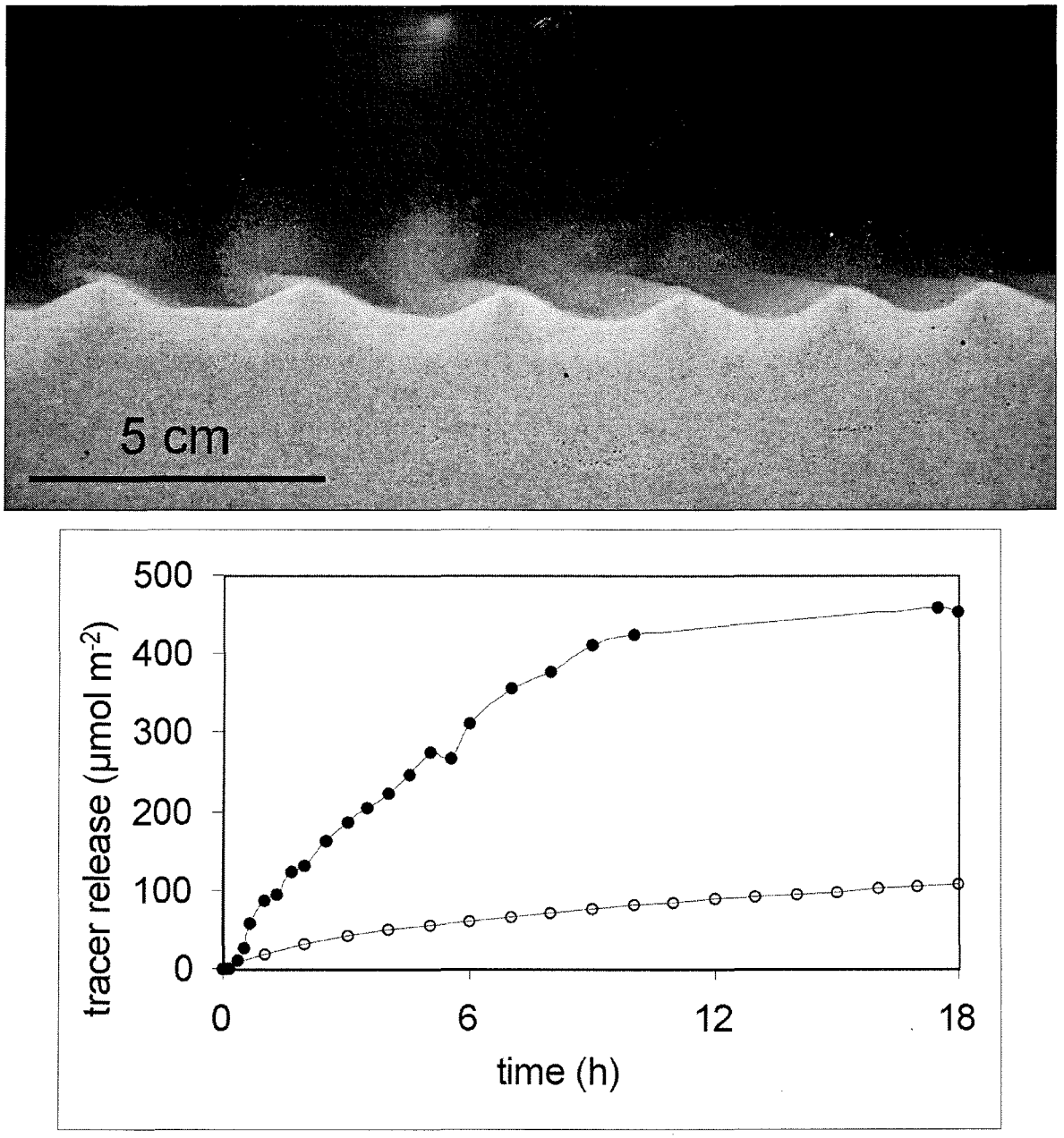

Fig. 2. Upper pane: Advective pore water exchange due to oscillating boundary currents interacting with ripple topography generated by waves. Stained pore water is released to the water column at the ripple crests, while unstained water intrudes the sediment in the ripple troughs. Experimental settings: median grain size: 250 µm, k: 2.9×10^{-11} m^2, water depth in wave tank: 20 cm, wave amplitude: 10 cm, wavelength: 120 cm, av. $u^* = 0.12$ cm s^{-1}, filtration rate: 90 L m^2 d^{-1}. Lower pane: Comparison of advective and diffusive release of solute tracer from the same sediment under stagnant flow conditions and exposed to the waves. Advective release due to waves in this case increased solute flux by factor 10 relative to diffusion.

The ecological relevance of the interfacial advective water flows is linked to the transport of reactive materials into permeable sediments. Laboratory and *in-situ* experiments showed that phytoplankton cells, bacteria and organic detritus particles are transported several centimetres into the sediment within 12 to 24 h (Pilditch et al. 1998; Huettel and Rusch 2000; Rusch et al. 2001) (Fig. 3). This process causes rapid particulate matter uptake in environments where strong boundary currents prevent the gravitational deposition of organic matter.

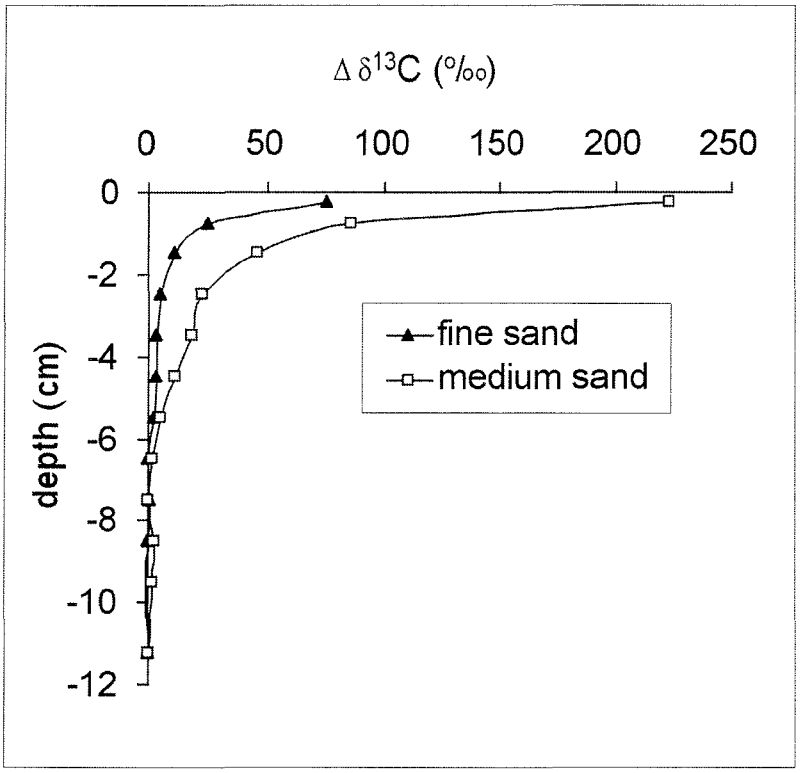

Fig. 3. Results of an *in-situ* experiment on transport of ^{13}C-labeled *Ditylum brightwellii* diatom cells into North Sea sediments of different grain size and permeability. Fine sand: k = 3×10^{-12} m^2, penetration time 32 h, medium sand: k= 26×10^{-12} m^2, penetration time 20 h. Interfacial water flows carried labeled diatoms down to 3 cm in the fine sand and down to 6 cm in the medium sand. In the latter this transport distance was covered in less than one day.

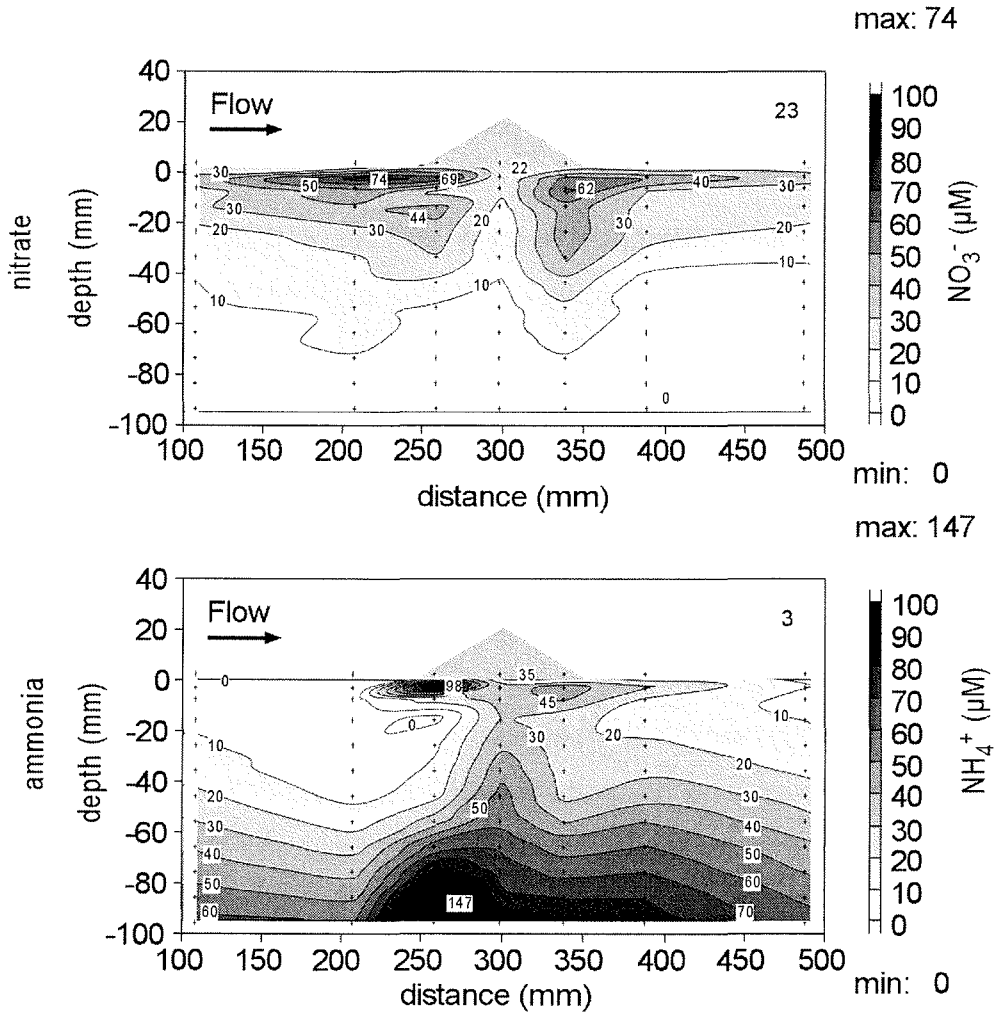

Fig. 4. Zones of enhanced nitrification are generated up- and downstream of protruding surface structures (in this case a small mound of 2.5 cm height, upper pane), while pore water rich in ammonia is drawn to the surface underneath the protrusion creating steep gradients between aerobic and anaerobic sediment zones (lower pane). Here ammonium-oxidizing bacteria find ideal growing conditions. Likewise metals are affected by the advective pore water flows. Dissolved ferrous iron and dissolved manganese are drawn from deeper anoxic sediment layers to the surface. The upwelling pore water flows, thus, create a pathway of reduced metals through the oxidized surface layer of the sediment permitting the release of these substances to the water column. Pollutants can be released from such sediments in the same manner. Median grain size 350 µm, permeability $k = 5.1 \times 10^{-11}$ m^2, porosity = 0.4, organic content = 0.2%, shear velocity $u^* = 0.38$ cm s^{-1}. (Modified after Huettel et al. 1998)

Concurrent with the transport of organic particles into the bed, water rich in oxygen and other electron acceptors (e.g. nitrate, sulfate) is forced into the sediment and, because the fluid experiences less friction than the particulate matter, passes through the layers where the intruding particles accumulate within the bed (Huettel et al. 1998). The pore water flow field associated with sediment topography dictates a directed flow from the area of intrusion to the release zone providing an efficient exchange mechanism for pore water and dissolved metabolites. More than 90% of the bacterial cells in sandy sediments are attached to the mineral grains (Rusch et al. 2001). When water rich in organic matter and electron acceptors is flushed through sand beds, the bacterial community converts these beds into efficient biocatalytical filters (Fig. 4).

Spatial and temporal heterogeneity in sedimentary biogeochemical processes due to boundary flow-topography interaction

Because in natural environments sediment topography as well as the boundary layer flow characteristics change on time scales ranging from seconds to seasons, the fast advective transport of particles and fluid caused by the topography-flow interaction generates a rapidly changing biogeochemical zonation of complex three-dimensional structure (Huettel et al. 1998) (Fig. 5). These rapid spatial and temporal changes further enhance the biocatalytical activity of permeable aquatic sediments and accelerate the transformation of matter in these beds (Aller 1994). A low content of reactive materials in such beds, thus, cannot be interpreted as low metabolic activity but rather is the consequence of rapid turnover and high exchange rates.

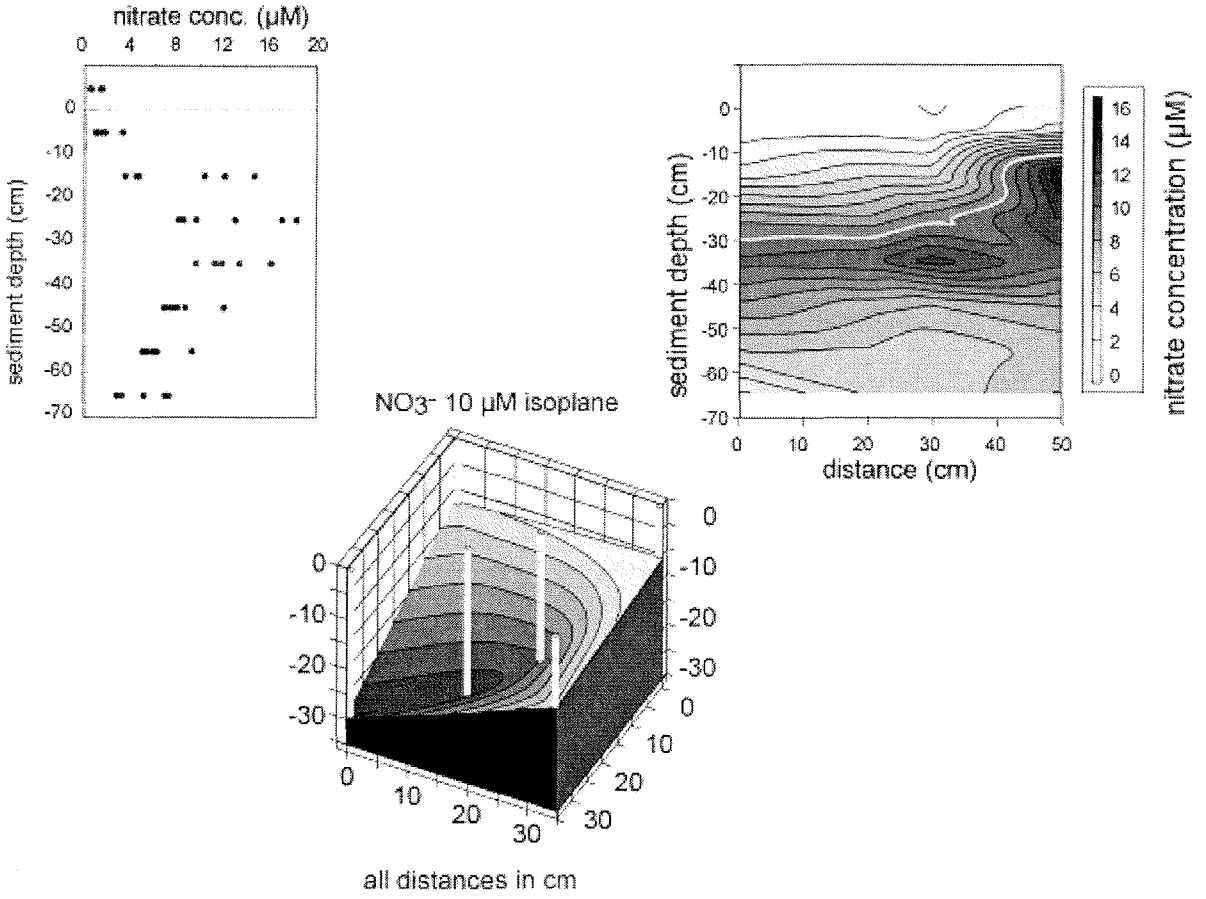

Fig. 5. The same set of nitrate pore water profiles originating from permeable carbonate sediment (Kaneohe Bay/Oahu, permeability $k = 5 \times 10^{-11}$ $m^2 - 9 \times 10^{-11}$ m^2) depicted in one- (upper pane), two- (middle pane), and three-dimensional (lower pane) plots. In permeable sediments the variation of concentrations between single vertical profiles may be caused by the complex three-dimensional nature of the biogeochemical zonation. By collecting horizontal spatial information with the vertical profiles, this three-dimensional structure can be shown.

Conclusions

The hydrodynamical boundary flow conditions and the permeability of the sediment define whether diffusion or advection dominates the exchange of substances between aquatic sediments and the overlying water column. When sediment permeability exceeds 10^{-12} m^2, advective transport surpasses diffusion (Fig. 6). In natural environments, this picture is complicated by the activity of benthic meio- and macrofauna organisms that enhance interfacial transport of solutes and particles by bioturbation and bioirrigation. In coastal permeable beds, this biological transport locally can be as efficient as advective exchange,

however, the biological activity is also controlled by the boundary hydrodynamics (e.g. due to supply of oxygen). Exchange of solutes and particles in aquatic environments is controlled by the hydrodynamic conditions at the sediment-water interface, and measurements attempting to quantify the interfacial exchange have to take the variability of the boundary flows and sediment permeability into account.

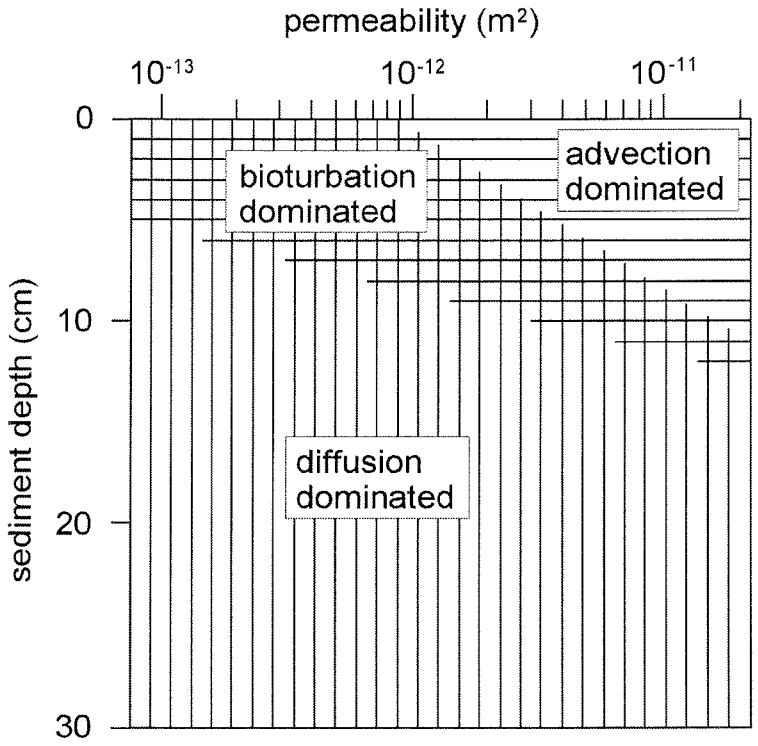

Fig. 6. The permeability and depth ranges of the main transport mechanisms in aquatic environments. The zone where bioturbation is dominant is depicted for marine coastal environments (modified after Huettel and Gust 1992).

6. Conclusions and Perspectives

In this thesis, the effects of shallow water waves on the interfacial exchange between sandy sediments and overlying water were addressed. The results of the laboratory wave tank experiments and the in-situ measurements with inert tracers agreed well: the main exchange process is advection driven by pressure gradients generated through the interaction between oscillating boundary flow and sediment topography. This leads to a release of pore water from deeper sediment layers at the ripple crests and intrusion of water in the ripple troughs. This pattern observed in the wave tank experiments could be verified for a natural environment, regardless of about the 10-fold larger spatial dimensions of the natural ripples and pore water flow field. Pore water velocities in the order of tens of cm h^{-1} were observed in the laboratory and in-situ. As these pore water velocities are matrix-averaged velocities, i.e. velocities of clouds of tracer moving through the sediment, the actual interstitial waters velocities are approximately 3 times larger in sediments of our tortuosity.

Advective pore water exchange rates in the laboratory experiments were up to 50-fold increased compared to exchange by molecular diffusion and amounted to values in the order of 100 L m^{-2} d^{-1}, which corresponded very well with the 140 L m^{-2} d^{-1} found in the field.

Based on field measurements, Riedl et al. (1972) calculated that the complete ocean volume could be filtered through the shelf sediments in only 14000 years. However, the interfacial exchange was attributed solely to wave pumping by hydrostatic pressure oscillations and exchange through the interaction of boundary flow and sediment topography was not taken into account. Our laboratory experiments were not designed to quantify the effects of wave pumping, but we could find a maximum exchange rate of 38 L m^{-2} d^{-1}, that probably was caused mainly by wave pumping. This implies that wave pumping may lose importance in those areas of the continental shelf where waves generate oscillating flows are at the seabed. Therefore, the wave-influenced continental shelf may be divided into three different zones: the beach, where large amounts of water are filtered through the sediment by percolation in a spatially limited zone; a shallow zone (water depth < wavelength/2) where wave orbital motion at the sea floor creates ripples and causes

topography-related advective filtering and a deeper zone (wavelength/2 < water depth < wavelength), where wave pumping enhances interfacial exchange by hydrostatic pressure oscillations. With variable wave energy, the spatial extent of these zones varies over time and the shallow zone may be subdivided into two zones in which topography-related advective exchange occurs permanently or episodically. With increasing water depth, the intervals between episodic advective events will increase.

The novel technique of an optode array that was employed in the field experiments proved to be a suitable tool for in-situ measurements of pore water velocities. This technique may be useful to assess in-situ pore water velocities in sands of different permeabilities and ripple spacing under variable wave conditions. The results might be used to infer filtering rates of shelf sediments not only based on wave pumping but also by topography-related advection.

The planar oxygen optode measurements in the laboratory wave tank revealed the oxygen dynamics in a natural permeable sand. It could be shown that the spatial oxygen distribution in the sediment was controlled by the pore water flow pattern linked to ripple topography, pore water flow velocity, oxygen consumption of the sediment, and molecular diffusion. Advective exchange created zones of sediment flushed by oxygen-rich water from the overlying water and zones where anoxic pore water reached the sediment surface. This led to horizontal oxygen concentration gradients in the sediment in the same order of magnitude as in the vertical. With slowly migrating ripples, the pore water upwelling zone could follow the ripple and sediment volumes were thus exposed to oscillating oxygen concentrations. When the sediment ripples propagated faster than the pore water velocity (experimental threshold $\approx$ 20 cm h^{-1}), a completely flushed, oxygen-rich sediment surface layer was formed and the sediment became redox sealed as no upwelling zones of anoxic pore water could reach the sediment surface. Planar oxygen optodes might be a useful tool for in-situ measurements of the oxygen dynamics in permeable sediments that are driven by the advective processes described in this thesis.

With the abundance of sandy sediments covered by ripples in shelf environments that are permanently or episodically exposed to oscillating flows induced by waves, it can be concluded that the processes described in this work affect large areas of the continental shelf. Filtering rates in the order of 100 L m^{-2} d^{-1} or larger suggest that these shelf sands are

effective filter systems that receive substantial input of particulate organic matter. In combination with rapid solute exchange, this means that shelf sands may be important sites for mineralisation and decomposition of organic matter to an extent that might have been overlooked in the past and that should receive further attention in the future.

7. References

Agrawal, Y. C. and D. G. Aubrey. 1992. Velocity Observations Above a Rippled Bed Using Laser Dopler Velocimetry. J. Geophys. Res.-Oceans. 97: 20249-20259.

Aller, R. C. 1982. The effects of macrobenthos on chemical properties of marine sediment and overlying water, p. 53-102. *In* P. L. McCall and M. J. S. Tevesz [eds.], Animal-Sediment Relations. Plenum Press.

Aller, R. C. 1994. Bioturbation and remineralization of sedimentary organic matter: effects of redox oscillation. Chem. Geol. 114: 331-345.

Aller, R. C. 2001. Transport and Reactions in the Bioirrigated Zone, p. 269-301. *In* B. P. Boudreau and B. B. Jørgensen [eds.], The Benthic Boundary Layer. Oxford University Press.

Andersen, F. O. and W. Helder. 1987. Comparison of Oxygen Microgradients, Oxygen Flux Rates and Electron-Transport System Activity in Coastal Marine-Sediments. Mar. Ecol. Prog. Ser. 37: 259-264.

Ayrton, H. 1910. The Origin and Growth of Ripple-mark. Proc. R. Soc. Lon. Ser. A. 84: 285-310.

Bagnold, R. A. 1946. Motion of Waves in Shallow Water - Interaction Between Waves and Sand Bottoms. Proc. R. Soc. Lon. Ser. A. 187: 1-18.

Ballew, R. M. and J. N. Demas. 1989. An Error Analysis of the Rapid Lifetime Determination Method For the Evaluation of Single Exponential Decays. Anal. Chem. 61: 30-33.

Berger, W. H., V. S. Smetacek and G. Wefer. 1989. Ocean productivity and paleoproductivity - an overview, p. 1-34. *In* W. H. Berger, V. S. Smetacek and G. Wefer [eds.], Productivity of the ocean: present and past. John Wiley & Sons.

Berner, R. A. 1976. The bentic boundary layer from the viewpoint of a geochemist., p. 33-55. *In* I.N.McCave [ed.], The Benthic Boundary layer. Plenum Press.

Berner, R. A. 1980. Early Diagenesis-A Theoretical Approach. Princeton University Press.

Berninger, U. G. and M. Huettel. 1997. Impact of flow on oxygen dynamics in photosynthetically active sediments. Aquat. Microbial Ecol. 12: 291-302.

Black, K. P. and J. W. Oldman. 1999. Wave mechanisms responsible for grain sorting and non-uniform ripple distribution across two moderate-energy, sandy continental shelves. Mar. Geol. 162: 121-132.

Blanton, J. O. 1991. Circulation Processes along Oceanic Margins in Relation to Material Fluxes, p. 145-163. *In* R. F. C. Mantoura, J.-M. Martin and R. Wollast [eds.], Ocean Margin Processes in Global Change. John Wiley & Sons.

Blondeaux, P., E. Foti and G. Vittori. 2000. Migrating sea ripples. Eur. J. Mech. B - Fluids. 19: 285-301.

Booij, K., W. Helder and B. Sundby. 1991. Rapid Redistribution of Oxygen in a Sandy Sediment Induced By Changes in the Flow Velocity of the Overlying Water. Neth. J. Sea Res. 28: 149-165.

Boudreau, B. P. 1996. The diffusive tortuosity of fine-grained unlithified sediments. Geochim. Cosmochim. Acta. 60: 3139-3142.

Cacchione, D. A., P. L. Wiberg, J. Lynch, J. Irish and P. Traykovski. 1999. Estimates of suspended-sediment flux and bedform activity on the inner portion of the Eel continental shelf. Mar. Geol. 154: 83-97.

Caldwell, D. R. and T. M. Chriss. 1979. The Viscous Sublayer at the Sea Floor. Science. 205: 1131-1132.

Canfield, D. E., B. B. Jørgensen, H. Fossing, R. Glud, J. Gundersen, N. B. Ramsing, B. Thamdrup, J. W. Hansen, L. P. Nielsen and P. O. J. Hall. 1993. Pathways of organic carbon oxidation in three continental margin sediments. Mar. Geol. 113: 27-40.

Canfield, D. E. and A. Teske. 1996. Late proterozoic rise in atmospheric oxygen concentration inferred from phylogenetic and sulphur-isotope studies. Nature. 382: 127-132.

Ciavola, P., R. Taborda, O. Ferreira and J. A. Dias. 1997. Field observations of sand-mixing depths on steep beaches. Mar. Geol. 141: 147-156.

Corbett, D. R., J. Chanton, W. Burnett, K. Dillon, C. Rutkowski and J. W. Fourqurean. 1999. Patterns of groundwater discharge into Florida Bay. Limnol. Oceanogr. 44: 1045-1055.

D'Andrea, A. F., R. C. Aller and G. R. Lopez. 2002. Organic matter flux and reactivity on a South Carolina sandflat: The impacts of porewater advection and macrobiological structures. Limnol. Oceanogr. 47: 1056-1070.

Darcy, H. 1856. Les Fontaines Publiques de la Ville de Dijon. Dalmont.

de Haas, H., T. C. E. van Weering and H. de Stigter. 2002. Organic carbon in shelf seas: sinks or sources, processes and products. Cont. Shelf Res. 22: 691-717.

Denny, M. W. 1988. Biology and the Mechanics of the Wave-Swept Environment. Princeton University Press.

Doucette, J. S., E. S. Harvey and M. R. Shortis. 2002. Stereo-video observation of nearshore bedforms on a low energy beach. Mar. Geol. 189: 289-305.

Durrieu De Madron, X., A. Abassi, S. Heussner, A. Monaco, J. C. Aloisi, O. Radakovitch, P. Giresse, R. Buscail and P. Kerherve. 2000. Particulate matter and organic carbon budgets for the Gulf of Lions (NW Mediterranean). Oceanol. Acta. 23: 717-730.

Elliott, A. H. 1990. Transfer of Solutes into and out of streambeds. Ph.D. Thesis. California Institute of Technology.

Elliott, A. H. and N. H. Brooks. 1997a. Transfer of nonsorbing solutes to a streambed with bed forms: Theory. Water Resour. Res. 33: 123-136.

Elliott, A. H. and N. H. Brooks. 1997b. Transfer of nonsorbing solutes to a streambed with bed forms: Laboratory experiments. Water Resour. Res. 33: 137-151.

Emery, K. O. 1968. Relict sediments on continental shelves of the world. Am. Assoc. Pet. Geol. Bull. 52: 445-464.

Epping, E. H. G. and W. Helder. 1997. Oxygen budgets calculated from in situ oxygen microprofiles for Northern Adriatic sediments. Cont. Shelf Res. 17: 1737-1764.

Eylers, H., N. H. Brooks and J. J. Morgan. 1995. Transport of Adsorbing Metals From Stream Water to a Stationary Sand-Bed in a Laboratory Flume. Mar. Freshw. Res. 46: 209-214.

Falter, J. L. and F. J. Sansone. 2000. Hydraulic control of pore water geochemistry within the oxic- suboxic zone of a permeable sediment. Limnol. Oceanogr. 45: 550-557.

Fleming, K., P. Johnston, D. Zwartz, Y. Yokoyama, K. Lambeck and J. Chappell. 1998. Refining the eustatic sea-level curve since the Last Glacial Maximum using far- and intermediate-field sites. Earth Planet. Sci. Lett. 163: 327-342.

Forster, S., M. Huettel and W. Ziebis. 1996. Impact of Boundary Layer Flow Velocity On Oxygen Utilisation in Coastal Sediments. Mar. Ecol. Prog. Ser. 143: 173-185.

Fossing, H., V. A. Gallardo, B. B. Jorgensen, M. Huttel, L. P. Nielsen, H. Schulz, D. E. Canfield, S. Forster, R. N. Glud, J. K. Gundersen, et al. 1995. Concentration and Transport of Nitrate By the Mat-Forming Sulfur Bacterium Thioploca. Nature. 374: 713-715.

Garcia, H. E. and L. I. Gordon. 1992. Oxygen Solubility in Seawater - Better Fitting Equations. Limnol. Oceanogr. 37: 1307-1312.

Golosov, S. D. and N. V. Ignatieva. 1999. Hydrothermodynamic features of mass exchange across the sediment-water interface in shallow lakes. Hydrobiologia. 409: 153-157.

Grasshoff, K., K. Kremling and M. Ehrhardt. 1999. Methods of seawater analysis. Wiley-VCH Verlag.

Haese, R. R. 2002. Macrobenthic Activity and its Effects on Biogeochemical Reactions and Fluxes, p. 219-314. *In* G. Wefer, D. Billett, D. Hebbeln et al. [eds.], Ocean Margin Systems. Springer.

Harris, C. K. and P. L. Wiberg. 1997. Approaches to quantifying long-term continental shelf sediment transport with an example from the Northern California STRESS mid-shelf site. Cont. Shelf Res. 17: 1389-1418.

Harris, C. K. and P. L. Wiberg. 2001. A two-dimensional, time-dependent model of suspended sediment transport and bed reworking for continental shelves. Comput. Geosci. 27: 675-690.

Harris, P. T. and R. Coleman. 1998. Estimating global shelf sediment mobility due to swell waves. Mar. Geol. 150: 171-177.

Harrison, W. D., D. Musgrave and W. S. Reeburgh. 1983. A wave-induced transport process in marine sediments. J. Geophys. Res. 88: 7617-7622.

Holst, G. and B. Grunwald. 2001. Luminescence lifetime imaging with transparent oxygen optodes. Sens. Actuator B-Chem. 74: 78-90.

Holst, G., O. Kohls, I. Klimant, B. Konig, M. Kuhl and T. Richter. 1998. A modular luminescence lifetime imaging system for mapping oxygen distribution in biological samples. Sens. Actuator B-Chem. 51: 163-170.

Hsü, K. J. 1989. Physical Principles of Sedimentology. Springer Verlag.

Huettel, M., S. Forster, S. Kloser and H. Fossing. 1996. Vertical migration in the sediment-dwelling sulfur bacteria Thioploca spp in overcoming diffusion limitations. Appl. Environ. Microbiol. 62: 1863-1872.

Huettel, M. and G. Gust. 1992. Impact Of Bioroughness On Interfacial Solute Exchange In Permeable Sediments. Mar. Ecol. Prog. Ser. 89: 253-267.

Huettel, M. and A. Rusch. 2000. Transport and degradation of phytoplankton in permeable sediment. Limnol. Oceanogr. 45: 534-549.

Huettel, M. and I. T. Webster. 2001. Porewater flow in permeable sediments, p. 144-179. *In* B. P. Boudreau and B. B. Jørgensen [eds.], The Benthic Boundary Layer. Oxford University Press.

Huettel, M., W. Ziebis and S. Forster. 1996. Flow-induced uptake of particulate matter in permeable sediments. Limnol. Oceanogr. 41: 309-322.

Huettel, M., W. Ziebis, S. Forster and G. I. Luther. 1998. Advective transport affecting metal and nutrient distribution and interfacial fluxes in permeable sediments. Geochim. Cosmochim. Acta. 62: 613-631.

Hutchinson, P. A. and I. T. Webster. 1998. Solute uptake in aquatic sediments due to current-obstacle interactions. J. Environ. Eng.-ASCE. 124: 419-426.

Ignatieva, N. V. 1996. Distribution and release of sedimentary phosphorus in Lake Ladoga. Hydrobiologia. 322: 129-136.

Jahnke, R. A., J. R. Nelson, R. L. Marinelli and J. E. Eckman. 2000. Benthic flux of biogenic elements on the Southeastern US continental shelf: influence of pore water advective transport and benthic microalgae. Cont. Shelf Res. 20: 109-127.

Johnson, H. D. and C. T. Baldwin. 1986. Shallow Siliclastic Seas, p. 229-282. *In* H. G. Reading [ed.], Sedimentary Environments and Facies. Blackwell Scientific Publications.

Jørgensen, B. B. 1994. Diffusion processes and boundary layers in microbial mats, p. 243-253. *In* L. J. Stal and P. Caumette [eds.], Microbial Mats. Springer-Verlag.

Jørgensen, B. B. 2001. Life in the diffusive boundary layer, p. 348-373. *In* B. P. Boudreau and B. B. Jørgensen [eds.], The Benthic Boundary Layer. Oxford University Press.

Jørgensen, B. B. and D. J. Des Marais. 1990. The diffusive boundary layer of sediments: oxygen microgradients over a microbial mat. Limnol. Oceanogr. 35: 1343-1355.

Kautsky, H. 1939. Quenching of luminescence by oxygen. Trans. Faraday Soc. 35: 216-219.

Kawamata, S. 1998. Effect of wave-induced oscillatory flow on grazing by a subtidal sea urchin Strongylocentrotus nudus (A. Agassiz). J. Exp. Mar. Biol. Ecol. 224: 31-48.

Klimant, I., V. Meyer and M. Kühl. 1995. Fiber-optic oxygen microsensors, a new tool in aquatic biology. Limnol. Oceanogr. 40: 1159-1165.

Klimant, I. and O. S. Wolfbeis. 1995. Oxygen-Sensitive Luminescent Materials Based On Silicone- Soluble Ruthenium Diimine Complexes. Anal. Chem. 67: 3160-3166.

Klute, A. and C. Dirksen. 1986. Hydraulic conductivity and diffusivity: laboratory methods, p. 687-734. *In* A. Klute [ed.], Methods of soil analysis - part 1 - physical and mineralogical methods. American Society of Agronomy.

Krögel, F. 1997. Einfluß von Viskosität und Dichte des Seewassers auf Transport und Ablagerung von Wattsedimenten (Langeooger Rückseitenwatt, südliche Nordsee). Ber. aus d. FB Geow. d. Univ. Bremen. 102.

Lambeck, K. and J. Chappell. 2001. Sea level change through the last glacial cycle. Science. 292: 679-686.

Li, L. and D. A. Barry. 2000. Wave-induced beach groundwater flow. Adv. Water Resour. 23: 325-337.

Li, L., D. A. Barry, F. Stagnitti and J. Y. Parlange. 1999. Submarine groundwater discharge and associated chemical input to a coastal sea. Water Resour. Res. 35: 3253-3259.

Li, M. Z. and C. L. Amos. 1998. Predicting ripple geometry and bed roughness under combined waves and currents in a continental shelf environment. Cont. Shelf Res. 18: 941-970.

Li, M. Z. and C. L. Amos. 1999. Field observations of bedforms and sediment transport thresholds of fine sand under combined waves and currents. Mar. Geol. 158: 147-160.

Li, Y. H. and S. Gregory. 1974. Diffusion of ions in sea water and in deep sea sediments. Geochim. Cosmochim. Acta. 38: 703-714.

Libelo, E. L., W. G. MacIntyre, R. D. Seitz and L. F. Libelo. 1994. Cycling of water through the sediment-water interface by passive ventilation of relict biological structures. Mar. Geol. 120: 1-12.

Liebsch, G., I. Klimant, B. Frank, G. Holst and O. S. Wolfbeis. 2000. Luminescence lifetime imaging of oxygen, pH, and carbon dioxide distribution using optical sensors. Appl. Spectrosc. 54: 548-559.

Lohse, L., E. H. G. Epping, W. Helder and W. Vanraaphorst. 1996. Oxygen Pore Water Profiles In Continental Shelf Sediments of the North Sea - Turbulent Versus Molecular Diffusion. Mar. Ecol. Prog. Ser. 145: 63-75.

Longuet-Higgins, M. S. 1983. Wave set-up, percolation and undertow in the surf zone. Proc. R. Soc. London Ser. A-Math. Phys. Eng. Sci. 390: 283-291.

Malan, D. E. and A. McLachlan. 1991. In situ benthic oxygen fluxes in a nearshore coastal marine system: a new approach to quantify the effect of wave action. Mar. Ecol. Prog. Ser. 73: 69-81.

Marinelli, R. L., R. A. Jahnke, D. B. Craven, J. R. Nelson and J. E. Eckman. 1998. Sediment nutrient dynamics on the South Atlantic Bight continental shelf. Limnol. Oceanogr. 43: 1305-1320.

McCave, I. N. 2002. Sedimentary Settings on Continental Margins - an Overview, p. 1-14. *In* G. Wefer, D. Billett, D. Hebbeln et al. [eds.], Ocean Margin Systems. Springer.

McLachlan, A. 1989. Water Filtration By Dissipative Beaches. Limnol. Oceanogr. 34: 774-780.

McLachlan, A. and I. Turner. 1994. The Interstitial Environment of Sandy Beaches. Mar. Ecol.-Pubbl. Stn. Zool. Napoli. 15: 177-211.

Migne, A. and D. Davoult. 1998. Macrobenthic metabolism as carbon and nitrogen fluxes in a coastal area exposed to strong tidal currents (Dover Strait, eastern English Channel). Hydrobiologia. 376: 307-315.

Milliman, J. D. 1991. Flux and Fate of Fluvial Sediment and Water in Coastal Seas, p. 69-90. *In* R. F. C. Mantoura, J.-M. Martin and R. Wollast [eds.], Ocean Margin Processes in Global Change. John Wiley & Sons.

Mix, A. C., E. Bard and R. Schneider. 2001. Environmental processes of the ice age: land, oceans, glaciers (EPILOG). Quat. Sci. Rev. 20: 627-657.

Moore, W. S. 1996. Large groundwater inputs to coastal waters revealed by Ra-226 enrichments. Nature. 380: 612-614.

Mu, Y. K., A. H. D. Cheng, M. Badiey and R. Bennett. 1999. Water wave driven seepage in sediment and parameter inversion based on pore pressure data. Int. J. Numer. Anal. Methods Geomech. 23: 1655-1674.

Musgrave, D. L. and W. S. Reeburgh. 1982. Density-driven interstitial water motion in sediments. Nature. 299: 331-333.

Nielsen, P. 1981. Dynamics and Geometry of Wave-Generated Ripples. J. Geophys. Res. 86: 6467-6472.

Nielsen, P. 1990. Tidal Dynamics of the Water-Table in Beaches. Water Resour. Res. 26: 2127-2134.

Nittrouer, C. A. and L. D. Wright. 1994. Transport of Particles Across Continental Shelves. Rev. Geophys. 32: 85-113.

O'Donoghue, T. and G. S. Clubb. 2001. Sand ripples generated by regular oscillatory flow. Coast. Eng. 44: 101-115.

Ogston, A. S. and R. W. Sternberg. 1999. Sediment-transport events on the northern California continental shelf. Mar. Geol. 154: 69-82.

O'Hara, S. C. M., P. R. Dando, U. Schuster, A. Bennis, J. D. Boyle, F. T. W. Chui, T. V. J. Hatherell, S. J. Niven and L. J. Taylor. 1995. Gas Seep Induced Interstitial Water Circulation - Observations and Environmental Implications. Cont. Shelf Res. 15: 931-948.

Oldham, C. E. and P. S. Lavery. 1999. Porewater nutrient fluxes in a shallow fetch-limited estuary. Mar. Ecol. Prog. Ser. 183: 39-47.

Packman, A. I. and N. H. Brooks. 1995. Colloidal Particle Exchange Between Stream and Stream Bed in a Laboratory Flume. Mar. Freshw. Res. 46: 233-236.

Pilditch, C. A., C. W. Emerson and J. Grant. 1998. Effect of scallop shells and sediment grain size on phytoplankton flux to the bed. Cont. Shelf Res. 17: 1869-1885.

Rey, V., A. G. Davies and M. Belzons. 1995. On the Formation of Bars By the Action of Waves On an Erodible Bed - a Laboratory Study. J. Coast. Res. 11: 1180-1194.

Riedl, R. J., N. Huang and R. Machan. 1972. The subtidal pump: a mechanism of interstitial water exchange by wave action. Mar. Biol. 13: 210-221.

Riedl, R. J. and E. A. Machan. 1972. Hydrodynamic patterns in lotic intertidal sands and their bioclimatological implications. Mar. Biol. 13: 179-209.

Riisgard, H. U. and P. S. Larsen. 2000. Comparative ecophysiology of active zoobenthic filter feeding, essence of current knowledge. J. Sea Res. 44: 169-193.

Rocha, C. 1998. Rhythmic ammonium regeneration and flushing in intertidal sediments of the Sado estuary. Limnol. Oceanogr. 43: 823-831.

Rocha, C. 2000. Density-driven convection during flooding of warm, permeable intertidal sediments: the ecological importance of the convective turnover pump. J. Sea Res. 43: 1-14.

Røy, H., M. Huettel and B. B. Jørgensen. 2002. The role of small-scale sediment topography for oxygen flux across the diffusive boundary layer. Limnol. Oceanogr. 47: 837-847.

Rusch, A. 2000. Dynamik der Feinfraktion im Oberflächenhorizont permeabler Schelfsedimente. Ber. aus d. FB Geow. d. Univ. Bremen. 155.

Rusch, A., S. Forster and M. Huettel. 2001. Bacteria, diatoms and detritus in an intertidal sandflat subject to advective transport across the water-sediment interface. Biogeochemistry. 55: 1-27.

Rutgers van der Loeff, M. M. 1981. Wave effects on sediment water exchange in a submerged sand bed. Neth. J. Sea Res. 15: 100-112.

Rutherford, J. C., J. D. Boyle, A. H. Elliott, T. V. J. Hatherell and T. W. Chiu. 1995. Modeling Benthic Oxygen-Uptake By Pumping. J. Environ. Eng.-ASCE. 121: 84-95.

Rutherford, J. C., G. J. Latimer and R. K. Smith. 1993. Bedform Mobility and Benthic Oxygen-Uptake. Water Res. 27: 1545-1558.

Savant, S. A., D. D. Reible and L. J. Thibodeaux. 1987. Convective Transport Within Stable River Sediments. Water Resour. Res. 23: 1763-1768.

Schlüter, M. 2002. Fluid Flow in Continental Margin Sediments, p. 205-217. *In* G. Wefer, D. Billett, D. Hebbeln et al. [eds.], Ocean Margin Systems. Springer.

Shum, K. T. 1992. Wave-induced advective transport below a rippled water-sediment interface. J. Geophys. Res. 97: 789-808.

Shum, K. T. 1993. The Effects of Wave-Induced Pore Water Circulation on the Transport of Reactive Solutes Below a Rippled Sediment Bed. J. Geophys. Res. 98: 10289-10301.

Shum, K. T. and B. Sundby. 1996. Organic matter processing in continental shelf sediments - the subtidal pump revisited. Mar. Chem. 53: 81-87.

Sleath, J. F. A. 1984. Sea Bed Mechanics. John Wiley & Sons.

Smetacek, V., U. Bathmann, E.-M. Nöthig and R. Scharek. 1991. Coastal Eutrophication: Causes and Consequences, p. 251-279. *In* R. F. C. Mantoura, J.-M. Martin and R. Wollast [eds.], Ocean Margin Processes in Global Change. John Wiley & Sons.

Thibodeaux, L. J. and J. D. Boyle. 1987. Bedform-generated convective transport in bottom sediment. Nature. 325: 341-343.

Traykovski, P., A. E. Hay, J. D. Irish and J. F. Lynch. 1999. Geometry, migration, and evolution of wave orbital ripples at LEO-15. J. Geophys. Res. 104: 1505-1524.

Turner, I. L. and G. Masselink. 1998. Swash infiltration-exfiltration and sediment transport. J. Geophys. Res.-Oceans. 103: 30813-30824.

VanRees, K. C. J., K. R. Reddy and P. S. C. Rao. 1996. Influence of benthic organisms on solute transport in lake sediments. Hydrobiologia. 317: 31-40.

Vaughn, C. C. and C. C. Hakenkamp. 2001. The functional role of burrowing bivalves in freshwater ecosystems. Freshw. Biol. 46: 1431-1446.

Ver, L. M. B., F. T. Mackenzie and A. Lerman. 1999. Carbon cycle in the coastal zone: effects of global perturbations and change in the past three centuries. Chem. Geol. 159: 283-304.

Villar, C., L. de Cabo, P. Vaithiyanathan and C. Bonetto. 1999. Pore water N and P concentration in a floodplain marsh of the Lower Parana River. Hydrobiologia. 392: 65-71.

Voulgaris, G. and M. B. Collins. 2000. Sediment resuspension on beaches: response to breaking waves. Mar. Geol. 167: 167-187.

Wainright, S. C., C. A. Couch and J. L. Meyer. 1992. Fluxes Of Bacteria and Organic Matter Into a Blackwater River From River Sediments and Floodplain Soils. Freshwater Biol. 28: 37-48.

Webb, J. E. and J. Theodor. 1968. Irrigation of submerged marine sands through wave action. Nature. 220: 682-683.

Webb, J. E. and J. L. Theodor. 1972. Wave-Induced Circulation in Submerged Sands. J. Mar. Biol. Assoc. U.K. 52: 903-914.

Webster, I. T. 1992. Wave Enhancement of Solute Exchange Within Empty Burrows. Limnol. Oceanogr. 37: 630-643.

Webster, I. T., G. J. Hancock and A. S. Murray. 1994. Use of Radium Isotopes to Examine Pore-Water Exchange in an Estuary. Limnol. Oceanogr. 39: 1917-1927.

Webster, I. T., S. J. Norquay, F. C. Ross and R. A. Wooding. 1996. Solute exchange by convection within estuarine sediments. Estuar. Coast. Shelf Sci. 42: 171-183.

Webster, I. T. and J. H. Taylor. 1992. Rotational Dispersion in Porous-Media Due to Fluctuating Flows. Water Resour. Res. 28: 109-119.

Wiberg, P. L. and C. K. Harris. 1994. Ripple Geometry in Wave-Dominated Environments. J. Geophys. Res. 99: 775-789.

Wollast, R. 1991. The Coastal Organic Carbon Cycle: Fluxes, Sources, and Sinks, p. 365-381. *In* R. F. C. Mantoura, J.-M. Martin and R. Wollast [eds.], Ocean Margin Processes in Global Change. John Wiley & Sons.

Wollast, R. 2002. Continental Margins - Review of Geochemical Settings, p. 15-31. *In* G. Wefer, D. Billett, D. Hebbeln et al. [eds.], Ocean Margin Systems. Springer.

Woods, R. J., S. Scypinski, L. J. C. Love and H. A. Ashworth. 1984. Transient Digitizer For the Determination of Microsecond Luminescence Lifetimes. Anal. Chem. 56: 1395-1400.

Wright, L. D. 1995. Morphodynamics of inner continental shelves. CRC Press.

Zabel, M. and C. Hensen. 2002. The Importance of Mineralization Processes in Surface Sediments at Continental Margins, p. 253-267. *In* G. Wefer, D. Billett, D. Hebbeln et al. [eds.], Ocean Margin Systems. Springer.

Ziebis, W., M. Huettel and S. Forster. 1996. Impact of biogenic sediment topography on oxygen fluxes in permeable seabeds. Mar. Ecol. Prog. Ser. 140: 227-237.

Manuscript not included in this thesis

Near-bottom performance of the Acoustic Doppler Velocimeter (ADV) -a comparative study

by Elimar Precht, Felix Janssen and Markus Huettel

(submitted to Aquatic Ecology 17.12.2002)

This manuscript was not included in this thesis, as it is a technical study not directly linked to the rest of the work presented here. The near-bottom performance of the ADV is of interest for many aquatic scientists as the ADV is widely used to characterise flows close to the seabed or around objects protruding into the benthic boundary layer. Manuscripts can be made available upon request.

Abstract

In a laboratory flume, a comparative study on the near-bottom performance of the Acoustic Doppler Velocimeter was conducted. We tested two different ADV systems at different configurations and two flow velocities (9 cm s^{-1}, 18 cm s^{-1}). The results were compared with synchronous measurements with a Laser Doppler Anemometer (LDA).

Near-bottom velocity measurements with the ADV have to be interpreted carefully as the ADV technique underestimates flow velocities in a zone close to the sediment. The height of this zone above the sediment varies with different ADV systems and configurations.

The nominal sampling volume height values given by the software often underestimate the true, effective sampling volume heights. Smaller nominal SVH improve the ADV near-bottom performance, but the vertical extent of the zone in which the ADV underestimates flow by >20 % may be larger than true SVH/2 by a factor of 2 (=true SVH).

When the measurement volume approaches the bottom, ADV data quality parameters (signal-to-noise-ratio and signal amplitude) exceeding the average "open water" level, are clear indicators that the ADV has begun to underestimate the flow velocity. Unfortunately, this is not a safe indicator for the range of reliable measurements as the ADV may begin to underestimate velocities even with unchanged "open water" data quality parameters. Thus, we can only recommend avoiding measurements below a distance from the bottom that we defined empirically comparing the ADV and the LDA velocity profiles. This distance is 2.5 × nominal sampling volume height.

Danksagung

Herrn Prof. Dr. Bo Barker Jørgensen sei herzlich gedankt für die Vergabe und Begutachtung dieser Arbeit.

Herrn Priv. Doz. Matthias Zabel danke ich für die freundliche Übernahme des Zweitgutachtens.

Mein besonderer Dank gilt Markus Hüttel, für die Initiierung und Betreuung dieser Arbeit. Er hat durch seine Ideen und die zahlreichen Diskussionen maßgeblich zu ihrem Gelingen beigetragen.

Finanziert wurde meine Arbeit durch die Max-Planck-Gesellschaft.

Von den Mitarbeitern des MPI geht mein Dank an alle TA's, und vor allem die der Flux-Gruppe; Gabi Schüßler, Susanne Menger, Martina Alisch. Ich danke außerdem Cecilia Wiegand für die Herstellung der Sauerstoff-Optoden, den E-Werkstättlern Paul Färber und Volker Meyer sowie Georg Herz von der Technik-Werkstatt.

Desweiteren gilt mein Dank Arzhang für hydrodynamische Antworten, Christian und allen weiteren Mitarbeitern der Flux-Gruppe. Ohne die Programmierkünste von Luboš wäre die Arbeit mit den planaren Optoden um ein vielfaches erschwert gewesen.

Ein ganz dickes Dankeschön geht an Felix Janßen, Uli Franke und Rebecca Ludwig und vor allem Hans Røy für Diskussionen, Ideen, Unterstützung, hilfreiche Anmerkungen zu den Manuskripten und kreative Kaffeepausen.

Auf keinen Fall unerwähnt bleiben dürfen natürlich Jean-Claude, Fanni, Solveig, Sandra, Jens, Tina (großartig, Ginger) und Herr Grötzschel.

Allen weiteren, hier nicht namentlich genannten Mitarbeitern des MPI's, die auf die eine oder andere Weise zum Gelingen dieser Arbeit beigetragen haben, sei hiermit ebenso gedankt.

Ich danke Markus Diesing von der Arbeitsgruppe Hydroakustik, Institut für Geowissenschaften der Uni Kiel, für Sonar-Bilder und immer zur Verfügung gestellten geologischen Sachverstand.

Nicht zuletzt möchte ich mich mich bei allen meinen Freunden (vor allem Schemel) und ganz herzlich bei meinen Eltern sowie meinen Geschwistern Lars und Kristina bedanken, auf die ich immer zählen konnte, wenn mal wieder nicht alles oder nichts so ganz richtig rund lief.